An

Ion Beam Complement to Electron Beam Writers

-

A Part of the Development, Characterisation and Utilisation

Dissertation
Zur Erlangung des Doktorgrades der Naturwissenschaften
angefertigt am
Lehrstuhl Experimentelle Physik I
der Fakultät Physik der Technischen Universität Dortmund
in Kooperation mit dem LPN CNRS (Marcoussis, F) und der Raith GmbH (Dortmund)

vorgelegt von
Lars Bruchhaus

März 2012

"... One should repeat that the prejudice invoked by the words damage or defects is unfortunate since the changes in structure produced by the passage of fast ions enables us to make materials which were not obtainable by normal thermodynamic processes. It is also true that the "damaged" material may have superior properties to the original solid..." [1]

I. Table of contents

II. List of Abbreviations

AFM	Atomic force microscope
Al	Aluminium
Ar	Argon
As	Arsenic
Au	Gold
Au_{55}	$Au_{55}(PPh_3)_{12}Cl_6$ ($(PPh_3)_{12}$ triphenylphosphine)
CAD	Computer aided design
Cl	Chloride
CPO	Charged particle optic
CP-ML2	Particle mask less lithography with high throughput
CO	Carbon monoxide
Co	Cobalt
CVD	Chemical vapour deposition
DNA	Deoxyribonucleic acid
EBID	Electron beam induced deposition
EBL	Electron beam lithography
EHDS	Electrohydrodynamic-induced liquid spraying
F	Flour
FBMS	Fixed beam moving stage
FC	Fraction of the current inside the diameter d_{NFC}
FIB	Focused ion beam
FOV	Field of view
FWHM	Full width half maximum
Ga	Gallium (usually as Ga^+ ions)
GFIS	Gas field ion source
H	Hydrogen
HOPG	Highly oriented pyrolytic graphite
HSQ	Hydrogen silsesquioxane
IBAD	Ion beam assisted deposition
IBID	Ion beam induced deposition
IBL	Ion beam lithography
Li	Lithium
LMIS	liquid metal ion source
ISE	Ion induced secondary electrons
MEBES	Manufacturing electron beam exposure system
MC	Monte Carlo (technique)
MFM	Magnetic force microscope
MIBK	Methyl isobutyl ketone
ML2	Maskless lithography with high throughput
N	Neutron number
Na	Natrium

NA	Numerical aperture (n·sin α)
Ni	Nitride
O	Oxide
OA	Optical axis
O-ML2	Optical mask less lithography with high throughput
PKA	Primary knock on atom
PMMA	Poly(methyl-methacrylate)
PRAL	Projected range algorithm
Pt	Platinum
R&D	Research and development
RIE	Reactive ion etching
SCALPEL	Scattering with angular limitation projection electron beam lithography
SE	Secondary electron
SEM	Scanning electron microscope
Si	Silicon
SIM	Scanning ion microscopy
SNOM	Scanning near field optical microscopy
SPM	Scanning probe microscopy
SRIM	Stopping and range of ions in matter
SThM	Scanning thermal microscope
STM	Scanning tunnelinig microscope
STEM	Scanning transmission electron microscopy
TEM	Transmission electron microscope
EUV	Extreme ultra violet (wave-length of 10 to 100nm)
UV	Ultra violet (wavelength < 400nm)
WD	Working distance
Xe	Xenon
Y	Sputter yield
Z	Proton/atomic number

III. List of variables / units

α	Angular semi angle of the objective
α_o	Beam defining aperture half angle or source side half angle / angular semi aperture of the beam emerging from the source
α_p	Half angle at the probe or lens system half angle image side / opening angle in the image space
ρ,β,γ,δ	Indices (= 1,2,3,…)
ΔE	Energy spread
ε_o	Vacuum permittivity ($8.854\ 10^{-12}$ F/m)
γ	surface tension of the liquid
λ	Wavelength of the applied light / equivalent wavelength of the accelerated charged particle
λ_{rel}	Relativistic equivalent wavelength of the accelerated charged particle
μA	Micro Ampere ($1 \cdot 10^{-6}$ A)
φ_o	Sample potential
φ_1	Axial electrical potential at the object plane
φ_2	Axial electrical potential at the image plane
φ_{source}	Ion source potential
φ_{ext}	Ion extractor potential
Ω	Unit solid angle
Θ	Beam deflection angle
ξ	Distance from the centre of the beam

Å Angstrom (10^{-10}m)

B Beam brightness

$\vec{B}$ Applied magnetic field

B_r Reduced brightness

b Image length

Cc Chromatic aberration coefficient

C_S Spherical aberration coefficient

c Speed of light (299,792,458 m/s)

$c_{\rho,\beta,\gamma,\delta}(z)$ Coefficient (with the indices comp. above)

D Area dose

D_L Line dose

d Minimum distance of two structures which can still be resolved as two separate objects

d_A Diffraction "disc of confusion"

d_{AFC} Diffraction image fractional current diameter (carrying FC% of the current, comp. above)

d_{CFC} Chromatic image diameter (carrying FC% of the current, comp. above)

d_{IFC} Gaußian image fractional current diameter (carrying FC% of the current, comp. above)

d_{SCF} Spherical aberration fractional current diameter (carrying FC% of the current, comp. above)

d_{NCF} Minimizing defocus plane diameter (carrying FC% of the current, comp. above)

d_c Disk of confusion due to chromatic aberration

d_G Gaußian image of the source

d_S Disk of confusion due to spherical aberration

$d_{S,eff}$ Effective source size

E Mean energy of particles (at the image plane)

dE/dx Ion energy losses per unit path length is defined

$\vec{E}$ Applied electric field

E_b Lattice binding energy

E_d Lower limit of energy the incident ion looses during the displacement process

E_s Surface binding energy

E_t Electrical field at the tip

e The elementary charge ($1.6 \cdot 10^{-19}$As)

eV Energy unit ($1.602 \cdot 10^{-19}$ J)

D Dose

FC Fraction of the current inside the diameter d_{NFC}

F(s) Force function between e.g. an impinging ion and a surface atom

f Focal length of the lens system

g Object length

h Planck constant $6.626176 \cdot 10^{-34}$ Js

I Average intensity measured inside for the "horizontal" or "vertical" gratings (two of the patterned areas)

$\mathbf{I_{em}}$ Ion source emitted current

$\mathbf{I_{bc}}$ Average intensity between the three patterns ("background")

$\mathbf{I_{cross}}$ Average intensity measured at the cross reference structure

$\mathbf{I_N}$ Total current

$\mathbf{I_{probe}}$ (Measured) particle current on the sample surface

$\mathbf{J_N(r)}$ Current density function of the beam

k "Physiological" factor takes into account the human eye's capability to resolve two features close to each other as difference in shape or intensity (usually ≥ 1)

L "Characteristic length"

M Magnification of the optical system

MeV Mega electron volt ($1 \cdot 10^{-6}$ eV, comp. above)

$\mathbf{M_1}$ Mass of the incident ion

$\mathbf{M_2}$ mass of the surface atom

m Mass of the (charged) particle

$\mathbf{m_{rel}}$ Relativistic mass

$\mathbf{m_e}$ $9.109534 \cdot 10^{-31}$ kg or $5.485 \cdot 10^{-4}$u (electron rest mass)

$\mathbf{m_{Ga}}$ Rest mass Ga = 69.72u = $1.157 \cdot 10^{-25}$ kg

$\mathbf{m_o}$ Rest mass

n Index of refraction

nm Nanometer ($1 \cdot 10^{-9}$ m)

$\mathbf{R_r}$ Radial range

$\mathbf{R_S}$ Spreading range

R_P^t Transverse projected range

$\mathbf{R_P}$ Projected range / distance at which the highest concentration of implanted ions will be found

r Distance to the optical axis

$\mathbf{r_a}$ Axis centre distance / radius of the beam defining aperture ($r_a \sim \alpha_o$)

$\mathbf{r_o}$ The radial coordinate in the object plane

$\mathbf{r_i}$ The radial coordinate in the image plane

$\mathbf{r_c}$ Radius of ion source

$\mathbf{r_r}$ Hard sphere radii

$\mathbf{r_t}$ Tip radius

pA Pico Ampere ($1 \cdot 10^{-12}$ A)

p_t Hydrostatic surface forces at the tip

q Charge of the particle

dS Area of the source emission site

s Distance between two particles / the centre of two hard-sphere atoms / two points in the discrete patterning grid

sr Steradian

T_D Point dwell time (time the beam rests at a point of the discrete pattering grid)

U Resolving power of an optical microscope (1/d)

UHV Ultra high vacuum ($<1\cdot10^{-8}$ mbar)

U_{blank} Blanking voltage

$U_{Defl.,n}$ Deflection voltage applied to one (n) of the deflection plates

U_{ex} Extractor voltage φ_{source}- φ_{ext}

$U_{St.,n}$ Stigmator voltage applied to one (n) of the stigmator plates

U Atomic mass = $1.66\cdot10^{-27}$ kg

u_o Intersection point of a trajectory with the object plane (u_0^* its conjugate complex)

u_a Intersection point of a trajectory with the aperture plane (u_a^* its conjugate complex)

V Acceleration voltage (φ_{source} - φ_0)

V(s) Interatomic potential functionV_1 = on axis voltage at the mid point of the lens

$\vec{v}$ Velocity of the charged particle

v_e Speed of the electrons

v_i Speed of the ions

v_{rel} Relativistic speed

X_S Implant depth

Z Focus position

1 Introduction

Craftsmen and artists creating something have the need for tools, the “art” of creating features at very small scales -called nanotechnology- has the same need.

Analysing and artificially fabricating features with at least one dimension below 100 nanometer ($1 \cdot 10^{-7}$ m or 1/10 million meter (m)) is generally referred to as “Nanotechnology” [2]. The human hair has a diameter of about 25 µm ($25 \cdot 10^{-6}$ m) which is 250 times larger.

Nanotechnology is regarded as a key enabling technology [3] and can be employed to:

- further improve (shrink/higher speed) current electronic devices (e.g., in computers)
- tailor surface properties (“tribology” [4])
- learn more from nature on the nanometer (nm) scale and transfer this into new machines or improve existing ones (“bionics” [5])
- ...

Various tools and techniques for nano analysis and patterning are in use and produce satisfactorily results for many applications (comp. chapter 2). Two of them are routinely employed: optical lithography and electron beam lithography (EBL), the first one for volume production and the second one for research and development (R&D) applications. We focus on the latter applications. In R&D nano patterning (comp. chapter 2) some processes have become quite complex [6] [7] while some challenges have yet to be solved:

- soft x-ray zone lens fabrication (comp. section 8.3)
- <10 nm reproducible hole fabrication for DNA encoding (comp. section 9.3)
- or locally modify surface properties at arbitrary shapes (comp. section 9.1 and 9.2).

In 1959 Feynman suggested the use of ions for nano fabrication in his talk (later published under [8]). About 3 years later S.P Newberry suggested ion beams for micro fabrication [9]. In the 1960s and at the beginning of the 1970s instruments suffered from ion source brightness limitations (comp. section 2.2.5) and a solution started to develop in the 1960s (comp. chapter 4).

An exemplary instrument set-up and the terminology of focused charged particle beam instruments are introduced in chapter 3. Although already realised in 1988 [10] -with the available technology by that time- an ion beam complement to electron beam lithography instruments was not accepted by the research community for various reasons (comp. chapter 7.2). Today the main application fields of focused ion beam (FIB) technology are: nano analysis, sample preparation for nano analysis and repair tool in the semiconductor industry [11] (comp. section 7.3). As a result, the available tooling has been designed for other purposes initially. Employing these instruments for nano patterning (comp. chapter 2) or trying to develop new processes have resulted in challenges, and an initial decline in usage from about 1995 to 2004 (comp. section 7.2 and 7.4). However, we have been encouraged by the:

- predicted and partially already proven capabilities,
- significantly larger amount of ion-matter interactions exploitable for nano patterning, some of them even with the potential for direct patterning (comp. chapter 6),
- theory behind charged particle optics (comp. chapter 5) for possible resolution,
- recent renaissance in focused ion beam patterning (comp section 7.2),
- available technology today and
- complementary knowledge of the European commission (EC) growth project NanoFIB team members [12] (comp. section 12.3.2),

so we have tried it again: We have converted the “ion beam nano structuring machine” idea into a proof of concept tool [13]. In addition we have employed the technology to reach various leading edge results (comp. chapter 9 and sections 8.3, 12.1.2 and 12.4).

The focus of this work is to describe the results of the development process (comp. chapter 8, section 12.1.1) of a nano patterning point liquid metal ion source (LMIS) instrument for research applications (comp. chapter 9) and rapid prototyping. In addition to taking part in the instrument development (personal contribution comp. section 12.1.1) two applications have been analysed in more detail. For the first one, the instrument architecture has facilitated the analysis of potential causes for a long known resolution limiting effect (comp. section 10.1). Finally, for the second one, we have employed it to study a potential process complexity reduction way for the creation of electrically conducting features (comp. section 10.2).
The following chapter takes a look at complementary technologies for nano analysis and patterning.

2 Some historical roots / current tools

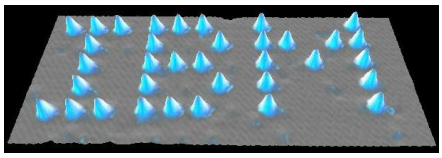

Various techniques with high resolution analytical and patterning capabilities on the small scale have been developed up to the single atom level (comp. Figure 2).

A review of technologies enabling analysis and pattering for „small things“ is presented as well as exemplary applications, advantages and limitations. They elucidate the need for further complementary tool concepts.

Four of these technologies have been developed for and applied to analysis purposes initially and after a while first patterning experiments have been carried out.

2.1 Nano analytics

There exist a large variety of potential nano analysis methods. Four exemplary ones will be described in more detail as they are the fundament for nano patterning techniques (comp. section 2.2).

2.1.1 Visible light microscope

The invention of the optical microscope has been an important milestone for the observation and creation of small things. Around 1600 the optical microscope has been developed (most likely by Z. Janssen) [14]. Since then it has been significantly improved many times, however it seemed as there has been a resolution limit which could not be overcome.

In 1873 E. Abbe published a way to model optical microscopes which he has worked out together with the master craftsman C. Zeiss. This has been the fundament for the manufacturing of optical microscopes based on theory [15]. Abbe has also published in this work a mathematical relation between the minimum distance (d) of two structures which can still be resolved as two separate objects due to diffraction phenomena. Almost at the same time (1874) H. v. Helmholtz developed a similar formula for the resolving power of an optical microscope:

$$U = 0.82 \cdot k \cdot \frac{n \cdot \sin\alpha}{\lambda}$$ [16]

Equation 1: resolving power U of an optical microscope

$n \cdot \sin\alpha$ = numerical aperture (NA)

α = angular semi angle of the objective

n = index of refraction

λ = wavelength of the applied light

U = resolving power, 1/d

k = “physiological” factor (usually ≥ 1)

The physiological factor k takes into account the human eye’s capability to resolve two features close to each other as difference in shape or intensity.

As a result objects separated by about half the wavelength of the applied light can be resolved with an optical microscope [16] using a high NA objective.

Following Equation 1 the resolving power could be further increased by either increase the numerical aperture (NA) or reducing the wavelength (λ):

The NA cannot be significantly increased, high end commercially available objectives have a NA of 0.95 (e.g. [17]) and immersion ones can even reach up to a NA of 1.45 NA (e.g. oil immersion [18]).

The wavelength of visible light is difficult to lower, as our eyes are sensitive to light wavelength from about 400-800 nm. However, classical photo, modern digital camera technology in combination with special sensors enable e.g. ultra violet optical microscopy (UV with a λ of about 10-400 nm). In addition even shorter wavelengths can be applied: e.g.: in 1912 M. v. Laue showed that a solid state consists of a periodic array of atoms [19] by x-ray diffraction experiments.

In spite of this well known limit, other derivatives like: e.g. confocal microscope [20], fluorescence microscope [21], scanning near field optical microscopy (SNOM) [22] have been developed. These efforts have been carried out e.g. keeping some advantages of optical microscopy e.g. [23]: non invasive to most samples, ambient operation conditions and ease of use. In addition a large variety of contrast mechanisms exist e.g.: amplitude, phase, polarisation, refractive index, fluorescence and spectroscopy. However, SNOM is more a mixture between optics and an SPM (comp. section 2.1.3).

Besides the use of electromagnetic waves there exist alternatives to visualise small things: electron microscopy (comp section 2.1.2), scanning probe microscopy (comp section 2.1.3) and ion microscopy (comp section 2.1.4).

2.1.2 Electron microscope

Early focussing attempts of “cathode rays” (electrons) by e.g. Hittorf (1869) and Birkeland (1869) used the rotationally symmetric field lying in front of a cylindrical magnet pole for focussing [24].

In 1924 d’Broglie discovered the wave nature of the electron [25], which has been published in his PhD thesis. This has been a starting point of the scientific field of electron diffraction (later called charged particle optics, CPO, comp. section 5.1). Already in 1926 H. Busch has been able to calculate trajectories in an electron ray bundle and found that the magnetic field of a short coil has the same effect on an electron bundle as has the convex glass lens with a defined focal length on a light bundle [24] [26]. Based on these calculations the first lenses have been created by Busch and Davisson and Calbick [24].

In his “Studienarbeit” (1929) E. Ruska sharply imaged a 0.3 µm aperture using electrons [24]. 2 years later an improved set-up has resulted in a two step microscope using electrons. The electrons have been focused by a magnetic lens (17.4 times magnification) [24]. Again a year

later Knoll and Ruska have employed for the first time the expression “Elektronenmikroskop” [27]. Finally, in 1933 Ruska has managed to brake for the first time the resolution barrier of an optical microscope (visible light) employing electrons (magnification of 12,000 with an edge resolution of 50 nm) [28]. Almost at the same time a competing group at AEG research labs (Germany, Brüche, Scherzer, and Recknagel) managed to fabricate a similar electron microscope instrument, as opposed to Knoll and Ruska, they have applied electrostatic lenses [26]. Further pioneering groups and information about the history can be found in [29] [26] [30] [31].

At the end of the 1930s technology advanced quickly due to the similar technology of electron microscopes, oscilloscopes and television sets. Applying d’Broglie’s theory Knoll and Ruska estimated in the same year (1932) the resolution limit for a 75 kV electron microscope to 2.2 Å [32], this has been reached about 40 years later [24]. Today leading edge transmission electron microscopes (TEMs) can reach a resolution below 1 Å (e.g. within the SESAM/UHRTEM Project 0.8 Å applying 200 kV acceleration voltage [33]) and special “correction lenses” e.g. K. Urban’s team [34] [35]. A further pioneer of electron beam technology is C. Oatley at Cambridge University in England who made a series of important technical advances in scanning electron microscopy and has also been involved in the commercialisation of electron beam techniques between the late 1940s and the early 1960s [36]. In addition the Oatley’s group has been involved in the commercial spin-out of scanning electron microscopes (SEMs) and electron beam (lithography) writers (EBL writers) to the Cambridge Instruments Company (later Leica Microsystems, now Vistec semiconductor systems [37] (further details about EBL comp. section 2.2.2 and 7.3.4).

2.1.3 Scanning probe microscope (SPM)

Already in 1929 an instrument called “stylus profiler” has been used to image sample surface topography [38]. In 1972 R. Young published the usage of a similar set-up. He developed it as non-contact instrument, detecting the field emission current between the tip and the sample, he called this instrument the “Topographiner” [39].

Later on in 1982 Binnig et al. published their outstanding results reached with the “scanning tunneling microscope” (STM). The STM made atomic surface lattices of some materials visible [40]. It senses the tunnelling current, which is more sensitive than the field emission current, between a conducting sample surface and the STM tip under ultra high vacuum (UHV) conditions. A few years later Binnig et al. [41] have published results from a similar technology visualising also insulating surfaces with the “atomic force microscope” (AFM)

even under ambient conditions by detecting surface forces. Under certain conditions it is possible to visualise surface atom lattices applying this technology [42].
Today many additional derivatives of this surface analysis method exist: magnetic force microscope (MFM), scanning near field optical microscope (SNOM), scanning thermal microscope (SThM), ...

2.1.4 First "ion microscope" and visualising atomic lattices of solid state

A few years after Ruska and Knoll in 1937 E.W. Müller invented the field (electron) emission microscope. It allows under most favourable conditions 10 Å resolution [43]. He has used electrons for a special kind of projection imaging of a sharp tip surface material. Fourteen years later in 1951 he has been able to significantly increase the resolution due to "field ionisation" and the development of the "Field Ion Microscope" [43]. With further improvements in 1955 it has been possible to visualize individual atoms as they form the crystal lattice of the tip metal with full resolution of high index net planes and with a resolution of 2.3 Å [43].
At the end of the 1960s Drummond and Long used a gas phase plasma source and have realised a scanning ion microscope, however it suffered from low beam brightness (comp. section 4.1, 2.1.4) at small beam diameters [44]. Fifteen year later Levi Setti has published first results from a scanning transmission ion microscope using hydrogen ions from a field ionisation source [45]. Further details about ion beam techniques and ionisation processes can be found e.g. in [46].

2.2 Nano patterning

The brief introduction of 4 high resolution analysis techniques will now be followed by patterning derivatives and an additional one without analysis roots.

2.2.1 Optical lithography

An exemplary derivative of the optical microscope technology (comp. section 2.1.1) is photolithography. In the 1950s J. Andrus [47] and W. L. Bond transferred photolithographic techniques (photoengraving) from defining patterns on printed circuit boards to silicon wafer processing [48]. At the end of the 1950s J. A. Hoerni integrated this technology into his "planar process" which in principle is still used in semiconductor manufacturing [49] (comp. patents: [50] [51]).

The instruments carrying out this photolithography are called “optical steppers” and are used within the semiconductor manufacturing process. The “stepper” projects the image of a desired photo mask pattern onto the surface of the semiconductor device being fabricated on a silicon wafer [52]. Although many times the “final” resolution limit has been predicted for „optical photo lithography“ [36], the technology is still capable in delivering the required resolution. However, mask costs increase significantly and optical proximity correction becomes more and more complex. It is the main lateral patterning technology for semiconductor industry, due to its high unmatched patterning speed, the existing infrastructure (e.g. mask fabrication facilities, resist technology) and lack of alternatives comp. [53].

As an example a currently commercially available tool employing ultra violet light (λ = 193 nm), the ASML Twinscan stepper [54] can resolve feature sizes down to 40 nm (immersion technique with a NA of 1.35).

2.2.2 Electron beam lithography (EBL)

Already in the 1930s e.g. P. H. Carr has studied the electron recording properties of various materials, as possible image formation process he suggested the creation of deposited layers [55].

According to Schmallenberg [36] and Owen et al. [56] Buck and Shoulder’s paper “An approach to microminiature printed systems” is among the first papers suggesting an electron beam resist patterning process creating devices in 1958. They suggested to locally deposit the gas tetraethoxysilane as silicaceous resist [57].

A comprehensive overview about the history of micro and nano patterning is given e.g. in [36], here further early electron beam patterning papers are cited.

In 1960 four decisive results have been published: W. E. Glenn (of General Electric Research) published his work using an electron beam causing deformation in the surface of a thermoplastic film [58]. W. Opitz from Carl Zeiss used an “electron beam milling machine” (milling, comp. section 6.2.1) with the capability to etch holes of a few µm diameter [59]. G.J. Selvin and W.J. Mc Donald outlined a complete microelectronics circuit fabrication process [60] which is for “the fine beam operation mode” similar to the Buck and Shoulder’s paper. Möllenstedt and Speidel of the University of Tübingen gave an impressive prove of the possible resolution with electron beam patterning down to 14 nm line width [61], an example of their pattering capabilities is given in Figure 1.

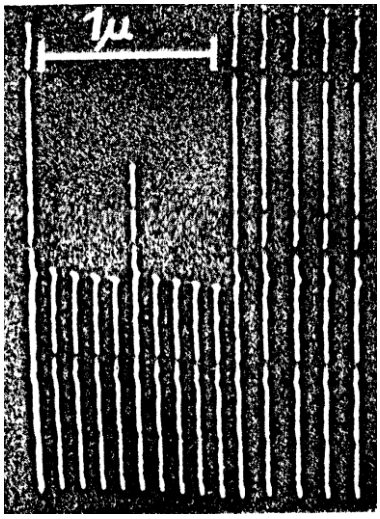

Figure 1: Electron micrograph of sub-100 nm lines written by e-beam lithography on collodion foil with the "Elektronenoptischer Mikroschreiber" (electron optical micro writer) [61].

In 1961 O. Wells has suggested a different electron beam processes for device fabrication [62], he is one of the first persons writing about electron beam "photo resist" processes in the way we use the term today (spinning a chemical resist on the sample surface, exposing it by electrons and developing it afterwards).Later on, in 1964 an IBM team (Thornely et al.) [63] invented an EBL writer to record e.g. dictionary data on a disk covered with Kodak high resolution photo emulsion. They used the "flying spot technique" (raster scanning the sample surface complemented by controlled blanking recalling the blanking data from a magnetic core buffer memory). In 1967 M. Hatzakis and R.F.M. Thornley have published the fabrication of solid state devices employing this technology [64]. The employed resist technique has been published a year later by another IBM team I. Haller, M. Hatzakis and R. Srinivasan. This has been the invention of the electron beam lithography resist poly(methyl-methacrylate) (PMMA, a thermoplastic and transparent plastic) [65]. PMMA is a high resolution organic resist which is sensitive to electron exposure and which is still employed by researchers today.

The first commercial available EBL system has been published by T.H.P. Chang and A.D.G. Steward in 1969 of Cambridge Scientific Instrument [66]. The Cambridge Instruments electron beam lithography systems (comp. section 2.1.2) replicated existing optical masks using a technology they also called "flying spot scanning technique" (comp. above) [66]. Later on T.H.P. Chang and B.A. Wallman have been the first demonstrating direct computer controlled e-beam patterning of chromium-glass photo masks, titled "A computer controlled electron-beam machine for micro-circuit fabrication" in 1971 [67]. Their company "Cambridge Instruments" (comp. section 2.1.2) has merged into Leica microsystems, now

Vistec semiconductor systems [37]. In 1976 Herriot et al. from Bell Laboratories published a new design and patterning scheme [68]. This technology has been licensed to the company ETEC e.g. [53] and has been used for many years within the EBL direct write mask writer family “MEBES” (Manufacturing Electron Beam Exposure System).

Serial computer controlled EBL (comp. section 7.3.4) is a rather slow technology compared to optical projection lithography. Nevertheless, for R&D and small scale production it possesses significant advantages: its high resolution capabilities, flexibility [69], the rapid prototyping capability without the need of mask generation. As a result even almost 40 years after the invention of the fundamental technology it is still the first choice for lateral nano patterning in R&D (e.g. [70] [71]) and for photo mask generation [72] employed e.g. in optical “stepper” instruments 2.2.1) in the semiconductor industry.

Multi column [73] or e-beam projection lithography like SCALPEL (scattering with angular limitation projection electron beam lithography) [74] could overcome the described speed limitations for semiconductor mass fabrication (comp. section 2.3), but work in these field have already been carried out in the 1990s and still none of them has been capable in replacing optical lithography. Just recently another promising concept, called reflective electron beam lithography (REBL) has been published [75]. Here a dedicated digital pattern generator combined with electron mirrors as beam switches have been realised as proof of concept.

Today an electron beam writer is the main lateral nano patterning tool in R&D and an essential part of many nano structuring activities (for volume semiconductor fabrication comp. 2.2.1). It is ideally suited for complex lateral batch nano pattering tasks from CAD designs, possesses an unmatched minimum beam diameter on the sample surface, relatively non destructive electron surface interactions compared to Ga^+ ions (comp. section 6.1.8), flexible process control and high automation level.

However, electron beam patterning possesses limitations: First it offers only a relatively little number of exploitable electron matter interactions compared to e.g. ions (comp. section 6.1.8). Second there exist limitations in 3D patterning. Third electron sample interactions lead to a relatively large interaction volume (comp. section 6.3.3, for acceleration voltages above 5 kV), which causes in combination with backscattering the proximity effect [56]. Forth it is usually an indirect technique with the need for pattern transfer which can lead to complex process chains.

EBL writers and their functionality will be described in more detail in section 7.3.4.

2.2.3 SPM patterning

All kinds of different experiments using SPM technology for nano fabrication have been reported (an overview over these techniques can be found e.g. [76] [77] [78] [79].

A very impressive prove of resolution has been given in a paper published by Eigler: His team managed to position individual Xe atoms on a Ni surface using a STM and afterwards read out the results with the same instrument (comp. Figure 2) [80] [81]. Together with Heinrich et al. D. Eigler has managed by positioning CO molecules to create a device acting as a three-input sorter that uses several AND gates and OR gates [82].

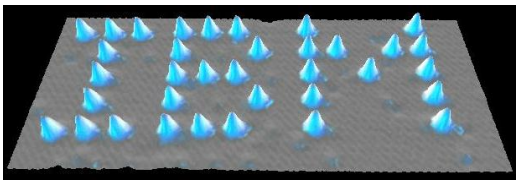

Figure 2: D. Eigler in 1989, individual Xe atoms on Ni (110) imaged with an STM [80] [81]

The fascinating capability of tailoring individual atoms/molecules is about the ultimate limit of resolution we can think of nowadays, however the technology is extremely slow.

2.2.4 Nano imprint

A further patterning technique without analysis roots is called nano imprint. In 1996 S. Chou's team has published a remarkable nano patterning publication proving 25 nm feature size utilising a new lateral nano structuring technology called "imprint lithography" [83]. The fundamental technology of compression moulding has been used already for some time as high throughput, low cost manufacturing technology with minimum feature sizes > 1 µm, e.g. for the fabrication of compact disks.

This invention is a complementary technique of nano patterning called "imprint".

If challenges like multi level placement, defect density and others [53] can be overcome in accordance to semiconductor industry requirements, this could be a promising -relatively cost effective and very fast- "next generation" lithography technique for the production of volume semiconductor devices. In addition it appears on the 2007 "international technology roadmap for semiconductors" [84].

2.2.5 Early focused ion beam (FIB) patterning

Already 1959 R. Feynman (comp. chapter 1) [8] has suggested to use ions for patterning tiny features and 3 years later S.P. Newberry has published a similar vision for ion beam micro fabrication [9].

According to Schmallenberg [36] K. Kanaya et al. presented among the first reported application of ion beams for micro fabrication in 1965 [85]. The paper title is "Micro colour recording, etching and machining by means of high voltage ion beams". They cut e.g. a 20 µm diameter hole into a thin Ni sheet and discussed possible advantages of ion beams over electrons beams due to their smaller particle wavelength and higher momentum.

At the beginning of the 1970s Seliger and his team [86] [87] added an "einzel lens" to an existing ion implantation (comp. section 6.2.2) system. The instrument was capable to create ions by various different techniques, e.g. RF, surface ionisation, sputtering, electron bombardment, ... [46]. They doped a Si sample by a boron focused ion beam and exposed electron beam lithography resist (PMMA, comp. section 2.2.5) using 60 kV He ions. The 300 keV instrument (comp. introduction of chapter 3) applied during these experiments is described in [46]. They discovered an about two orders of magnitude higher resists sensitivity of ions compared to electrons. In addition they reported a beam diameter of about 3.5 µm. However, they have been limited because of the low beam current due to the small beam brightness (comp. section 4.1, 2.1.4) of the applied source technology [88] (comp. chapter 4), at that time for probe sizes below 10 µm [44]. At about the same time J.H. Orloff, and L.W. Swanson studied a field ionization source and performed micro etching [89].

Some currently used so called focused ion beam (FIB) instruments and their applications applying a different source technology called liquid metal ion source (comp. chapter 4) will be described in more detail in chapter 7.

Computer controlled FIB nano patterning is a similar serial fabrication process as electron beam lithography (EBL, comp. section 2.2.2 and 7.3.4) and therefore rather "slow" compared to e.g. optical projection lithography or nano imprint (comp. section 2.2.4). However, an FIB instrument similar to modern EBL writers would offer complementary patterning capabilities (comp. section 6.1.8 and 7.3.4). The focus of this work is the development of a versatile, computer controlled, vector scan, nano patterning ion beam instrument for research applications and rapid prototyping with sub 10 nm patterning capabilities.

2.3 Future perspectives

Some nano analysis and patterning techniques have been summarised in this chapter. As mentioned, there are fast technologies for mass production on one hand (optical projection lithography, next generation „optical lithography“ or potentially projection charged particle beams, “multi column approaches” and imprint) and an extremely slow but fascinating single atom manipulation one on the other hand.

For the semi conductor industry new methods [84] [90] are potential “next generation” lithography candidates: like EUV (extreme ultra violet, λ of 10 to 100 nm, or soft x-rays [91]), ML2 (maskless lithography with high throughput [71]), CP-ML2 (charged particle mask less lithography with high throughput) and O-ML2 (optical mask less lithography with high throughput). The latter one uses conventional optical lithography scanner architecture, but the photo mask is replaced by an addressable array of light modulating elements. In addition the described nano imprint technology could also be applied if the encountered challenges can be overcome (comp. section 2.2.4). Finally, x-ray lithography (λ from 0.01 nm to 10 nm [14], [92]) possesses also the necessary resolution capabilities. However, these are new technologies, e.g. conventional lenses absorb EUV [91] and also x-rays need different optical elements.

Applied fundamental research and small scale prototype fabrication have a need for further and complementary technologies. Direct write serial focused charged particle beam technology is an option, since many years direct write electron beam lithography is the main tool for lateral nano patterning in research and development. Direct write EBL writers will be discussed in more detail in section 7.3.4.

This technology is too slow for mass production, but offers many advantages for R&D applications e.g.: Sub 10 nm resolution capability (e.g. the creation of a 5 nm gap used as part of a tunnelling device [93], or 12 nm period [94]), flexibility and cost efficiency for low volumes (maskless CAD (computer aided design) designs can be quickly transferred onto all kinds of different sample systems). A maskless technology has no need for expensive and “inflexible” masks / templates, as CAD designs can be easily and quickly modified. For example an optical projection instrument would always require the fabrication of a new mask (set) for each device modification.

Further advantages are: versatility and sophistication (e.g. varying different kinds of charged particles and acceleration voltages cause different interaction volumes (comp. section 6.3.3) with various interaction processes. Some of them can be catalysed by inserting gases into the process chamber [95]).

These capabilities are valuable during the prototyping phase, when devices and circuitry are often altered [71].

Seliger and his team as well as Orloff and his team pioneered promising application areas of direct write ion beam tools. If source brightness limitations could be overcome and the source stability is adequate for patterning applications, the large variety of ion beam mater interactions can be exploited (comp. chapter 6 and section 6.1.8). Within the next chapter we will introduce the general instrument set-up and the terminology of a focused ion beam (FIB) instrument.

3 Focused ion beam instrument set-up and terminology

Before 1970 ion implanters have been employed for semiconductor fabrication [46] and around 1970 one of these instruments has been converted to explore further direct patterning applications (comp. section 2.2.5).

Within this chapter an exemplary instrument set-up including the technical terms (in **bold)** are presented.

A "**Point / focused ion beam instrument**" consists of a **charged particle optics** (**CPO**) **column** (comp. section 5.1), detectors, a sample positioning system, a vacuum system, driving electronics and software.

Inside the CPO column the ion beam generation, ion extraction, focussing, deflection and acceleration are taking place.

If one or more electrons have been separated from or added to atoms they are called ions (single or multiple ionised atoms). Currently, most ion beam sources so called focused ion beam (FIB) instruments are "**blunt needle**" Gallium (Ga) **liquid metal ion sources** (**LMIS**, comp. chapter 4).

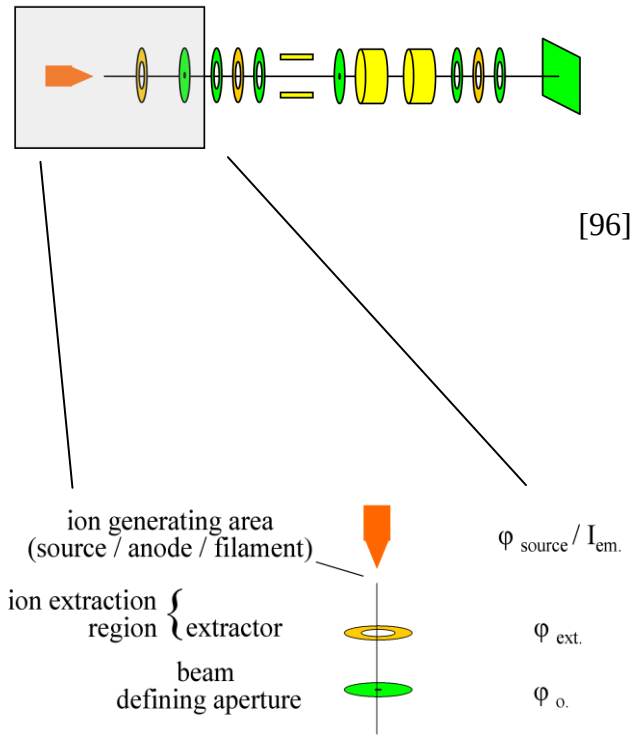

[96]

An applied **extractor voltage** ($\mathbf{U_{ext.}} = \varphi_{source} - \varphi_{ext.}$) extracts and ionises the atoms from the liquid metal ion source (LMIS, comp. section 4.3) via a mechanism called **field evaporation** (comp. section 4.4), [97].

The extracted ions define the **source emission current** ($\mathbf{I_{em}}$).

The beam defining aperture limits the emission current to the desired **probe current** value ($\mathbf{I_{probe}}$). Probe currents from a few hundreds fA to a few tens of nA are possible e.g. [98].

I_{probe} divided by the elementary charge (e = $1.6 \cdot 10^{-19}$As) equals the number of ions hitting the sample surface per second, which is usually measured inside a **Faraday cup** (comp. section 8.1).

Figure 3: Point ion source instrument CPO system part I (Ion generation and extraction region)

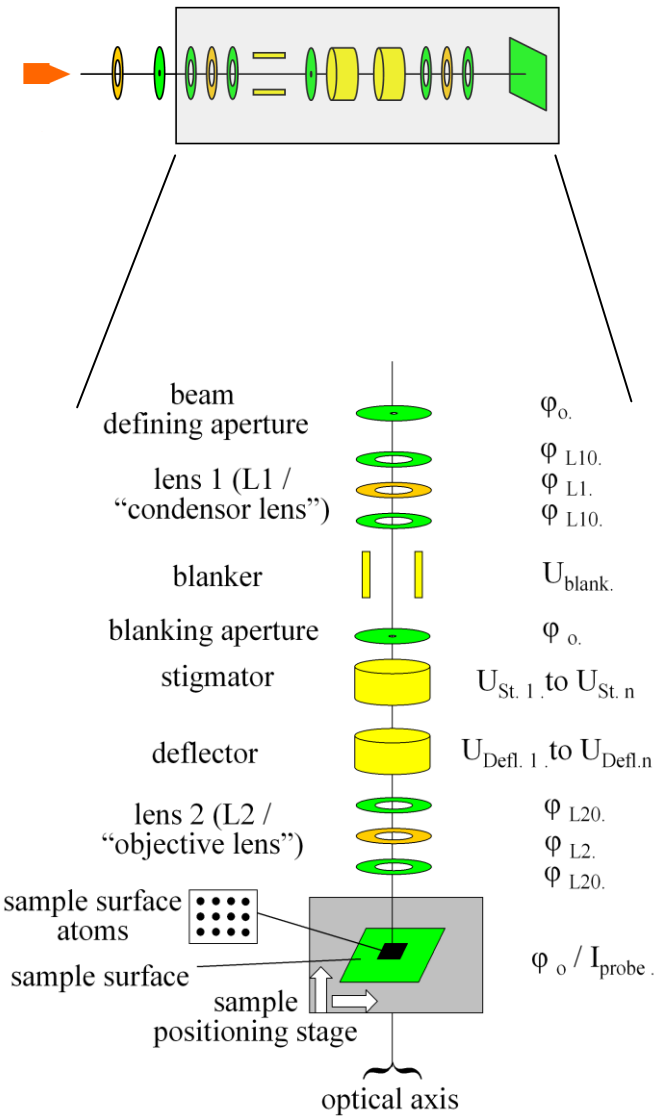

The ion beam is in most charged particle optic (CPO, comp. section **2.1.2** and **5.1**) columns focused by two **electrostatic lenses** (condenser and objective lens, comp. section 5.1.4). The **instrument resolution** (comp. section 5.1) can be as small as 2.5 [99] and 4 nm [100].

If a **blanking voltage** (**U_{blank}**) is applied to the **beam blanker** (plates) the beam is deflected away from the optical axis onto the **blanking aperture**, so the ion beam cannot hit the sample surface anymore.

Applying the **deflection voltages** (**$U_{Defl.,n}$**) to an **electrostatic deflection unit** (**“deflector”**) the beam can raster scan (for imaging applications) or create arbitrary patterns on the sample surface. These voltages are generated in a raster scan unit or inside a pattern generator (comp. section 7.3.2, 8.1), both are controlled by the software.

Some **aberrations** (beam imperfections, comp. section 5.1.2 and 5.1.3) can be corrected with an **octopole electrostatic stigmator** applying the stigmator voltages (**$U_{St.,n}$**).

Figure 4: Point ion source instrument CPO system part II (focussing and deflection)

The ions are accelerated onto the sample surface by the potential difference between the source and the sample ($V = \varphi_{source} - \varphi_{o,}$ e.g. 30 kV).

Here they interact with sample surface atoms (comp chapter 6).

If the instrument is used for imaging secondary electrons can be detected by a secondary electron (**SE) detector** e.g. an **electron multiplier** type [101] or a **multi channel plate** detector. The latter one can also detect secondary ions. (comp. section 7.1). The amplitude of the signal in combination with the position of the raster scanned beam on the sample surface forms an image of the **field of view** (**FOV**, the area raster scanned by the beam, without moving the stage, usually < 2.5 mm [98]). The ratio of the image edge displayed usually on a computer screen to the edge of the raster scanned area defines the magnification for the imaging process.

The sample positioning system is also controlled by the software. This allows processing larger areas on the sample surface extending the field of view (FOV).

Acceleration voltages can be usually varied (e.g. in the range from 5 kV up to 30 kV (e.g. [100]) in most commercially available systems) as well as probe currents (I_{probe} e.g. in the range of a few hundred fA to a few tenth of nA).

These instruments have to be operated under vacuum conditions: to minimise filament contamination (about $1 \cdot 10^{-8}$ mbar) and to minimise disturbing interactions with the chamber gas molecules (better $1 \cdot 10^{-4}$ mbar) as the main free path of incident ions increase with better vacuum [101].

Scanning electron microscopes (SEM) (comp. section 2.1.2) and electron beam writers (comp. section 7.3.4) possess a similar general instrument set up, with an electron source instead of an ion one.

Depending on the main application the instruments can be especially optimised e.g. in these aspects:

- ion beam column (including ion beam generation, deflection),
- driving electronics / software
- sample manipulation stage

Exemplary set-ups for currently available instruments and their applications will be described in section 7.3.1 and 7.3.2).

Being familiar with the terminology and an exemplary instrument set-up, in the following chapter ion source concepts will be introduced possessing the potential to overcome the source brightness limitation (comp. section 2.2.5).

4 Ion sources

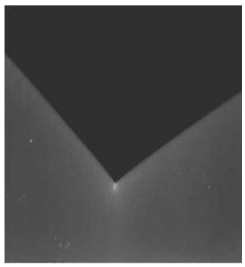

As described in chap. 2, ion beam source technologies which have been available before the 1970s have not been suitable for long term nano patterning applications (comp. section 2.1.4 and 2.2.5). Since the 1990s one ion source technology is dominating focused ion beam (FIB) applications [102]: Liquid metal ion sources (LMIS, comp. Figure 10).

Recent developments have enabled two complementary technologies: a “super-tip” noble gas field ion sources (GFIS) [103] and a noble gas magnetically enhanced, inductively coupled plasma ion source [102]. They have reached the commercialisation level for ion microscopy and milling (comp. section 6.2.1) applications, respectively.

We will describe parameters/characteristics indicating a well suited source for ion beam nano patterning, take a look at different ion source principles and will focus on one of them.

4.1 Source characteristics required for patterning

The quality of an ion source is defined by specific application dependant source performance parameters e.g. [46]. For nano fabrication applications the following ones are relevant: Energy spread (comp. section 5.1.3), virtual source size diameter, angular intensity, beam brightness, source life time, source stability (over many hours) and a chance for selecting different ion species.

Optimum charged particle optical focusing requires a small energy distribution of the emitted ions, reducing chromatic aberrations (comp. section 5.1.3). A distribution value below 1 eV would be ideal, like current scanning electron microscope/electron beam lithography writer thermally assisted field emission sources (e.g. 0.3 eV [104]).

In addition a small spot on the sample surface depends on the virtual source size [105] (comp. chapter 5). The diameter should be as small as possible, for achieving minimum feature sizes and patterning periodicity.

Angular intensity is described as the emitted current per unit solid angle [97]:

$AI = \frac{dI_{em}}{d\Omega}$, AI = angular intensity, I_{em} = emitted current, Ω = unit solid angle

Equation 2: angular intensity [97]

If this angular intensity is divided by the area of the source this is called beam brightness, the emitted current density per unit solid angle (Ω) of beam divergence [46]. Patterning and analysis applications require a large beam current in a small spot and therefore a large beam brightness which is the result of a high angular intensity and a small emission site (virtual source size). Both enable e.g. a sufficient image contrast at the maximum resolution (comp. section 5.1.7) or reasonable patterning speeds at high resolution.

$$B = \frac{dI}{d\Omega \cdot dS} = \frac{I}{\pi^2 \cdot r_C^2 \cdot \alpha_o{}^2}$$

Equation 3: beam brightness [46]

B = beam brightness

dS = area of the source emission site

r_c = radius of ion source;

α_o = angular semi aperture of the beam emerging from the source

In addition the concept of reduced brightness is often employed, as it is conserved throughout an optical system [106]:

$B_r = \frac{B}{V}$, B_r = reduced brightness, V = acceleration voltage

Equation 4: reduced brightness [106]

As described above (comp. section 2.2.5), at the end of the 1960s patterning applications have been limited mainly by the brightness of the available ion sources (10^5 to 10^6 A/(m^2·sr) [88]. As a result alternative ion source technologies should possess significantly higher brightness values.

In addition the source lifetime is an important parameter for the usability of the source in a patterning instrument. It has to exceed at least the time to carry out the patterning job.

Unattended batch nano fabrication jobs over hours require additional stable source characteristics, e.g. the acceleration voltage stability influences the focus, as the electrostatic lenses focus the ions relative to the applied acceleration voltage (comp. section 5.1.5) and the probe current stability (comp. chapter 3 and section 6.1.9) influences the patterning process reproducibility.

The usability of more than one type of ion would be required to increase the potential application space of a direct write ion beam instrument.

4.2 Different types of ion sources [106]

Today most FIB instruments are equipped with LMIS. In addition further ion generation techniques exist: e.g.: 3 general types of noble gas ion sources: gas field ion sources, plasma gas ion sources and other types of gas ion sources like: laser ion sources, electron impact gas ion source, electron beam ion sources and traps. The general operation principle and some figures of merit will be given for two promising recent developments.

4.2.1 Gas field ion sources (GFIS)

Gas field ion sources are based on the field ionisation process, it takes place at high electric fields (≥10 V/nm). Around 1940 Müller employed this ion generation technique in his field ion microscope [43]. There exist 3 general types of GFIS: needle, capillary and integrated and needle in capillary type [106]. The needle type GFIS “super-tip” has reached the commercialisation level in a FIB microscope called “Orion” [107]. It is capable to resolve sub

nm features in imaging [108] and to pattern 6 nm minimum feature sizes [109] (comp. sections 7.3.3 and 7.3.4).

Researchers from Alis Corp. (now Carl Zeiss AG) [103] have managed to overcome the technical challenges, however it is not possible to use it for applications like long term nano patterning [110].

This is a technology breakthrough with a large future potential: small virtual source size, high beam brightness and a large number of possible ions. For exemplary application results compare section 7.3.3.

A feature of nm scale formed on a regular tip is called “super-tip”. Ward and his team (at Alis Corp. comp. above) have realised it as a three sided pyramid. This tip is operated in a noble gas molecules environment applying electric extraction fields [103]. They have assumed a virtual source diameter of 0.3 nm, measured an angular intensity of 2.5 µA/sr and calculated from this a brightness of $4 \cdot 10^9$ A/(sr·m^2). In addition they have assumed an energy spread (comp. section 5.1.3) 0.25 to 0.5 eV.

More details about the operation principle can be found in [106] [103] [97].

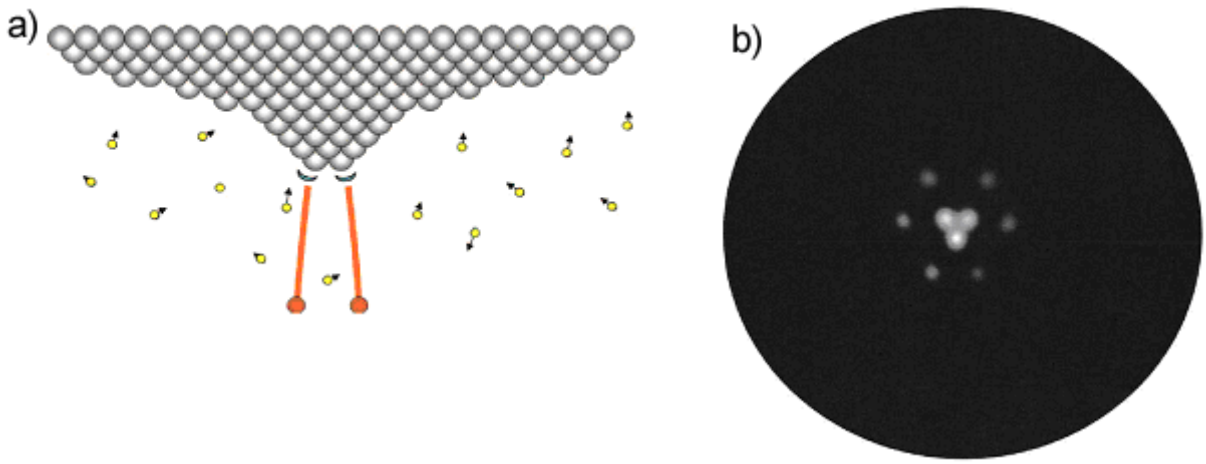

Figure 5: a) Sketch of the Orion “super-tip” GFIS and b) field ion microscope image (comp. section 2.1.4) of the corresponding emission pattern [103] (there Fig. 5 and 6).

The high (reduced) beam brightness and the small energy spread are well suited for high resolution imaging applications.

4.2.2 Plasma gas ion sources

In plasma gas ion sources ions are extracted through a small aperture from a plasma. The virtual source size can be altered by selecting different beam defining apertures. The polarity

of the emitted ions can be selected by the polarity of the extraction electrodes [106]. It is a reliable and robust emission technique [106].

Recent developments have been commercialised by Oregon Physics ("Hyperion") [111], [112]. Oregon physics has managed to create a plasma ion source with 5-6 eV energy width, 10 nm beam diameter and 10^4 A/(sr·m^2) with mostly single ionised ions in the beam [111]. The main application is high current milling / etching (comp. section 6.2.1), here the LMIS spot on the sample is not optimum [111].

4.2.3 Nano patterning relevant characteristics of ion sources overview

The parameter and more detailed description of LMIS will be given in section 4.3 to 4.5 for comparison of the different source technologies the parameter are summarised in Table 1.

Ion sources	Reduced brightness [A/(sr·m^2·V)]	Energy spread (comp. section 5.1.3) [eV]	Employable resolution for patterning [nm]	optimum probe current range	Probe current stability for long term nano patterning	References
Plasma	$1 \cdot 10^4$	5-6	100 (10 "assumed"')	>1 nA	yes	[111], [111], [111], [111] and [106]
GFIS	$1 \cdot 10^9$	0.25-0.5	6	≤1 pA	no	[103], [103], [109], [110], [110]
LMIS	$2 \cdot 10^6$	4.5	7	0.3 - 100 pA	yes	[113], [114] [115] and comp. section 7.2, [116] + [111], [7] and [117]

Table 1: Nano patterning relevant source characteristics ([106])

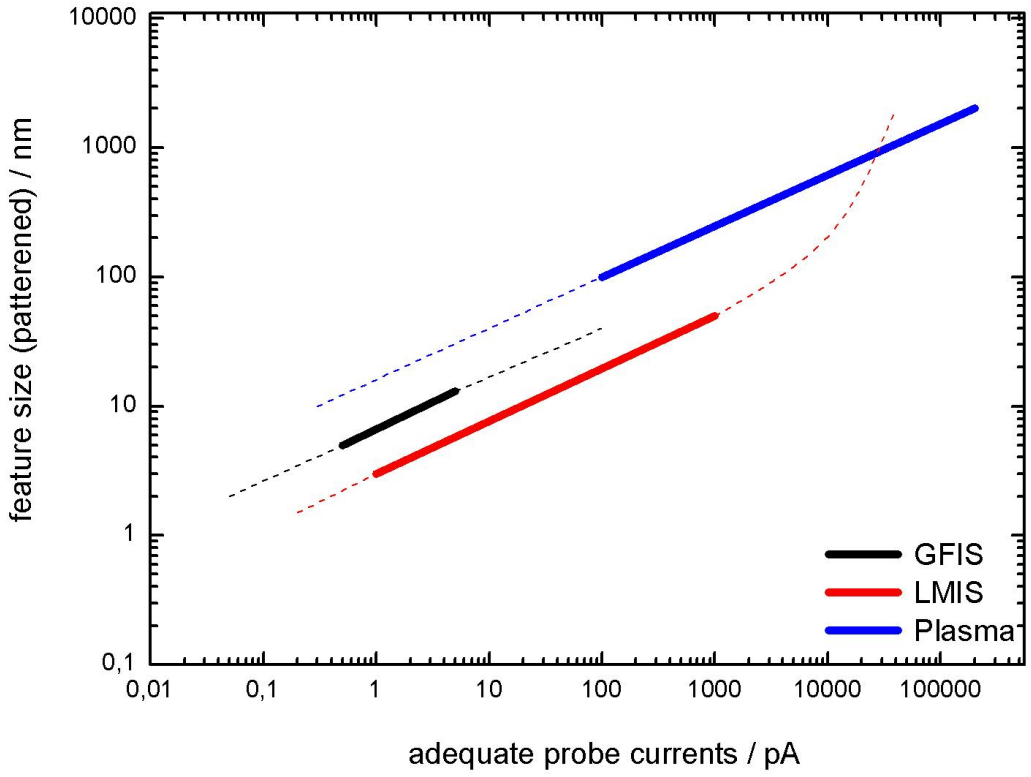

Figure 6: approximated patterning feature sizes versus adequate probe currents for different ion sources (LMIS [116] [111], Plasma [111], GFIS estimated from [110])

Table 1 and Figure 6 visualises the source characteristics for three ion source technologies. It becomes evident, that the plasma source is well suited for material removal (milling/etching, comp. section 6.2.1), the GFIS "super-tip" for high resolution imaging with a low probe current and LMIS for long term nano patterning (stable and high resolution) over a large probe current range. LMIS spot size degradation above 1nA. This derives from beam energy distribution which is called "beam tails" which requires defocusing (comp. section 4.4) [111]. Further ion beam generation mechanisms are described e.g. in [46] [97] [118] [106] [119] [120] [121] [122]. As LMIS are currently the optimum choice for nano patterning, they will be discussed in more detail in the following sections.

4.3 Liquid metal ion sources (LMIS): Historical background

The fundamental effect is already known at least since the year 1600 [123], it has been further studied in the 19th century by Rayleigh [124]. W. Gilbert has reported the discovery that

liquids around a tip are attracted by amber (electric fields) leading to a conical shaped droplet ("... in the case of a spherical drop of water standing on a dry surface, for a piece of amber held at suitable distance pulls toward itself the nearest particles and draw them into a cone...") [123].

In 1932 Gray first employed the term electrohydrodynamic-induced liquid spraying (EHDS) [97] for this effect. However, it took until the 1960s that the fundamental effect could be technologically exploited. V.E. Krohn jr., working at a spacecraft laboratory (Thomson Ramo-Wooldridge Inc.), has published his work about liquid metal droplet experiments. He has been the first who technologically exploited this long known effect as possible heavy particle propulsion system for "space thrusters" [125]. Krohn has been mainly interested in the droplet emission, so he "complaint" about the large number of "disturbing" emitted ions ("Unfortunately, additional measurements indicate that large numbers of metal ions are produced along with the droplets ...") [125]. He employed a so called liquid metal ion source (LMIS) consisting of a capillary tube [97] in which liquid metal flows down to the apex and is extracted by strong electric fields. They have already been capable in delivering satisfactorily current/intensity levels. However, it has been difficult to operate them at emission currents below 10 µA [44].

Further pioneers have been Mahoney [126] and Ringo and his team at Argonne National Laboratory [127]. They have used a "hollow needle" LMIS and already determined experimentally that the energy spread (ΔE, comp. section 5.1.3) is minimal at low emission currents and increases with increasing emission current (comp. section 4.5).

1971 Clampitt et al. carried out experiments with very sharp tips [44]. However, emission currents here have been limited to 10^{-6} A [44]. Later on, by "accident" [97] he and his group discovered the blunt needle LMIS, which increased the upper stable emission current limit by at least two orders of magnitude with respect to the sharp tips (comp. above) to about 200 µA [44]. The "blunt needle LMIS" was born [128], combining a significantly higher usable intensity than the sharp needle types and keeping the possibility for lower emission currents than the capillaries, allowing to operate the source with a smaller energy spread (ΔE, comp. above).

Seliger and his team at Hughes research labs have carried out among the first tests of focused ion beam nano patterning [86] [87] (employing non LMIS). The applications have been limited by the brightness [129] (comp. section 2.2.5). At the end of the 1970s Seliger and his team pioneered also the examination of nano structuring applications with this new type of (liquid metal ion) source technology. They have integrated a LMIS into an ion beam system

equipped with an electro static focussing lens (comp. section 5.1.5 and 5.1.6) [88] [129] (comp. section 2.2.5). They reached 100 nm probe size at an acceleration voltage of 57 kV.
Another pioneering LMIS groups in the early 1980s has been: Sudraut and Benassayag first University Paris Sud, later L2M CNRS (today LPN CNRS, F) [44]. Prewett and Mair have called them "the Orsay group" [44]). The successors (Gierak et al.) have led the joined instrument development project (comp. chapter 8 and section 12.3). Further pioneering groups and early manufacturer are described in [44].
More details about the historical background of LMIS can be found in [97] [44].

4.4 Model / theory for these kind of LMIS

The main atom extraction / ionisation process of LMIS's is called "field evaporation" [97] [44]. One of the image forming mechanisms in E. Müller's field ion microscope (comp. section 2.1.4) is also caused by this effect [43] [19].
The actual emission is based on a surface process, the ions are generated at the LMIS apex, due to high electric fields of the order of 10 V/nm (for Ga, depending on the metal). The bonds holding an atom to the surface are simultaneously breaking as ionisation takes place [97]. Figure **7** shows a schematic emitting needle LMIS. In 1964 Taylor published a mathematical model for the disintegration of drops in strong electric fields [130]. He modelled the static shape with a half angle of 49.3° for the meniscus (Figure **8**). He was the first to find a mathematical model for the electrohydrostatic equilibrium of an electrically conducting liquid [97]. At the apex a cone similar to Taylor's theory is formed and a jet like elongation builds up at the very end.
The field evaporation model is only consistent in combination with liquid flow and space charge (comp. section 5.1.3) effects assuming the existence of a jet like elongation at the apex region of the emitter [44]. This has been observed e.g. by P. Sudraud and G. Benassayag (comp. section 4.3, comp. Figure **9**) [132] using a MeV TEM (transmission electron microscope). They estimated the jet dimensions from the TEM images to be 3 nm diameter and 10 nm length at 9 µA emission current [132]. However, the actual virtual source size is significantly larger than that: about 40-45 nm [133], due to a possible lateral movement of the jet (jet wobble) and space charge effects (local broadening or trajectory displacement, comp. 5.1.3) [97] at the apex region, here millions of amperes per square centimeters can be reached [134].

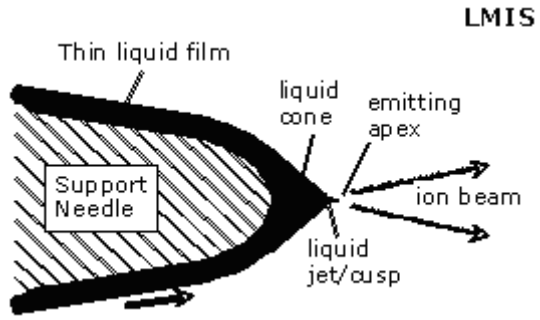

Figure 7: Emission area of an LMIS, [97]

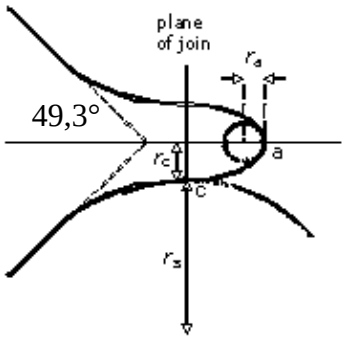

Figure 8: Magnified liquid apex ("meniscus" with little "jet", Gilbert-Gray cone-jet) [97] (angle added)

The pressure at the end of the jet can be described by:

$$p_t = \frac{2 \cdot \gamma}{r_t} - \frac{1}{2} \cdot \varepsilon_0 \cdot E_t^2$$

Equation 5: pressure at the end of the jet corrected version of Kingham and Swanson for streamline and non-turbulent liquid flow [131]

γ = surface tension of the liquid

p_t = hydrostatic surface forces at the tip

r_t = tip radius

ε_0 = vacuum permittivity

E_t = electrical field at the tip

In an equilibrium between the electric field and the hydrostatic surface forces $p_t = 0$:

$$\frac{2 \cdot \gamma}{r_t} = \frac{1}{2} \cdot \varepsilon_0 \cdot E_t^2$$

In addition, the emission is not a stable, steady and constant process, there exist high frequency oscillations of the Taylor cone [135] [136] [137].

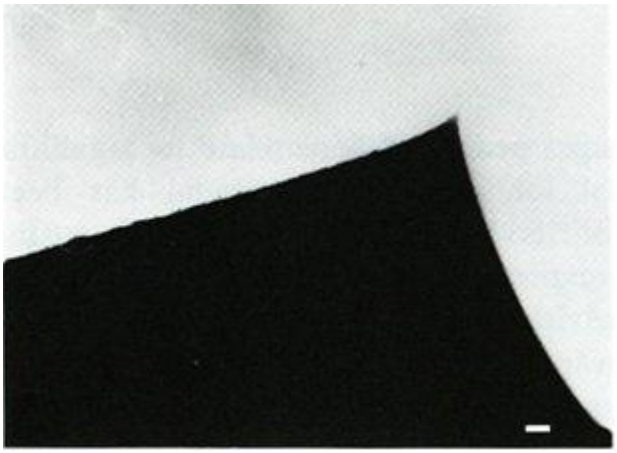

Figure 9: Early 2.5 MeV TEM image of the liquid cone with emitting jet of an operating LMIS at 30 µA emission current and an extraction voltage of 5.5 kV (100 nm scale bar has been copied into this image from image f within the same publication), Fig. 2e in [132]

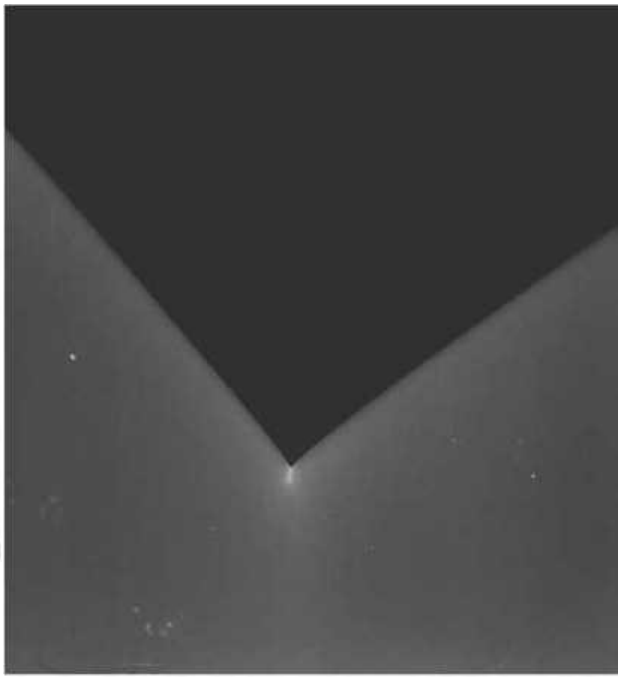

Figure 10: MeV TEM image of an LMIS in operation (2004), without scale bar Fig. 6b, in [117]

The natural energy width caused by field evaporation is 1 eV or less at low emission currents, but the measured value of the emitted ions is significantly larger (about 4.5 eV at 1 to 2 µA emission current [114]). This results in chromatic aberrations (comp. chapter 5.1.3). The reason seems to be again space charge broadening [97] (comp. section 5.1.3).

Further on although a relatively small final ion probe size (<10 nm) can be proved by either image resolution or patterning, there exist lower energy ions causing interactions even more than a µm away from the point of incident e.g. [138] [44] [139] [140] (comp. section 5.1.8). This effect is the already mentioned “beam tails” or “a tail of low energy ions”. Ward et al. suggest that the distribution is better fit by a Holtsmark velocity distribution (describes $1/r^2$ force dependences (e.g. Coulomb) interacting with a constant charge density) [141] instead of the often applied Maxwellian distribution (comp. section 5.1.8). This effect can be explained if either many of these ions deriving from free space field ionized neutrals or by charge exchange between an energetic primary ion and a slow neutral in the vacuum space [97]. The above described beam tails could result in patterning artefacts away from the point of impact and as a result can e.g. limit the minimum patterning periodicity for some applications. The

effect has been studied for LMIS, as it becomes quite obvious for large probe currents (comp. section 4.2.3), we expect it to be present also in other high current density charged particle sources/columns, but we are not aware of experimental results.

4.5 More detailed and further characteristics of LMIS

In section 4.1 the fundamentals of source characteristics, in section 4.4 the model of LMIS emission and in section 4.2.3 some relevant source characteristics for nano patterning have been summarised, more details will be given in this section.

LMIS in current instruments reach an angular intensity of about 20 µA/sr [142], combined with a virtual source size of about 40 to 45 nm [133] this results in a beam brightness of about 10^{10} A/($m^{-2}sr^{-1}$) e.g. [95] which is sufficient for most applications. In addition for LMIS in the emission current range of interest (1-5 µA) the angular intensity dI/dΩ (comp. section 4.1) is constant over a considerable range of axial angle [97]. This enables a large variety of selectable beam defining apertures which results in different beam currents (comp. section 4.2.3).

Although the described energy spread (comp. section 5.1.3) of a Ga LMIS is quite large: about 5 eV, it is almost constant for emission currents between 1 and 2 µA. It increases with increasing emission current [114] (comp. section 4.3). This limits the final possible resolution in some operation modes (comp. section 5.1.3).

The source lifetime for Ga is about 1500 h [98], which is sufficient for many nano fabrication applications.

A low vapour pressure metal (like Ga) is preferred, avoiding vapour arcs between the anode and extractor [128].

Many metals or alloys can be employed as source material / incident ions (comp. section 6.1.8, e.g. [143]). Metals which are not liquid at room temperature under ultra high vacuum (UHV) conditions need constant filament heating which increases the energy spread [144]. Ga possesses a low melting temperature (303.05 K-273.15 K = 29.9° C) and -depending on purity and enviromental conditions- a large undercooling behaviour down to -8.26° C (for example from 273.15 K down to 264.89 K) [145]. As a result it is liquid at room temperature inside the instrument and can emit [146] if heated before. During operation no steady heating is required.

Finally, Ga LMIS sources produce mainly single charged ions (> 99%) [44] and [140]. This means each ion carries the elementary charge of $1.6 \cdot 10^{-19}$ As.

Although not all of the target source characteristics (comp. section 4.1) are optimum and additional challenges exist, 7 nm patterning has already been proven [115].
Nevertheless, additional issues might limit unattended long term batch nano patterning. E.g. the emission characteristics of currently applied LMIS change during operation. This requires a “refresh”/cleaning cycle: heating every 40-100 hours [147]. This procedure removes tip contamination and supplies fresh liquid Ga to the apex.
More details can be found: [44] [148] [97].

4.6 Summary

The two complementary ion source techniques described above: GFIS (comp. section 4.2) or plasma (comp. section 4.2.2) have reached remarkable performance levels.
However, among the available ion sources (comp. section 4.2) for nano patterning liquid metal ion sources are the first choice, because of the large variety of usable ions (comp. section 4.5 and 6.1.8) and the relevant source characteristics (like brightness, resolution, comp. section 4.2.3 and 4.5).
Although not all described source characteristics are optimum for ultimate patterning applications (comp. section 4.5), the successor of one of the pioneering LMIS groups called the “Orsay group” (comp. section 4.3) have improved Ga LMIS technology for high resolution unattended long term structuring applications (comp. section 4.4). From 2001-2004 the EC funded NanoFIB research project team [12] has integrated this into a proof of concept tool (comp-. chapter 8).
In addition to potential further improvements in “super-tip” GFIS or plasma sources, promising further techniques like e.g. “atomic-size metal ion sources...” [149] (“super-tip” concept also for LMIS [106]) could enable complementary capabilities in the future.
With the LMIS as currently the best source technology for nano patterning application the possible resolution of such an instruments and how it is influenced, will be described in the following chapter.

5 Resolution

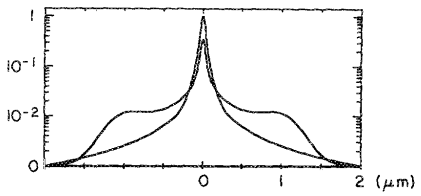

In focused ion beam (FIB, and other scanning particle beam) instruments the minimum achievable probe size at the sample surface determines the "theoretical" analysis (imaging) and patterning resolution [150]. This is an important parameter, but other factors influence resolution as well, e.g. the achievable signal to noise ratio in imaging and the minimum achievable distances (periods) for pattering applications, especially on "non ideal" sample systems [150] (comp. Figure 16).

The fundamental resolution concept for a point source ion beam nano patterning instrument is the same as the one described in section 2.1.1 and 2.1.2. The smaller the resolvable features or periods are, the higher the resolution.

For real applications it is better to differentiate between two different -although not independent- terms for resolution: "(theoretical) instrument resolution" (comp. section 5.1) and "application resolution" (comp section 5.2) derived from the term "analytical resolution" used in [44].

In addition care has to be taken to avoid significant contribution from the environment (vibration, electromagnetic fields, ...) [150].

5.1 Instrument resolution / charged particle optics (CPO)

5.1.1 Introduction

Some historical roots of charged particle optics (CPO) are described in section 2.1.2 together with references summarising the historical evolution.

Instrument resolution is the technological and fundamental limit of the instrument hardware. The concept describes the general capability of an instrument to create a small spot of an ion beam for example on a sample surface. It can be calculated for FIB instruments by CPO modelling based on the virtual source size (comp. section 4.5) and the focusing capability of the column. It depends on beam parameters (source brightness, acceleration energy and energy spread ΔE (comp. section 4.1, 5.1.2 and 5.1.3)), lens system parameters (chromatic and spherical aberration coefficient C_c and C_s, respectively (comp. section 5.1.2 and 5.1.3)), application settings such as probe current (I_p) and aperture half angle (α_0), defocus [151] [140] and space charge effects (comp. section 5.1.3) [150].

The instrument resolution can be measured using e.g. "ideal" material systems. In [95] [134] some exemplary methods are described.

The scope of charged particle optics analysis for a scanning point source ion beam instrument is the transformation of the shape and the size of the current density distribution of a beam of ions at the object plane (the source) into a different shape and size distribution at the image plane (e.g. on the sample surface) [134]. In the image plane the beam is usually raster scanned [134] over the sample surface. However, the analytical formulas for real CPO set-ups reach a mathematical complexity level that make it difficult or even impossible to employ them as simple analytical models, so these are only calculated in complex computer algorithms (inspired by [152] comp. section 6.1). Nevertheless, simplified analytical models are presented to assist users in finding parameters to ameliorate the system.

5.1.2 Geometrical CPO, imaging and intrinsic aberrations

Geometrical CPO has an analogy in light optics: the index of refraction. In addition geometric light optics models like the thin lens formula, illumination and imaging rays can be used to visualise CPO systems. However, the equations of "motion" are different.

The „index of refraction" of an electrostatic lens can be defined in the following way: $n_1 = \sqrt{\varphi_1}$ and $n_2 = \sqrt{\varphi_2}$ [153] (φ_1 and φ_2 denote the axial electrical potential at the object and image planes, respectively). This is physically not particularly meaningful [153], but provides up to a certain limit a vivid analogy, for modelling some of the fundamentals of CPO. In

contrast to light optical lenses with the change of index of refraction is abrupt at the surface of refraction, in charged particle optics the index of refraction changes smoothly in the lens [26] [35].

As in geometrical light optics the thin lens formula (with $f = f_u = f_v$) and the magnification definition can be employed. In addition the magnification definition for a point source ion beam instrument for small angles is given.

$\frac{1}{f}=\frac{1}{b}+\frac{1}{g}$	$M=\frac{b}{g}$	$M=\frac{\alpha_O \cdot V}{\alpha_P \cdot U_{ext.}}$
Equation 6: Thin lens formula	Equation 7: Definition of magnification	Equation 8: Magnification in point source ion beam instruments for small angles after [150]

f = focal length of the lens system

g = object length

b = image length

M = magnification of the optical system

α_o = beam defining aperture half angle or source side half angle (comp. Figure 11)

α_p = half angle at the probe or lens system half angle image side (comp. Figure 11)

$U_{ext.}$ = extractor voltage (comp. chapter 3)

V = acceleration voltage (comp. chapter 3)

The ion emitting source (the object) is demagnified onto the sample surface (image plane). How this can be done and optimised is described/analysed/optimised in the field of “charged particle optics”.

In a real field emission system the object (which is usually virtual) is the source, which is of the order of a few tens of nanometers in size [154] (virtual source size, $d_{S,eff}$, comp. section 4.4). A charged particle optical system is characterised by the system magnification M (usually < 1 “demagnification”) combining all lenses, in a point source ion beam column. They usually consist of a classical “two” lens system: gun/extractor/entrance electrode [46], condenser and objective lens.

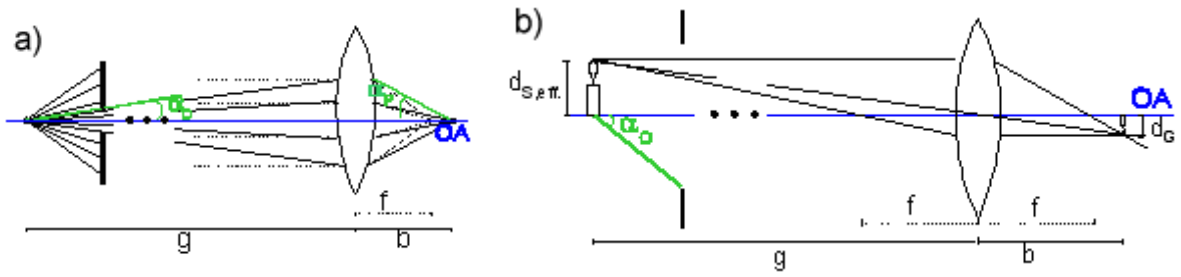

Figure 11: a) illumination and b) imaging rays for thin lenses (with $f = f_u = f_v$)

$d_{S,eff}$ = effective source size

d_G = Gaußian image of the source

OA = optical axis

The particle motion in electromagnetic fields can be described by this ordinary differential equation (Lorentz' equation):

$$\frac{d}{dt}\left(m \cdot \vec{v}\right) = q \cdot \left(\vec{E} + \vec{v} \times \vec{B}\right).$$

Equation 9: Lorentz' equation e.g. [155]

m = mass of the charged particle

$\vec{v}$ = velocity of the charged particle

q = charge of the particle

$\vec{E}$ = applied electric field

$\vec{B}$ = applied magnetic field

Neglecting space charge effects (comp. section 5.1.3) and taking only ions close to the optical axis with low slope [155] into account ("paraxial rays") the paths can be approximated by linear imaging equations.

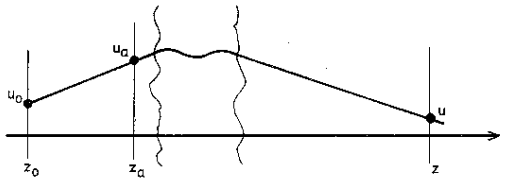

Figure 12: particle path linear approximation [155]

If the z axis is the optical axis, one way modelling the paths of ions is to employ complex notation u(z) = x(z) + i y(z) (u(z) is a linear complex function of z, u_o and u_a, which is defined by the initial values x_o / y_o and x_a / y_a of the points u_o and u_a, respectively), comp. Figure 12. The position at z_a is the aperture plane, so u_a describes the intersection point of a trajectory with the aperture plane, whereas u_o denotes the intersection point of a trajectory with the object plane.

$$u(z) = g(z, x_0, x_a, y_0, y_a) = f(z, u_0, u_a, u_0^*, u_a^*)$$

with $u^*(z) = x - iy$ as the conjugate complex of u(z), f can be series expanded in powers of u and u^*:

$$u(z) = \sum_{\rho,\beta,\gamma,\delta} c_{\rho,\beta,\gamma,\delta}(z) \cdot u_0^{\rho} \cdot u_0^{*\beta} \cdot u_a^{\gamma} \cdot u_a^{*\delta}$$

Equation 10 series expansion of the imaging equation in complex notation [155]

u(z) = intersection point of a trajectory with the xy plane at z

ρ, β, γ, δ = indices (= 1, 2, 3,…)

$c_{\rho,\beta,\gamma,\delta}(z)$ = coefficient (with the indices comp. above)

u_o = intersection point of a trajectory with the object plane (u_0^* its conjugate complex)

u_a = intersection point of a trajectory with the aperture plane (u_a^* its conjugate complex)

In the simplest case of rotationally symmetric systems the coefficients must satisfy the following equation:

$$\rho - \beta + \gamma - \delta = 1$$

Equation 11: allowed combination of coefficients for systems with rotational symmetry [155]

and for symmetry after 180° rotation (“two fold symmetry”):

$\rho+\beta+\gamma+\delta=1,3,5,...$ only odd values are allowed.

Equation 12: allowed combination of coefficients for systems with two fold symmetry [155]

The first order of Equation 10 describes the linear imaging process. The rotationally symmetric case is described in Equation 13:

$$u(z_i)=c_{1000}(z)\cdot u_o+c_{0010}(z)\cdot u_a$$

Equation 13: first order and rotation symmetric case of Equation 10 [155]

$c_{1000}(z)$ and $c_{0010}(z)$ = coefficients $c_{\rho,\beta,\gamma,\delta}(z)$ comp. Equation 10 with $\alpha = 1$ and $\beta = 1$, respectively

Then $z = z_i$ can be selected in a way that $c_{0010}(z)$ equals 0, which results in:

$u(z_i)=c_{1000}(z_i)\cdot u_o$ [155] and could be written as

$d_G = M \cdot d_{S_{eff}}$ [156].

Equation 14: Gaußian image

M is the overall magnification of the column (comp. above) and $d_{S,eff}$ is the effective virtual source size (about 45 nm for a Ga LMIS compare 4.4, comp. Figure 11).

The best achievable resolution (spot diameter (d_G, FWHM) is the „Gaußian image“ (“stigmatic image” [14]). A perfect lens system could image a small region of space on the object side of the lenses into a small region of space on the image side of the lens. A point in object space would be imaged onto a point in image space with the magnification M. Infinitesimally small points in image space would be only limited by the current producing capability of the source and the minimum current required for reproducible patterning [134]. A perfect lens will reverse the spherical expanding wave and so form a perfect point image, (comp. Figure 11) [134].

However, imaging suffers from aberrations. In CPO it is not so easy to combine several lenses to cancel these aberrations as in light optics. A visible light objective can resolve feature sizes of about the wavelength of the applied light (comp. section 2.1.1), but the best electron microscopes are only capable in resolving features about a 100 times larger than their wavelength, and they usually employ magnetic lenses, which are better than electrostatic ones

(comp. section 5.1.6, [134]). In a rotationally symmetric CPO system chromatic and spherical aberration cannot vanish which is known as the Scherzer theorem [157] [35].

If the order of Equation 10 is larger than one it represents deviations from the Gaußian optics and the "order of aberration". Second order aberrations do not exist for two fold symmetry (comp. Equation 12). Table 2 gives an overview of the allowed third order aberrations and their names for rotationally symmetric systems [155]:

ρ	β	γ	δ	Aberration type
1	1	1	0	Third order astigmatism and curvature of field
2	0	0	1	
1	0	1	1	Third order coma
0	1	2	0	
0	0	2	1	Third order spherical aberration
2	1	0	0	Distortion

Table 2: Third order aberration coefficients for perfect rotationally symmetric lenses [155]

5.1.3 Aberrations limiting the minimal probe size close to the optical axis

For a scanning point LMIS optical system, some of the third order aberrations listed above (comp. Table 2) limit the minimum spot size on the sample surface in the centre of the deflection field (optical axis): astigmatism, coma and in particular spherical aberrations [134]. In addition chromatic aberrations [134] and space charge effects (comp. section 5.1.3) [150] contribute. The last three (spherical, chromatic and space charge) usually limit current point source ion beam lens systems, depending on the operating conditions (column operation modes, comp. below) [44].

Spherical aberrations are a result of the variable focusing strength of a lens, depending on the distance of the trajectory at the lens plane from the optical axis r_a. The resulting factor from Table 2 in Equation 10 is c_{0021}. It is proportional to the spherical aberration coefficient C_S which can be found in lens tables (it is often written as $C_S(\infty)$ or $C_S(f)$) [155]. Rotationally symmetric electrostatic lenses possess a positive spherical aberration, which means that the spherical aberration coefficient is also positive. As a result, rays further away from the optical axis are more strongly focused and hence intersect the optical axis in front of the Gaußian image plane. The reason for the positive spherical aberration is that the electrical field increases to the border of the lens aperture resulting in stronger focussing as in the centre. The

spherical aberration coefficient C_S can be e.g. employed to calculate the optimum focus plane (comp. Figure 13) in front of the Gaußian plane with the disk of confusion d_S:

$$d_S = C_S \cdot \alpha_0^3$$

Equation 15: disk of confusion due to spherical aberration [158]

d_S = disk of confusion due to spherical aberration
C_S = spherical aberration coefficient
α_o = beam defining aperture half angle or source side half angle

A further formula for estimating the spherical aberration coefficient will be described in section 5.1.7. The contribution of the spherical aberration becomes more and more significant for larger probe currents in focused ion beam instruments [44] (large apertures = large α_o, α_o has to be increased if the source brightness remains constant in order to increase the probe current (I_P)).

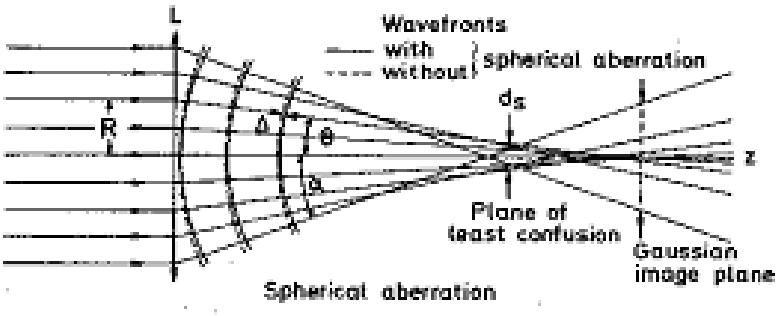

Figure 13: Effect of positive spherical aberration [159]

Chromatic aberration results from particles carrying (slightly) different energies which get focused more or less strongly by the lenses.
The chromatic aberration is proportional to α_o (the opening angle of the beam defining aperture, comp. Figure 11) and the ratio of the „energy spread“ to the acceleration energy ($\Delta E/E$) [134]. As described in section 4.4 the energy spread for a LMIS is quite large (about 4.5eV, comp. section 4.4) compared to a electron field emission sources (<1 eV comp. section 4.1) limiting the final achievable resolution of a point source ion beam system with a LMIS at “medium” beam currents (medium aperture sizes, medium α_o) [44].

$$d_C = C_C \cdot \frac{\Delta E}{E} \cdot \alpha_0$$

Equation 16: disk of confusion due to chromatic aberration [158]

d_c = disk of confusion due to chromatic aberration

C_C = chromatic aberration coefficient

ΔE = energy spread of the ions.

E = acceleration energy

α_o = beam defining aperture half angle or source side half angle / angular semi aperture of the

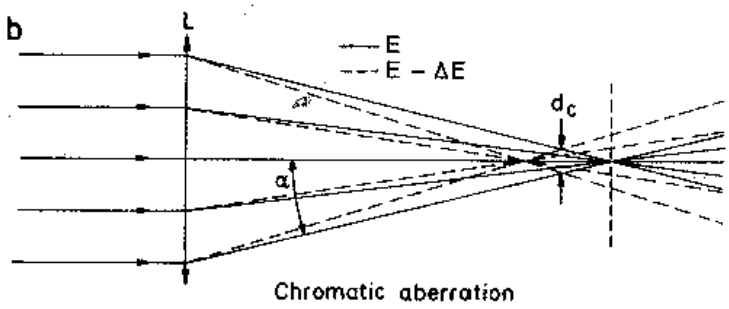

Figure 14: Chromatic aberration [159]

A simple way of estimating the impact of optical components (in geometrical CPO) on the minimum probe size of the beam on the sample surface at the optical axis is to calculate the square root of the sums of the contributing "discs of confusion". This model will not be presented here (but can be found in many CPO books, for example [159] [44] [134] [156]), because a more accurate and equally simple one will be presented in section 5.1.7.

In addition space charge and Coulomb effects are the results of interactions of the charged particles among themselves [134] [113]. They have to be taken into account in addition to the aberrations described above (comp. section 5.1.2 and 5.1.3). These effects are more serious for ions than for electrons, as the particle density is higher and the time of flight through the system is longer because the ion velocity is smaller than that of electrons (accelerated by the same acceleration energy, the ratio is about $3.5 \cdot 10^2$ for Ga^+ to electrons, comp. section 12.5.1) [113]. These effects can be divided into three different categories: space charge, trajectory displacement (first investigated by Loeffler) and energy broadening (Boersch) effects, the latter two are of statistical nature [113] [160].

Space charge effects cause deflection of the "total, averaged charge of all the particles in the beam" [113]. The deflections are proportional to the distance from the axis for uniform charge distribution in round beams (rotation symmetric), mainly resulting in a defocus which can be

compensated by the lenses. If the charge distribution is non-uniform, aberrations can be caused [113]. The effect increases linearly with the beam current. Wide charged particle beams of high current deriving from low brightness sources are dominated by this effect [113].

Energy broadening describes the axial velocity change resulting from particle interactions. The energy broadening (increase in ΔE) influences the instrument resolution via an increase in chromatic aberrations (lens and deflector) [113]. They are usually most severe close to the source which is the place with the lowest particle velocities (for a 30 keV system for example) and their densities are highest [113].

Trajectory displacement describes the lateral shift in the positions and velocity of the particles perpendicular to the optical axis, this causes direct degradation of the instrument resolution [113]. In addition the beam brightness is reduced.

The stochastic nature of the energy broadening and trajectory displacement effect derives "from the discrete nature of the charges" [161]). As a result they cannot be corrected [113]. "These effects become dominant in narrow beams of low and moderate densities" [113].

Summarising the rules of thumb of the main limiting aberrations for three exemplary column operation modes are [44]:

1. at small beam currents (small beam defining aperture half angle / small beam defining apertures) the effective source size (Gaußian image of the source)
2. at medium probe currents (medium beam defining apertures) the chromatic aberration limited and
3. for large beam currents (large beam defining apertures) the spherical aberrations.

In addition to the intrinsic aberrations of perfect rotationally symmetric lenses (comp. section 5.1.2) parasitic aberrations due to imperfect alignment and/or mechanical manufacturing exist. The parasitic ones must not be confused with the intrinsic ones, especially as in both groups exist some with the same name in the literature. This is the case because the dependence on position and angle of the object (or target in a probe forming system) are similar.

E.g. two fold symmetric first order parasitic astigmatism can be observed in SEM images (the beam on the sample surface forms an ellipsoid instead of a circle). This can be corrected by an octopole stigmator unit [134]. Astigmatism aberration is proportional to α_o (the opening angle of the beam defining aperture, comp. Figure 11) [159].

Paraxial coma is also a parasitic aberration. Coma can be produced by misalignment of the lens electrodes, imaging a point object into something with three fold symmetry [134],

resulting in beam shapes on the sample surface similar to a comet. Coma aberration is proportional to α_o^2 (the square of the opening angle of the beam defining aperture, comp. Figure 11).

5.1.4 Further point LMIS charged particle optics (between 5 and 50keV)

Ga LMIS based ion beam instruments have to be treated differently from electron instruments, because of the significantly higher mass, resulting lower speeds, and the different ion generation principle (comp. chapter 4). In electron charged particle optics relativistic effects and wave considerations like diffraction, have to be taken into account.

Fraunhofer diffraction is caused by a diaphragm (aperture) in the objective lens („Airy discs“) [159]. At the focal plane of an electron microscope the following diffraction disc of confusion (d_A, comp. section 5.1.3) is formed:

$$d_A = \frac{1.2 \cdot \lambda}{\alpha}$$

Equation 17: Disk of confusion due to Fraunhofer diffraction caused by a diaphragm [158] (same as Equation 1 with k = 1, n = 1 and the approximation for small angles $\sin \alpha_o = \alpha_o$)

d_A = diffraction “disc of confusion” (similar to d_{A50} in section 5.1.7)

λ = the equivalent wavelength of the accelerated charged particle (comp. section 12.5.1)

α_o = the half angle beam defining aperture with respect to the source comp. Figure 11

The disc of confusion (comp. section 5.1.3) for 50 kV electrons (with an equivalent relativistic wavelength (λ_{rel}) of about 5 pm, comp. section 12.5.1) and an objective aperture of 20 mrad results in about 0.2 nm at the sample surface [159]. This contribution can become relevant for higher resolving power electron microscopes (like transmission electron microscopes, TEMs, comp. section 2.1.2) or if the aperture size has to be reduced.

Ga^+ ions at 30 keV have a wavelength of about 0.02 pm (classical approximation, comp. section 12.5.1), which is about $3.4 \cdot 10^2$ times smaller than the one of electrons of the same energy, so current point ion source instruments are not diffraction limited.

In electron microscopy relativistic effects have to be taken into account, because electrons accelerated by 5 to 50 kV possess much higher speeds than Ga^+ ions. At 50 kV the speed of Ga^+ ions is about 371 km/s (electrons reach this speed at an acceleration voltage of about 0.392 V, comp. section 12.5.1). The 371 km/s result in a relativistic mass difference between the rest mass and the corrected one (e.g. [155]) of:

$$m_{rel} = \frac{m_0}{\sqrt{1-\frac{\vec{v}^2}{c^2}}} = \frac{m_0}{\sqrt{1-\frac{(371 km/s)^2}{(300000 km/s)^2}}} \approx \frac{m_0}{1}$$

Equation 18: Mass correction due to high speeds

m_{rel} = relativistic mass

m_o = rest mass

$\vec{v}$ = speed of the ions accelerated by 50 kV

c = speed of light

In the acceleration range of interest (ion beams accelerated below 50keV) relativistic effects can be ignored (comp. also [162]) and the rest mass of the particles can be used for the calculations.

Particles are in perfect coherence when they carry all the same energy after emission [163]. On one hand field emission guns for electrons emit from a small area with a narrow energy spread, so they deliver highly coherent electron beams. Here interference cannot be neglected [159] [163]. A similar concept to light optics can be applied to electrons, based on an extension of Kirchhoff's theory of light ("diffraction theory of aberrations") [134]. On the other hand LMIS have a relatively large energy spread (comp. section 4.5) and emit from a larger area (comp. section 4.5), so their coherence is poor [163]. Here interference can be neglected and a different concept based on the beam current density can be used (comp. section 5.1.7).

As a result geometrical optics is sufficient to describe ion beam CPO [151] e.g. for point LMIS nano patterning instruments below 50 kV.

5.1.5 Lenses

Ion beam focusing is usually performed by electrostatic lenses only, with $\vec{F}_e = q \cdot \vec{E}$ (from Lorentz's law, comp. section 5.1.2). It is in the nonrelativistic case independent of the particle velocity [134] as opposed to magnetic lenses with $\vec{F}_m = q \cdot \vec{v} \times \vec{B}$ (comp. section 12.5.1).

If we attempt to create the same force created by means of a magnetic field for electrons and Ga^+ ions (with the same charge) accelerated by the same voltage:

$$\frac{\vec{B}_i}{\vec{B}_e} = \frac{v_{e,rel}}{v_i} \approx 3.4 \cdot 10^2$$

Equation 19: Necessary magnetic field ratio causing the same effect to charged particles of different mass (with $9.8 \cdot 10^7$ m/s for 30 kV electrons (relativistic) and ions $2.9 \cdot 10^5$ m/s (classical approximations), comp. section 12.5.1)

$\vec{B}_i$ = magnetic field required to apply the same force to an ion

$\vec{B}_e$ = as to an electron accelerated by the same acceleration voltage

m_i = rest mass of a Ga^+ ion

m_e = rest mass of an electron

v_e = speed of the electrons

v_i = speed of the ions

The magnetic field for ions must be about $3.4 \cdot 10^2$ times higher (comp. above) to apply the same force to 30keV electrons and ions, however the significantly different masses have to be taken into account in addition, therefore here electrostatic lens technology is employed.

Electrostatic lens property evaluation can be separated into two parts: the derivation of the potential distribution and the calculation of the electron optical properties of the lens [26]. In order to calculate the electric field distribution of an electrostatic lens, the Laplace equation $\Delta\Phi = 0$ [155] has to be solved [26]. Often the dilemma exists, that simple electric field distribution integrals, which can be solved analytically cannot be fabricated mechanically and vice versa [164]. In addition many geometrical parameters are involved influencing the potential distribution: thickness of the electrodes, distances between electrodes and diameter as well as the electrode shapes (e.g. rounding of the electrodes) [26].

The exact electrostatic field distribution („shape of the potential“) is required to analyse the optical properties of electrostatic lenses. “In the early days” of CPO, computers didn’t exist, so field distributions were acquired from experiments in an electrolytic tank or resistor arrays [153]. If adequate field distributions have been found by computer modelling, lens electrodes should be manufactured to reproduce the equipotentials.

Computer aided design methods became available for potential computation around the 1970s, today the field distribution of electrostatic lenses can be calculated on personal computers [26]. However, care has to be taken that the results are in agreement with experimental results [164]. The simulation accuracy for rotational symmetric lenses can be better than 0.1% using the correct boundary conditions (for potential and the first derivative) [26].

In principle, electrostatic lenses could consist of many electrodes however the majority consists of three. The outer two at the same potential (usually for ion beam instruments on ground potential) and the central one at a different potential [165]. This type of electrostatic lens is called an “einzel lens” or “unipotential lens”.

5.1.6 A simple analytical model for an electrostatic einzel lens

Focusing in an einzel lens (unipotential lens) is performed by changing the particle energy while passing through the lens, however the overall acceleration/deceleration is not altered by this type of lens [165].

In 1991, Crewe [164] published a simple analytical model for the asymptotical behaviour of a symmetric einzel lens. He carefully simulated three different potential distributions and came to the conclusion: “The most significant result of all these calculations is that the properties of the symmetrical einzel lens do not depend very much on the shape of the potential distribution and that we can give very simple approximations to these properties that are good to a factor of two throughout the whole range of practical values for the potential” [164].

Crewe has developed asymptotic approximation formulas for spherical and chromatic aberration coefficients (comp. also section 5.1.3) as well as the focus length. They can serve as a vivid guideline for system designers and users by giving them rules of thumb: e.g. a shorter working distance (as it depends on f) will reduce C_C and C_S. However, neither L nor V_1 can be easily determined by a user, so it is not possible to obtain reliable values.

$$C_C = 2 \cdot f \,,\; C_S = 20 \cdot \frac{f^3}{L^2} \text{ and } f = 1.06 \cdot \frac{L}{\left(\ln\left(\frac{V_1}{V} \right) \right)^2} .$$

Equation 20: Approximation for C_C, C_S and f (definitions comp. section 5.1.2 and 5.1.3) of an einzel lens [164]

f = focus of the lens

L = “characteristic length”

V_1 = on axis voltage at the mid point of the lens

V = acceleration voltage

Chromatic aberrations are about double and spherical aberrations about 4 times higher for einzel lenses than for magnetic ones with similar characteristics [26].

The central electrode can have a positive ("decelerating" einzel lens for Ga^+ ions) or a negative potential ("accelerating" einzel lens for Ga^+ ions), usually the accelerating mode ones show better optical performance [166], but need higher voltages than the decelerating modes, so it's not easy to fulfil the necessary electrical insulation requirements [165].

5.1.7 An alternative approach of analytically estimating the probe size

Barth and Kruit [151] have developed and verified by computer models an accurate, alternative and simple analytical model which could replace the commonly applied disc of confusion one (comp. section 5.1.3). They have called it: "the-root-power-sum algorithm". This approach is different, because it is based on the diameter (d_{PFC}) of the circle that contains a given fraction FC of the probe current (usually 50 for 50%), as opposed to the diameter of a vaguely defined probe size in the disc of confusion model. The corresponding diameter is defined by the integral over the current density distribution:

$$FC = \frac{2 \cdot \pi}{I_N} \cdot \int_0^{\frac{d_{NFC}}{2}} J_N(\xi) \cdot \xi \, d\xi$$

Equation 21: Current density distribution [151]

FC = Fraction of the current inside the diameter d_{NFC}

I_N = Total current $J_N(\xi)$ = Current density function of the beam

ξ = distance from the centre of the beam

d_{NFC} = Minimising defocus plane diameter (similar to the plane of least confusion comp. Figure 14).

The source image (d_{IFC}) is often neglected, but this is only permissible at very low probe currents. As a rule of thumb for e^- Schottky field emitters (reduced brightness (comp. section 4.1) about $2 \cdot 10^7$ $Am^{-2}srV^{-1}$, comp. section 4.1, [113])) and LMIS (reduced brightness of about $2 \cdot 10^6$ $Am^{-2}V^{-1}$, [113]) d_{IFC} can only be neglected for beam currents smaller than 20 pA and 2 pA, respectively [151]. The following formulas give the contributions of the individual aberrations for 50% of the current inside the diameter (d_{x50}):

spherical aberration	source image
$d_{S50} = \left(\frac{1}{2}\right)^{\frac{5}{2}} \cdot C_S \cdot \alpha_P^3$	$d_{I50} = \frac{(2 \cdot \pi)}{\alpha_P} \cdot \left(\frac{I_{probe}}{B_r \cdot V}\right)^{\frac{1}{2}}$
diffraction aberration	chromatic aberration
$d_{A50} = 0.54 \cdot \frac{\lambda}{\alpha_P}$	$d_{C50} = 0.34 \cdot C_C \cdot \frac{\Delta E}{E} \cdot \alpha_P$

Table 3: Analytical models for contributions except for space charge effects (comp. section 5.1.3) [151]

I_{probe} = probe current α_p = half angle at the probe (comp. Figure 11)

λ = equivalent wavelength of the accelerated charged particle (comp. section 12.5.1)

B_r = reduced brightness (comp. section 4.1) ΔE = energy spread

C_C = chromatic aberration coefficient C_S = spherical aberration coefficient

d_{S50} = spherical aberration fractional current diameter (for 50% of the probe current)

d_{I50} = Gaußian image fractional current diameter (for 50% of the probe current)

d_{A50} = Diffraction image fractional current diameter (for 50% of the probe current)

d_{C50} = Chromatic aberration fractional current diameter (for 50% of the probe current)

E = mean energy of particles V = acceleration voltage

In addition they have developed the following way of adding them:

1) "adding" d_{SFC} and d_{AFC}	2) "adding" d_{IFC} to the result from 1)	3) "adding" the d_{CFC} to the result from 2)
$d_{D50} = \left(d_{S50}^4 + d_{A50}^4\right)^{\frac{1}{4}}$	$d_{B50} = \left(d_{D50}^{1.3} + d_{I50}^{1.3}\right)^{\frac{1}{1.3}}$	$d_{P50} = \sqrt{d_{B50}^2 + d_{C50}^2}$

Table 4: root-power-sum algorithm [151]

For a non diffraction limited system like FIB below 50 keV, these can be simplified to:

$$d_{PFC} = \sqrt{\left(\left(d_{SFC}^{1.3} + d_{IFC}^{1.3}\right)^{\frac{1}{1.3}}\right)^2 + d_{CFC}^2}$$

Equation 22: Root-power-sum algorithm neglecting the diffraction

5.1.8 A spot current distribution model [167] [140]

A LMIS can be regarded as a "point" source with a high angular intensity ion emission. As described in section 4.4, the effective ion optical source diameter is around 45 nm (comp. section 4.4).

Addition of the square root of the sums of the discs of confusion (comp. section 5.1.3) and root-power-sum (comp. section 5.1.7) are vivid and helpful models, but give no indication of the actual current distribution on the sample target (in the image plane) [134]. In 1991 Orloff and Sato have developed a mathematical model for the current distribution in the image plane, including chromatic aberrations [167] [140]. The beam current distributions results of their model fit better to the author's experiment results, than for example the discs of confusion model (comp. Figure 15).

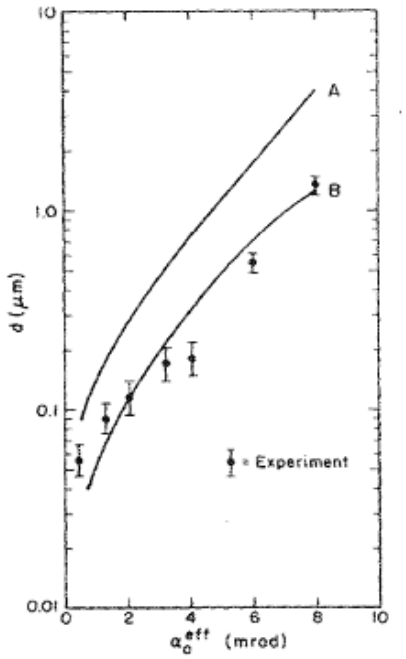

Figure 15: A: beam size calculated from the discs of confusion method, B: by calculations of trajectories (new model), compared with experimental measurement points Fig. 1 in [140]

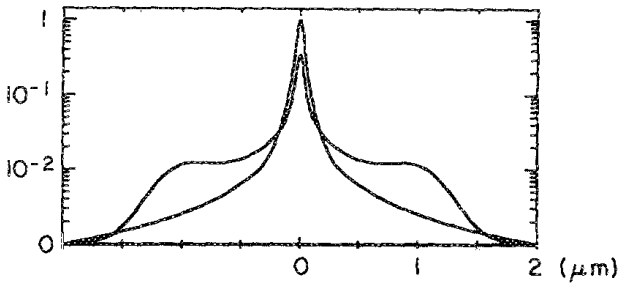

Figure 16: Calculated current density distribution profiles for the case of large aberrations (at different focus positions Z) mod Fig. 2 in [140]

The calculated beam current density distribution in the image plane can be Fourier transformed, resulting in the "optical transfer function" of the instrument [134]. A higher value of the optical transfer function at a certain spatial frequency f_0 means that features in the size range of $1/f_0$ will be resolved at a higher contrast.

Different focussing conditions (electrostatic lens excitation voltages) result in different focus positions (comp. section 5.1.2), this has an impact on the current distribution on the sample surface (Figure 16). For some applications, such as imaging very small features, a different probe profile is optimum (e.g. realized at Z = -1.6 mm focus position in Figure 16) than for patterning small periods in a material that is very sensitive to ion irradiation. Here another profile might be more appropriate (e.g. Z = -0.18 mm in Figure 16) [140].

5.1.9 Aberrations of particles deflected away from the optical axis

Analytical instruments such as transmission electron microscopes are optimised for on optical axis high performance, however patterning instruments have to maintain a certain level of performance even in the corners of a patterning field (write-fields, calibrated field of view, comp. section 7.3.4), so deflection aberrations have to be taken into account, in particular deflection distortion, curvature of field, transverse chromatic aberration, astigmatism of deflection and coma of deflection.

Deflecting the beam away from the optical axis causes misplacements created by "field of curvature effects on deflection over a planar target" [168], called deflection distortion. The misplacement is proportional to Θ^3 (the third power of the deflection angle, more details can be found in section 12.5.2) [162]. This aberration can be corrected dynamically by dividing the write-field into sub fields and adding a position off-set to each individual field, as in electron beam writers e.g. [169].

Objects away from the optical axis are imaged onto a curved surface in the image space, leading to a wrong focus (excitation of the lenses) on planar samples and therefore a position dependent spot broadening within the write-field. The curvature of field focus error is proportional to Θ^2 (the square of the deflection angle). This aberration can be corrected by adjusting the focal length by an amount proportional to Θ^2, this correction is called "dynamic focus correction" [134].

In addition to the described longitudinal chromatic aberration on the optical axis (comp. section 5.1.3) there exists also a transverse chromatic aberration. It influences the deflection accuracy of the particles of (slightly) different energies, as the electrostatic deflection field applies slightly different deflection angles to particles of slightly different energy. It is

proportional to $\frac{\Delta E}{E}\cdot\theta$ and $\frac{\Delta E}{E}\cdot\alpha_p$ (the energy spread and the deflection angle and the energy spread and the opening angle in the image space) [163].

Astigmatism of deflection results in an elliptical spot which is proportional to $\alpha_0\cdot\theta^2$ (the beam defining aperture opening half angle (comp. Figure 11) times the square of the deflection angle) [162], detailed formulas are cited in section 12.5.2.

Finally, a coma of deflection exists. It results in similar coma shapes away from the optical axis as from the parasitic coma on the optical axis (comp. section 5.1.3). It is proportional to $\alpha_o^2\cdot\Theta$ (the square of the beam defining aperture opening half angle (comp. Figure 11) times the deflection angle) [162], the detailed formula is cited in section 12.5.2.

5.1.10 Modelling CPO system

Since the 1970s computer modelling has been possible (comp. section 5.1.4). There exist different techniques: charge density, finite difference method (e.g. "SIMION" [170]) or finite elements ("EOD" [171] or "OPTICS" [172]) can be used to simulate potential distributions (electrostatic field lines). The charge density method has the highest accuracy in potentials and field simulation [26]. In addition ray tracing ("EOD" [171], can be used to calculate ion trajectories from the source through the column onto the sample surface and wave optics for diffraction limited systems (e.g. [172]).

5.1.11 Focused ion beam (FIB) instrument's imaging resolution

Commercially available point ion source instruments advertise sub 10 nm imaging resolution on ideal material system, like Au on C. This is comparable to the "instrument resolution" described above. Example specifications are: 4 nm [100] [173], 2.5 nm [99], 5 nm [174].

5.1.12 Attainable patterning resolution with LMIS ion beam instruments

Kubena et al. have already managed in 1991 to structure down to 7 nm dots into PMMA resist [115] and in 1998 Gierak et al. were able to mill (comp. section 6.2.1) a sub 10 nm line into 50 nm thick AlF_3 on GaAs [175]. However, in 2001 Li has been only capable in milling (comp. section 6.2.1) about 60 nm holes into Si_3Ni_4 membrane. Afterwards they have reduced it down to 1.8 nm by employing an additional Ar^+ broad ion beam exposure process, the closing takes place due to increased atom mobility or a kind of redeposition of sputtered atoms [176]. The have called the process "sculpturing".

There usually exists a difference between the instrument resolutions (comp. section 5.1) and the resolution obtained in experiments, therefore we'll take a closer look at them in the following section..

5.2 Application resolution

Application resolution is a result-oriented concept. It is formed by the convolution of the instrument resolution (comp. section 5.1) with all mechanisms involved exploited for the specific application (contrast creating or structuring mechanisms) such as chemical or physical processes including their corresponding process sensitivities, lateral as well as depth distributions (comp. chapter 6) and disturbing side effects (comp. above). The distribution of these processes define the effective interaction volume (comp. section 6.3.4) which can be exploited for specific patterning applications. It determines the "application resolutions".

The effective interaction volume is created by complex many body interaction processes (comp. chapter 6), it can be influenced by many parameters e.g. angle of incidence, acceleration voltage, ... (comp. chapter 6), depending on the actual patterning goal.

Imaging or patterning "ideal" material systems which can proof the instrument resolution (comp. section 5.1) is different from using a nano structuring instrument for the fabrication of certain structures. For the latter one the "application resolution" usually dominates the achievable resolution. Acceleration energies between 5 and 50 keV in Ga LMIS point source ion beam instruments induce near surface processes with a few tens of nm penetration depth / interaction volume (comp. section 6.3.3 and 6.3.4). A high "instrument resolution" (comp. section 5.1) enables extremely small lateral spot sizes to be achieved (e.g. a few nm, comp. section 5.1.11). However, if the effective interaction volume for the target application is of the order of a few tens of nm this will dominate the effective usable resolution.

On one hand the application resolution can -for some applications- be even orders of magnitude larger than the instrument resolution or make certain special instrument differences important, which are invisible in instrument resolution figures like full width half maximum (FWHM, comp. section 5.1.8). An example is that different focus values can result in different beam profiles and hence influence the pattering results (comp. section 5.1.8).

On the other hand for some applications ion beam imaging / structuring can be more suitable than electron beam imaging / patterning, although the instrument resolution is worse. E.g. clever processing can allow to pattern with an application resolution above the actual instrument resolution. For example direct pattering of sub 5 nm holes ("application

resolution") on the rear side of a membrane (comp. section 9.3). This exploits the lateral extension of the interaction volume (comp. section 6.3.3) at the membrane rear side, when patterned from the top [177].

Also in ultra high resolution imaging all interaction processes have to be taken into account, when imaging on non ideal material systems. An incident ion beam surface interaction phenomenon is called "sputtering" (comp. section 6.2.1): surface material is removed by the incident ion beam. The relatively large material removal rate for 5 to 50 keV Ga^+ ions limits the resolving capability of an ultra sharp edge ("small feature"), because the edge is removed / smoothed out during the imaging process: "For extended small features (e.g. layered structures), rearrangements, redepositon, and differential sputtering rates may limit the resolution in some cases" [134].

5.3 Summary

The exploitable resolution is determined by two inter-related terms for resolution called instrument and application resolution.

The instrument resolution can be analysed and optimised with charged particle optics (CPO) theory. Today's point liquid metal ion source (LMIS) optical systems are mainly limited by spherical and chromatic aberrations [134] as well as charge effects [150], which one actually dominates depends on the "column operation mode" (comp. section 5.1.3). For patterning applications with large write-fields, aberrations due to the deflection of the beam away from the optical axis have also to be taken into account.

Analytical models have been presented, which offer the possibility to optimise system parameters for specific applications and getting a feeling which parameter influence the resolution in which way. In addition a further model is presented to calculate the current density distribution in the image plane. State of the art instruments can image feature sizes below 10 nm and some of them have also been used for patterning lateral features sizes in the same regime.

The instrument resolution is important and can for some applications define the ultimate patterning resolution capability. However, for many applications, the finest reachable feature sizes and periods depend also on the actual current distribution inside the spot on the sample surface -which can be influenced by the excitation of the lenses- (comp. section 5.1.8). In addition each application has "its own resolution" which can be described by the term application resolution. This concept takes "all" interaction process into account.

In addition, clever processing even allows patterning of feature sizes above the instrument resolution (comp. section 5.2).

Ion matter interaction processes are usually complex many body interactions, so understanding them is essential for users and mandatory for opening new application fields.

6 Ion matter interactions

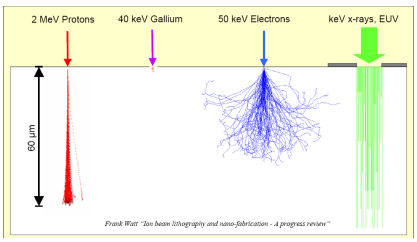

A few tens of nm interaction volume (comp. section 6.3.3) *of* Ga^+ *ions (comp.* Figure 23*) combined with a large variety of possible interaction effects offer fascinating nano fabrication opportunities for a point source vector scan ion beam complement to a Gaußian beam vector scan electron beam lithography instrument, which is currently the most widely used tool for lateral nano pattering.*

Structural changes caused by impinging ions onto surfaces are often referred to as radiation "damage". "... One should repeat that the prejudice invoked by the words damage or defect is unfortunate since the changes in structure produced by the passage of fast ions enables us to make materials which were not obtainable by normal thermodynamic processes. It is also true that the "damaged" material may have superior properties to the original solid..." [1] and in addition they "... may be controlled, understood and even utilized for nano structure creation ...." [178]. In spite of the fact that the term radiation "damage" is misleading it is widely spread within the literature. We will employ the terms: surface modification, atomic disorder, atomic modifications, atomic lattice modification or atom order modification instead.

There exist quite different general ways (instrument set-ups) how ions are generated and hit the surface for exploiting ion-matter interactions. Three exemplary ones are: a plasma close to the target surfaces, volume ion sources and point ion sources.

Understanding ion-matter interactions is essential for carrying out current and opening potential new application areas for ion beam nano patterning besides well trodden paths.

6.1 Introduction to ion-matter interaction mechanisms

Historically e.g. ion implantation (comp. section 6.2.2) depth prediction had to rely on experimental results and empirical formulas. In 1963 the Lindhard, Scharff and Schiott (LSS) theory has been the first unified approach for a comprehensive statistical model of atom-atom collisions [179] [96]. It is still the base for current numerical methods (comp. 6.3) [96].
First some fundamentals and terminology will be briefly described, then an overview over ion-matter interactions will be given, followed by a more detailed analysis of ion-matter interactions and finally current possibilities to model ion-matter interactions including the remarkable accuracy the results have nowadays for some parameter.

6.1.1 Modelling of interatomic potentials

Ion matter collisions are a complicated many body process, due to the composition of an atom as core and many electrons [180]. For modelling and understanding experimental results force or interatomic potential functions would be required, e.g. the central force approximation (dependence on other co-ordinates is neglected):

$$F(s) = -\frac{d}{ds} \cdot [V(s)]$$

Equation 23: Central force approximation [152]

F(s) = force function between e.g. an impinging ion and a surface atom.
V(s) = interatomic potential function
s = distance between two particles

The simplest potential function is called hard sphere potential (can e.g. be applied to two billiard balls):

$$V(s) = \begin{cases} \infty, & s < r_r \\ 0, & s \geq r_r \end{cases}$$

Equation 24: Hard sphere potential [152]

s = is the distance between the centre of two hard-sphere atoms
r_r = hard sphere radii

More accurate quantum mechanical derived charge distributions result in analytical functions reaching a mathematical complexity level which makes it difficult or even impossible to be applied for analytical models, as a result these are only used in some complex computer

calculation algorithms [152]. Simplified analytical models are presented here assisting researchers using such tools especially to determine how certain patterning goals could be achieved by varying the process parameters.

6.1.2 A simplified model

Estimating ion surface interactions, e.g. with the computer simulation using a program called SRIM (comp. section 6.3.1), three energies are defined. The first one is called displacement energy (E_d). The energy of the incident ion E must be larger than E_d to displace a hit atom from its initial position (typical values are 15 eV for semiconductors and 25 eV for metals and 2-5 eV for e.g polymers). The next one is the lattice binding energy (E_b). Every replaced (recoiled) target atom looses this energy while leaving its lattice site and dissipates it mainly as phonons. Typical values for E_b are about 1-3 eV, however it is only known for a few materials. During displacement the incident ion looses at least E_d. The surface binding energy (E_s) is the third one (it takes surface effects into account, so it's different from the traditional chemical binding energy). To remove an atom out of the target (sputter, comp. section 6.2.1) the energy normal to the surface must be larger than the surface binding energy (E_s) at the moment when it crosses the plane of the surface [179].
More details about ion stopping / energy losses can be found e.g. in [152] [179].

6.1.3 Fundamentals of ion-matter interactions

Point source Ga^+ ions in the 5 to 50 kV acceleration voltage regime, result in ion speeds of hundreds of km/s (comp. section 12.5.1). Ga^+ ions possess a significantly higher rest mass than e.g. electrons (about six orders of magnitude between Ga^+ 69.72 u and electron $5.485 \cdot 10^{-4}$ u [181]). As a result a large momentum is transferred onto the sample surface and strong interactions are expected, causing various effects. Most of the energy is dissipated as heat. For periods longer than about a nano second and distances larger than 100 nm the ion beam can be approximated as a continuous heat source [182]. If an incident ion displaces a target surface atom, this is called recoiling [152]. A vivid analogy is a collision between two billiard-balls (comp. hard sphere potential section 6.1.1).
Ion matter interaction effects can be caused by incident ions or further atoms taking part in the collision process. Ion beam instruments employing 5 to 50 kV acceleration voltages exceed the displacement energies (in the order of 5 to 20 eV) by orders of magnitude, so primary collisions are usually followed by secondary ones, forming a collision cascade. All atoms or ions in motion can create further cascades (Secondary, tertiary,... knock-on atoms) [152]). A

collision cascade can be regarded as “a moving sea of particles” [11]. This process continues until the remaining energy -of every participating particle- has fallen below the final energy (E_d+E_b). There is not sufficient energy left which could cause further atom displacements [179]. As a result all particles which have participated are finally resting again, sharing the residual energy with their neighbours and dissipating it as phonons [152].

6.1.4 Classification of collision cascades [11]

Ion matter interactions and the resulting collision cascades (comp. section 6.1.3) can be differentiated into three regimes (low velocity, linear cascade and spike regime), each can be exploited for different kinds of nano patterning applications.

The first regime is called “very low velocity or single knock on regime”. The mass of the incident ion (M_1) is significantly lower than the mass of the surface atoms (M_2) or the acceleration voltage is low. Incident ions do not transfer enough energy to the recoiled atoms, so those won’t generate cascades and sputtering is minimal, e.g. for a He ion microscope (comp. section 4.2.1).

The second regime is called “linear cascade regime” or (low velocity regime). The mass of the incident ion is in a similar range than the mass of the surface atoms ($M_1 \sim M_2$) and the acceleration voltage is moderate (E_0 = 5 to 50 keV).

The third regime is called “spike regime”. The mass of the incident ion is significantly larger than the mass of the surface atoms (M1 >> M2, can be reached for example by bombarding the sample surface with clusters) and/or the acceleration voltage is large, this regime “is seldom reached during conventional FIB operation” [11]. Spikes formation is a nonlinear effect, definition from [152]: “…a high density cascade which possesses a limited volume in which the majority of atoms are temporarily in motion.” [152]. This can lead to spatially limited volumes with more atomic disorder, compared to linear cascade regimes (for more details comp. [152]). If spike effects could be modelled reasonably accurate, they might also be exploitable for nano patterning.

Our instrument (comp. chapter 8) operates in the linear cascade regime using Ga^+ ions in the 15 to 40 kV regime.

6.1.5 Nuclear / electronic interactions

Interaction mechanisms -as a first approximation [183]- can be analysed separately, as elastic (nuclear) and inelastic (electronic) interactions, because of the large mass difference between

the incident ions or surface atoms with respect to electrons [180] and the resulting different respond times to impacting ions [179].

Ions interacting with other atoms cause elastic/nuclear interactions often referred to as radiation "damage" (6.2, further reading [11] [180]). We will employ the term radiation interaction instead. Incident ions transfer momentum to target surface atoms and loose initial kinetic energy (E_d, comp. section 6.1.2) until they come to rest, within the collision cascade region.

Ions interacting with electrons of the target atoms are called inelastic/electronic interactions (comp. e.g. [152] [11] [180]). This process can be regarded as a continuous viscous drag phenomenon between the incident ions and the sea of electrons [152].

The nuclear contribution usually dominates the stopping process (comp. Figure 22 and [152]) in the linear cascade regime. Exemplary results will be described in section 6.2. In certain cases (e.g. channeling, comp. section 6.1.7 or for high acceleration voltages comp. section Figure 22a) the electronic stopping gets important too.

6.1.6 Terminology for travel ranges of ions in matter [152]

The travel range of an incident ion depends on the ion energy loss. The rate of ion energy losses per unit path length is defined as dE/dx [11]. There exist different range definitions (comp. Figure 17) for one and multi ion impacts [152].

A single ion moving in matter looses energy by discrete steps and finally stops after travelling a certain path [180] (comp. section 6.1.3). This path is called range (R) (the integrated averaged distance that an ion travels while moving in the target surface). Projected range (R_P), means the range projected onto the incident trajectory vector. If the incident beam is normal to the sample surface, it equals the implant depth (X_S), which is measured perpendicular to the sample surface. Further less common definitions like radial range (R_r), spreading range (R_S) and transverse projected range R_p^t can be derived from Figure 17 or [11] [152].

In the case of many impacting ions [180] [11], the stopping of ions can be regarded as a stochastic random process [152], therefore atomic collisions of many incident ions onto the sample surface can be modelled applying statistical means.

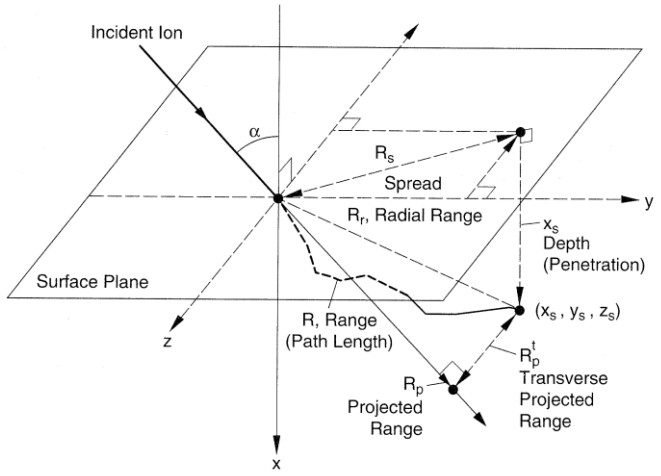

Figure 17: 3D ion trajectories [152]

The path lengths vary randomly from ion to ion (even for ions with the same energy, same incident angle entering the same material) [152] The resulting ranges can be statistically fit by a Gaußian distribution inside the sample surface, with a deviation around the mean value called “range straggling”. Here the projected range (R_P) is the distance at which the highest concentration of implanted ions will be found.

6.1.7 Channeling

If ions enter the sample surface along a low index crystal axis or plane, they can pass through the crystal much further than the calculated range for amorphous samples [180]. During this channeling the relative importance of nuclear stopping (comp. section 6.1.5) is reduced, the ions lose more energy in electronic stopping (comp. section 6.1.5). As a result processes related to nuclear stopping like radiation interactions like lattice disorder or sputtering are also reduced [152]. E.g. ranges of incident ions with energies between 50 to 100 keV can exceed predicted ranges (for amorphous samples) by factors of 2 to 50 [152]. Even ions hitting the sample surface with angles which initially cause no channeling, can be scattered into a channeling direction [152]. It can be employed as contrast mechanism for ion beam imaging applications [11].

On one hand there exist difficulties like predicting doping and interaction [178] as well as obtaining e.g. implantation (comp. section 6.2.2) near the surface. On the other hand advantages like possible deeper implantations and less lattice disorder could be exploited for certain applications [152].

6.1.8 Ion matter interactions overview

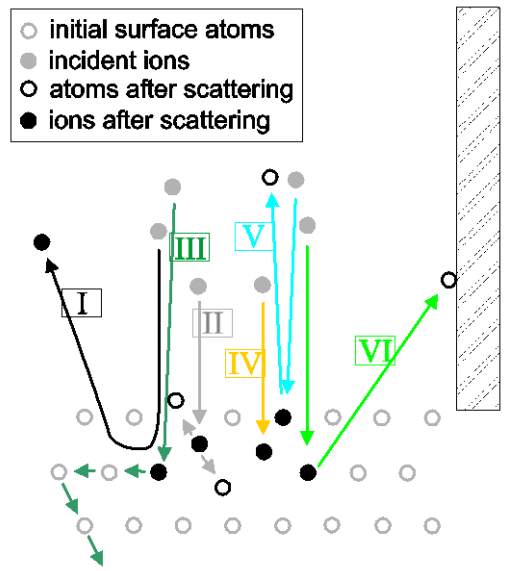

Figure 18: Exemplary interactions (incident ions are: I) backscattered, II) implanted at interstitial sites influencing the original crystal structure, III) implanted at lattice sites and causing further interactions, IV) implanting at interstitial sites and come to a rest, V) target atoms are sputtered out of the sample, VI) target atoms are sputtered out of the sample and redeposit at a surface in the vicinity.

In the linear cascade regime (comp. section 6.1.4)	
Ga^+ ions can	**Electrons can**
cut / crosslink organic molecules	cut / crosslink organic molecules
excite atoms (comp. section 7.1)	excite atoms (comp. section 7.1)
generate heat	generate heat
be backscattered (**I**)	be backscattered
initiate gas assisted processes (milling, comp. section 6.2.1 and 6.2.3) / deposit (M/D))	initiate gas assisted processes M/D
participate in gas assisted processes	-
implant at interstitial (**II**, **IV**) or lattice places (**III**, **V**, **VI**) in crystalline or into amorphous surfaces	-
cause surface modifications, move surface atoms to other positions (interstitial (**II**) or lattice (**III**) ones)	-
remove surface atoms (“sputtering”), these atoms can either “redeposit” (**IV**) at surfaces in the vicinity or escape into the vacuum chamber (**V**)	-

Table 5: Ga^+ and electron matter interaction (Roman numerals, refer to Figure 18)

Possible interactions are visualised in Figure 18. Incident ions can interact for example with surface atoms and electrons as well as groups of surface atoms (molecules), in addition Table 5 gives an overview about processes for ions and electrons (comp. section 6.2.1):

The most spread lateral nano patterning instruments are currently Gaußian beam vector scan electron beam writers (comp. section 7.3.4), however the larger variety of ion-matter interactions, opens an enormous application space for ion beam nano patterning. This variety can even further be increased by varying the incident ion species (comp. Figure 19).

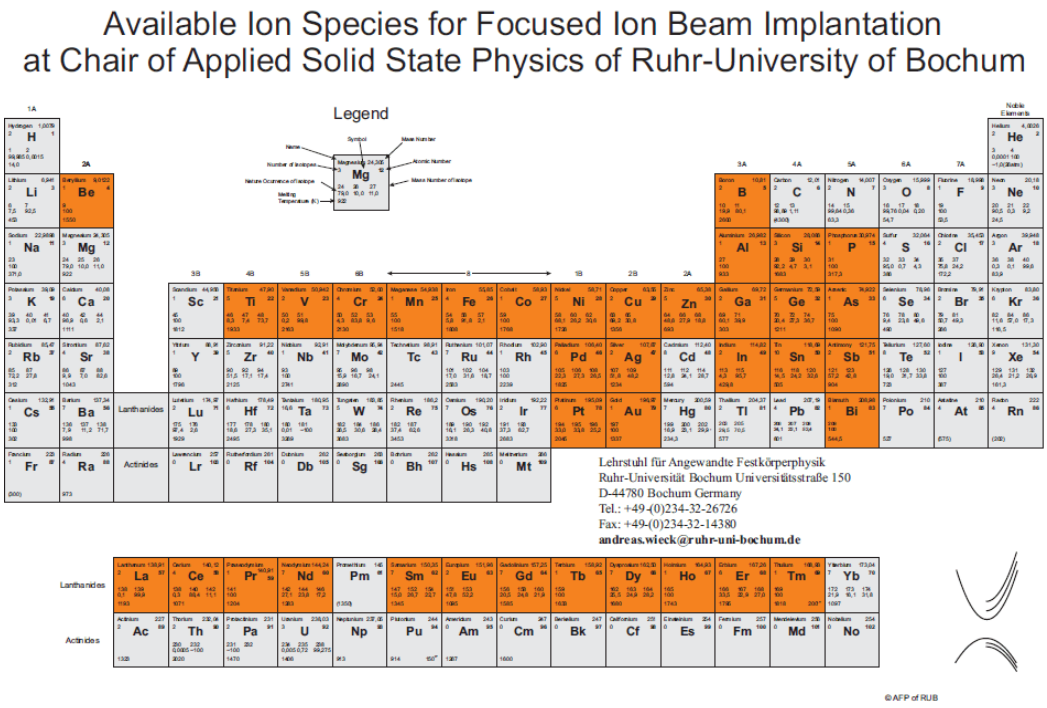

Figure 19: Exemplary large variety of available ion species at the Ruhr University Bochum [143]

6.1.9 Definitions of ion dose [11]

As described above (comp. section 6.1.4) our instrument operates in the linear cascade regime, however together with other research groups we explore non conventional patterning applications. For all these applications the dose plays a significant role. Dose is the quantity of particles absorbed by a medium within a certain area [11].

$$D = \frac{I_p \cdot T_D}{s^2},\ D_L = \frac{I_p \cdot T_D}{s}$$

Equation 25: Area and line dose

D = area dose

D_L = line dose

I_P = probe current (comp. chapter 3)

T_D = point dwell time (time the beam rests at a point of the discrete pattering grid)

s = distance between two points in the discrete patterning grid (“(exposure) step size”)

Fluence describes the number of particles passing through a defined area before hitting the target. The unit for both is [ions/cm^2]. A further term often used in ion beam technologies is dose rate, it equals the beam current with the unit [A] [184].

The ion dose can be classified into three regimes (low/medium/large) e.g. for Ga^+ ions in the linear cascade regime, causing different surface effects [183]. Varying dose experiments have been carried out revealing surface bumps in cross sectional images, due to local amorphisation and surface modifications (comp. Figure 20) [185].

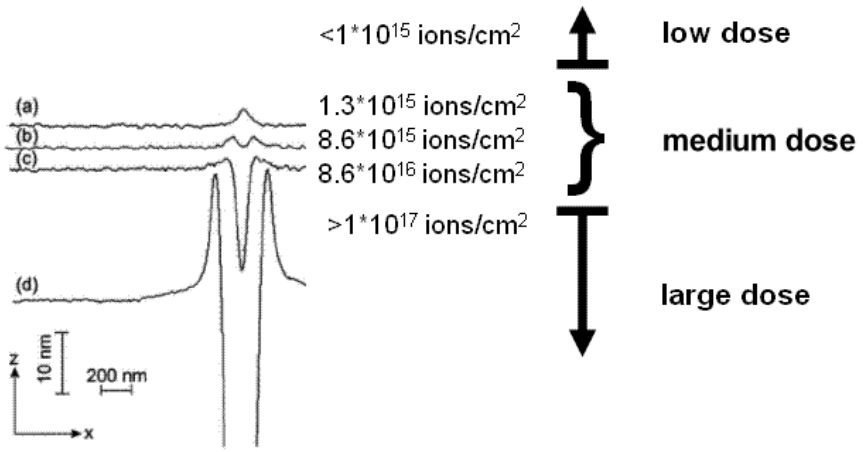

Figure 20: Cross sections of a Si (100) surface applying different doses (50 keV Ga^+ ions) modified Figure from [185]

In the low ion dose regime (10^{11} to 10^{15} ions/cm^2) the global crystallographic order of some materials (metals, metal alloys and oxides) will not be modified. If ions hit solids with covalent bonds the surface phase can be rendered locally into the amorphous phase and if they hit amorphous oxide surfaces they may become locally crystalline. The depth concentration profile of implanted ions can be characterised by a Gaußian distribution around the projected range R_p (comp. section 6.1.8) [152]. Significant sputtering does not take place in this dose

regime (comp. Figure 20), but other effects like atomic lattice modification, atom mixing, phase transitions, surface cleaning, ... occur (comp. section 6.2.1 and 6.2.2).
In Figure 20 can be seen that milling (comp. section 6.2.1) starts in the medium (intermediate, 10^{15} to 10^{17} ions/cm^2) ion dose regime. In addition the other effects (comp. above) are present and if the dose is further increased, e.g. multi dimensional atomic lattice modifications and complex configurations can be generated [11].
The high dose regime (>10^{17} ions/cm^2) is usually applied for material removal applications, however the other effects (comp. above) are still present. Sputtering effects in the linear cascade regime (comp. section 6.1.4) and the high dose regime can be modelled with the linear cascade model and the binary collision approximations [179]. It is a quite well understood and studied regime, because of the commercial interest e.g. in the semiconductor industry (comp. section 6.2.1 and chapter 7).
However, the medium and low dose regime has so far been relatively little studied and applied for patterning applications.

6.2 A closer look at the interaction results

Nuclear interactions (comp. section 6.1.5) create structural modifications in the target surface [152], which can cause structural changes and modify the surface composition, as surface atoms can be removed from their initial position. E.g. in crystalline surface regions they can stop again at interstitial (Figure 18: II), other “lattice” (Figure 18: III) positions or even outside the surface. These (local) surface modifications can be simple one dimensional ones [183] [152] as well as more complex ones like track formation [180]. The structural modifications can be permanent [180] or non permanent (comp. section 6.1.9). Many atom order modifications are created along the ranges of the individual impacted ions and the ranges of the secondary processes. All these atom order changes are important for material modification applications [180].
Electronic interactions (comp. section 6.1.5) can alter the length of organic substrate molecules or excite and ionise surface atoms.

6.2.1 Radiation interactions causing structural surface changes

A widely exploited and quite well understood application of intended surface modification by sputtering is called milling milling (comp. section 6.2.1) starts with the side effect of redeposition (e.g. [11] [180]). The majority of the sputtered particles origin from a very thin

surface layer 1 nm^3 volume around the point of impact (zero diameter beam) [178], depending on incident ion energy and mass. Atoms can be moved out of the sample surface (as neutral, cluster or ion), which results in a surface material removal. These particles can either "redeposit" (Figure 18: VI) at surfaces in the vicinity or escape into the vacuum chamber (Figure 18: V), the latter ones can be detected for analysis purposes (e.g. with an secondary ion detector or be analysed by a mass analyser, comp. section 7.1). Some of these will also be of the kind of the incident ones, which have been implanted earlier. During milling operation (comp. section 6.2.1), ions are implanted into the surface and milled at the same time, so after an initial phase the ion implantation (comp. section 6.2.2) concentration inside the surface reaches the maximum value called "steady state. The sputter yield (Y) describes the number of substrate atoms removed under certain process conditions. Different sputter yields of the components lead to a phenomenon called differential/preferential sputtering [180]: the different components of the surface are sputtered with different speeds. Further details can be found e.g. [134] [11] [180] [150].

Another example of intended surface modification is called replacement collision in monoatomic materials. If a primary knock-on atom (PKA, comp. section 6.1.3) possesses sufficient energy (>Ed comp. section 6.1.2) to displace an atom from its original lattice site, but is left with insufficient energy to leave this lattice side again ($<E_d$), this is called a replacement collision. These events have usually little effect on the chemical order of monoatomic materials, so structural changes dominate, however incident ions are implanted. These sites can serve as nucleation sites for growth process.

In addition in polyatomic materials this can lead to chemical disorder.

6.2.2 Radiation interactions modifying the surface composition

Intended surface modification opens fascinating nano patterning opportunities by modifying the surface composition resulting in e.g. replacement collision of a multi species target, atom intermixing, doping and local surface changes.

If replacement collisions take place in a polyatomic material the chemical stoichiometry can be altered. An exemplary polyatomic lattice consists of atoms of type A and B. Atoms from type A can be replaced from their initial lattice sites and take lattice sites of type B atoms, this is called an "antiside defect" [152].

Ion irradiation of a thin surface layer of one material followed by another material initiates a similar effect which is called atom intermixing or chemical alloying. It takes place at the interface separating the surface layer from the layer below [152] [178]. These effects can be

exploited as complementary pattering / implantation processes. E.g. the possible amount of Au which can be mixed into a Cu layer (20 nm Au layer irradiated by Xe ions) significantly exceeds the maximum concentration possible by direct implantation, which is limited by the steady state condition (comp. section 6.2.1) [152].

"Implantation" is a commonly exploited example in the semiconductor industry of changing physical material properties (in particular conductance). Incident ions resting in the substrate are called implanted. They can rest e.g. at interstitial sites in crystalline surfaces (Figure 18: II, IV) or at lattice places (Figure 18: III, V, VI) intermixed with the original surface atoms. Within the implantation process most of the kinetic energy is converted to heat, only a small fraction remains as atomic order modifications in the sample or are emitted as energetic particles or radiation [182]. The implanted ions can change the physical properties of e.g. semiconductors which is called doping. The actual applications will be described in more detail in chapter 7. Implantation around tens of atomic per cents are usually maximum values [152]. Avoiding channeling in ion implantation the incident angles are carefully selected (off-axis, off-plane or random incidence) [180]. However, a careful selection of the angle of incidence and crystal orientation could be tested exploiting these effects e.g. for locally controlled implantation and surface modification injection at range levels larger than those predicted for amorphous surfaces (comp. section 6.1.7). Here careful pioneering experiments are required for creating reliable models.

Radiation interactions can locally cause phase transformations e.g. amorphous surface regions or crystallisation [180]. In crystalline metallic alloys the crystalline phases can become amorphous or change to a different crystalline structure (this transformation can be a metastable or an equilibrium state). The observation of amorphous phase is strongly material dependant (further reading [152]).

Radiation interactions can initiate surface functionalisation and cleaning processes [152]. Contaminant thin surface layers are removed ("texturing") by the incident ion beam e.g. absorbed water, hydrocarbons and oxides which can result in favourable high bonding surfaces for chemical or morphology (texture) influenced adhesion facilitating film growth / coating (e.g. Teflon on metal growth). This is a widely spread surface preparation technique in surface science [186], however usually volume ion sources (comp. section 4.2.2) are employed to process large surface areas.

6.2.3 Gas assisted interactions

Complementary to pure ion sample interactions are those with additional process gases available in the vicinity of the point of impact of the energetic ion beam. These gases can catalyse, initiate processes or induce molecule disintegration [187].

Gas assisted processes can be separated into two groups: non reactive and reactive ones. In the first case the (process) gas contains all process relevant components and the ion beam delivers mainly the energy causing the reactions. In the second case the incident ion species takes part in the process, it chemically reacts on the sample surface with the other components delivered by the process gas [152].

Reactions with residual or intentionally induced gases inside the vacuum vessel are called ion beam assisted/induced deposition (IBAD/IBID) [152] [95], respectively or reactive ion etching (RIE). For deposition the term IBID (ion beam induced deposition) is currently more frequently used e.g. [95]. The deposition rate for IBID is higher than for EBID (electron beam induced deposition) [188] but the incident ions will be partially deposited into the target. The mechanism is a kind of chemical vapour deposition (CVD) and the reactions are comparable to e.g. laser induced CVD [189]. Gases like H_2O can increase the etch speed.

The presence of an energetic ion beam during film growth facilitates atom densification, because the adatom mobility is increased and nucleation sites for island formation are created (about 4 times higher nuclei density and 5-15 times smaller nuclei seize) [152]. The etching speed (rates) for milling (comp. section 6.2.1) applications can be influenced by process gases. This technique is called reactive ion etching (RIE). Gas assisted processes can further influence residual stress, texture (orientation control), composition and modification of grain sizes as well as the surface morphology, the susceptibility to corrosion, optical properties (e.g. of semiconductor masks), the surface hardness and ductility, the adhesion and further tribological [4] properties (friction, lubrication and wear) [152].

A detailed recent analysis for gas assisted processing by ion and electron beam is given in [95].

6.2.4 Electronic interactions and exemplary results

In addition to the nuclear interactions discussed above, electronic interactions can also be exploited for patterning and analysis applications e.g. for polymer resist exposure [190] and diverse atom excitations products.

In electron beam lithography electrons alter polymer molecule chain length, which causes the resist exposure [191]. Ion irradiation can also alter surface molecule chain length. Similar to

the exposure with electrons the molecules can either be cut into shorter molecules e.g. poly poly(methyl-methacrylate) (PMMA) in positive resist exposure regime, or cross linked to longer molecules, e.g. PMMA in negative resist exposure regime. However, ions offer a third contrast mechanism, if the dose is further increased, then milling (comp. section 6.2.1) of the resist will start.

Atoms can be excited by electron as well as ion bombardment (comp. Table 5). Electrons can be removed from surface atoms or be excited to higher shells. These removed electrons can interact with other molecules, e.g. causing additional resist exposure (comp. above), be added to surface atoms or leave the sample (ion induced secondary electrons, ISE). These can be detected by conventional SE detectors (e.g. used in scanning electron microscopes) for imaging and further analysis purposes. Excited electrons can relax producing e.g. phonons, plasmons or photons (e.g. x-rays [44]).

6.3 Modelling ion-matter interactions

The routine and reproducible application of ion beam surface interactions requires the possibility to model them e.g. interaction areas and parameters influencing the spreading [180]. An overview about existing models is given in [180].

6.3.1 The stopping and range of ions in matter (SRIM) possibilities and limitations

Monte Carlo computer programs (e.g. “SRIM” (The stopping and range of ions in matter) by Ziegler at al. [192] [179], e.g. chapter 1 and chapter 7) simulate statistical interaction events. SRIM takes direction changes due to binary collisions into account and nuclear and electronic energy loss.

This kind of model predicts sputter yield very well for light targets. However, the yield for heavier targets and heavier incident ions increases significantly faster with Z than predicted. Binary binding and mass effects are well taken into account, but SRIM fails to predict density effects (depending on N the atom density in the target material) [180]. If the energy deposit into the target is small enough, Monte Carlo simulations predict experimental results quite well [180]. In SRIM only amorphous substrates are taken into account, e.g. an effect like channeling is neglected.

Figure 21a) and c) show exemplary interaction volumes (comp. section 6.3.3) for 40 keV Ga^+ and Li^+ ions impacting into an amorphous silicon substrate simulated by SRIM, respectively. Figure 21b) displays the analogue result for 40 keV electrons simulated by Casino (a Monte

Carlo electron matter interaction calculation software [193]). As can be seen, the lateral (2·b) and vertical (2·a) spread for Ga^+ ions are each smaller than 100 nm and about two orders of magnitude smaller than those of electrons.

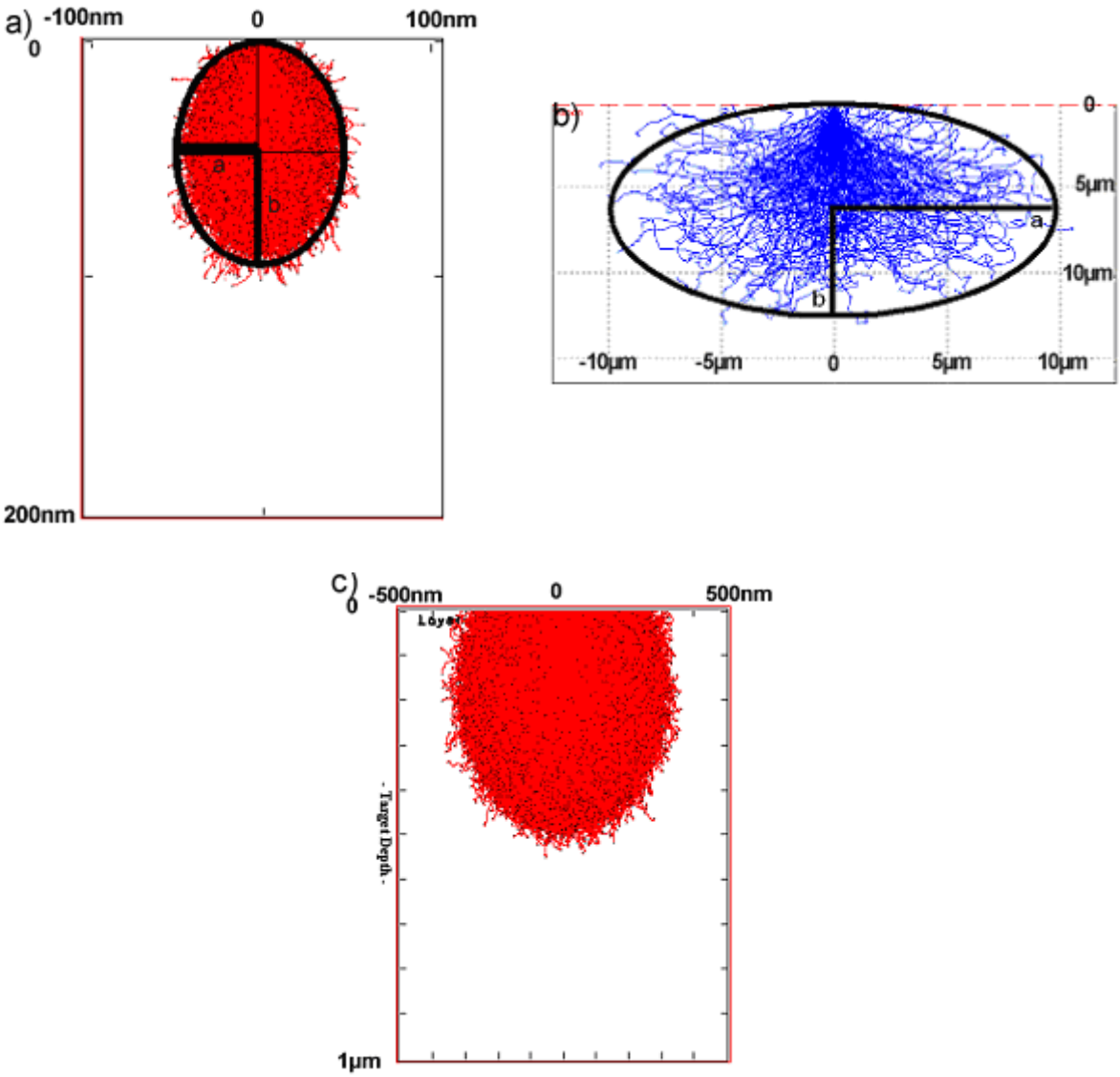

Figure 21: Monte Carlo simulation results of interaction volumes (comp. section 6.3.3) for 3 different charged particles accelerated by 40 keV (1,000,000 trajectories, modelling parameters details comp. section 12.7.1, 12.6 and 12.7.2 respectively)
a) Ga^+ ions into an amorphous Si substrate (SRIM)
b) electrons into silicon (Casino [193], only forward scattering)
c) Li^+ ions into an amorphous Si substrate (SRIM)

As can be seen in Figure 21 for ion beam matter interactions around 40 kV the interaction volume (comp. section 6.3.3) is usually in the range of a few tens of nanometers in 3 dimensions (e.g. approximated by an ellipse with a = 44 nm (9.8 µm for electrons) and b = 48 nm (6,2 um for electrons) the volume of an ellipsoid rotating around "2b" is 3.89 10^{-22} m^3 or 0.000389 μm^3 (2.5 10^{-15} m^3 or 2500 μm^3, electrons, without backscattering)). By varying the incident ion species (comp. section 6.1.8), the interaction volume can be influenced, e.g. light ions like Li^+ would result in a smaller interaction volume as electrons, but in a larger one than Ga^+ (comp. Figure 21a) and c).

As discussed above (comp. section 6.1.5) the stopping processes can be –as a first approximation- analysed separately for nuclear and electronic stopping.

Stopping power is the amount of energy an ion looses per travel range (comp. section 6.1.8). Figure 22 displays the exemplary stopping power of Ga^+ ions inside an amorphous Si substrate with different acceleration energies. They are plotted from the stopping and range tables generated by "PRAL" (projected range algorithm, [179]) inside the software SRIM. Figure 22a) shows the contribution of nuclear and electronic stopping over a large acceleration voltage regime (0 to 1000 kV) and Figure 22b) the acceleration voltage regime of interest (linear cascade regime, 5 to 50 kV, comp. section 6.1.4). It can be seen that nuclear interactions (stopping power, dE/dx Nucl.) dominate in this acceleration voltage regime, so it can be relatively accurately modelled by interatomic potentials (comp. section 6.1.1) between the incident ion and the target atom [11].

For electrons the stopping power decreases and for ions increases with increasing collision energy onto the sample surface Figure 22c). For Ga^+ ions into silicon the electronic stopping power results in SRIM and [194] are similar, whereas for nuclear stopping they differ between a factor of 2 and 3, which can be explained by different applied models / formulas.

When a large momentum is transferred into the sample surface, additional phenomena have been observed; spikes, large cluster emission, chemical effects (comp. above). These effects cannot be explained in the linear cascade regime, therefore have to be treated by e.g. molecular dynamic models. This can take into account complex many body interactions, electron phonon coupling and atom internal excitation inside a limited region of the sample.

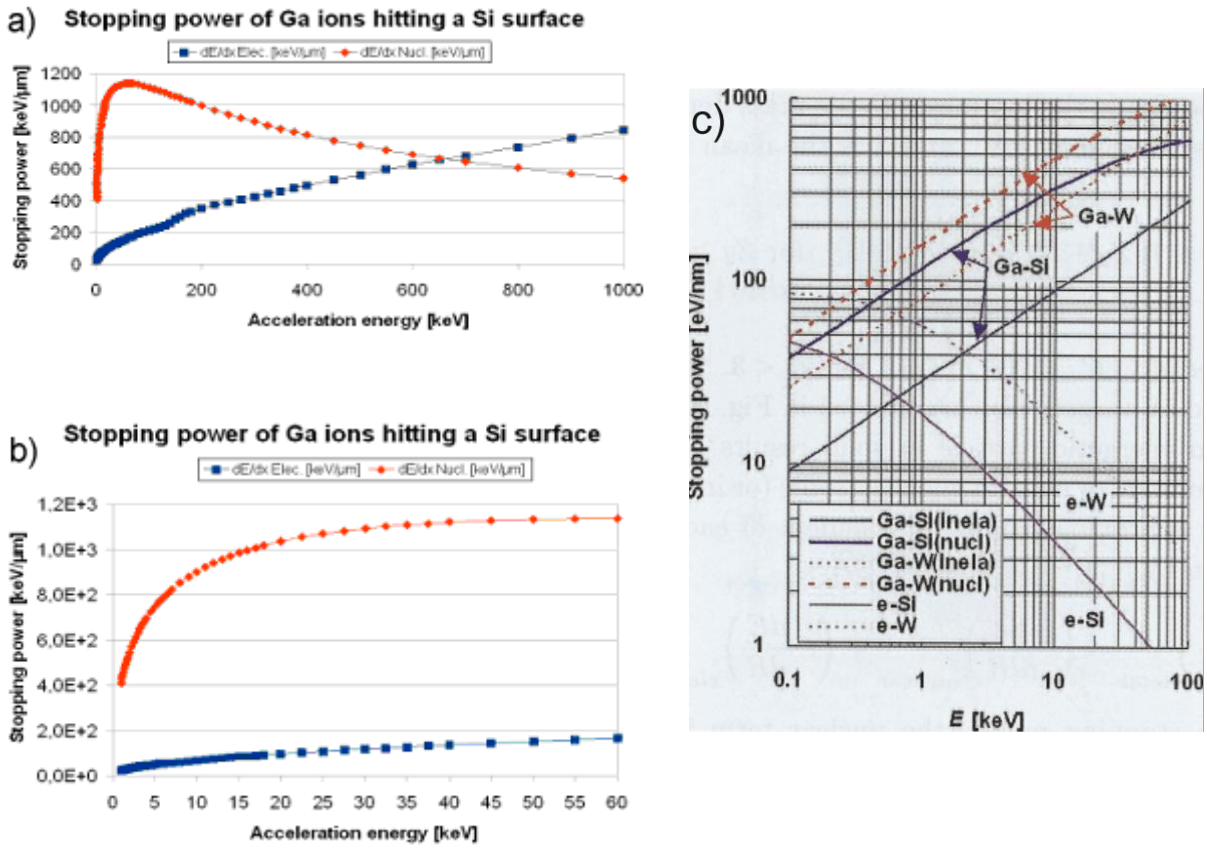

Figure 22: Simulated electronic and nuclear stopping power of Ga^+ ions hitting a silicon surface
a) from 1 to 1000 keV by SRIM 2008 (applied parameters comp. section 12.7.1 and the corresponding table 12.7.4)
b) as a) but results displayed from 1 to 60 keV
c) comparison between stopping power of electrons and ions [194]

6.3.2 Molecular dynamics simulations for ion-matter interactions

Molecular dynamics simulation codes use sophisticated interatomic potentials [180], they model the temporal and spatial evolution of atoms in a cascade. An event is modelled by giving a chosen energy to an atom which will act as primary knock on atom (PKA) [152]. To understand self assembly into nano clusters and heavy ion nonlinear impacts, a combined code of MC, diffusion and molecular dynamics has been developed [180] (an example is given on the following www page [195].

6.3.3 Interaction volume

The complete area which takes place in the various interaction processes and collisions is called the interaction volume. It extends to the maximum travel range of the incident ions and initiated collision cascades (comp. section 6.1.3) in all 3 dimensions. For patterning applications the volume extension and how it can be influenced are important parameters.

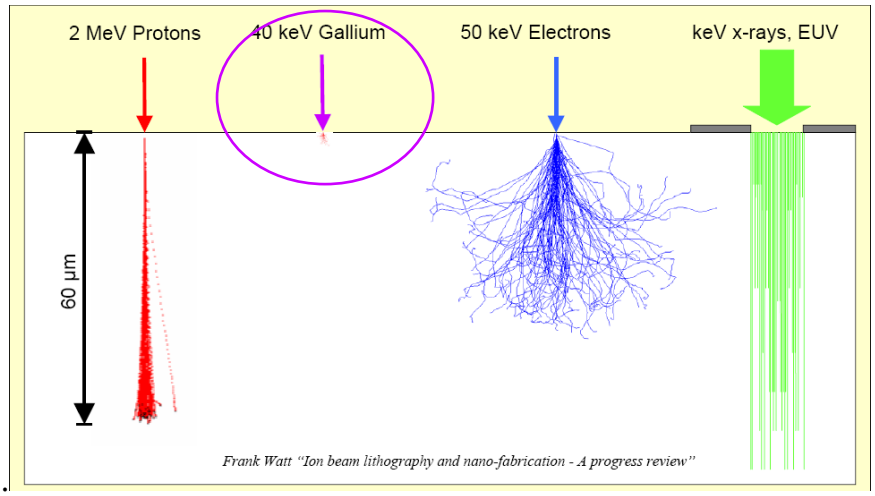

Figure 23: Interaction volumes of different accelerated particles within the sample [188]

Figure 23 shows the promising small interaction volume (usually around tens of nm in all 3 dimensions for Ga^+ ions, compared to other technologies. As a result surface pattering is possible with a high selectivity and high resolution in all three dimensions.

6.3.4 Effective interaction volume

The term effective interaction volume can be used to describe the volume of altered surface properties in the desired manner for a specific application.

The effective interaction volume can be called “voxel” [196] and [44], in the example above this would be a value of 3.89 10^{-22} m^3 for 40 kV Ga^+ ions and 2.8 10^{-15} m^3 for 40 kV electrons into Si (comp. section 6.3.1). Although the surface probe size can be significantly smaller (electrons comp. section 2.1.2 and Ga^+ ions comp. 5.1.11) the process relevant voxel size for Ga^+ ions is significantly lower (7 orders of magnitude) than that for e.g. electrons ([44] (comp. section 6.3.1)).

However, if larger impacts e.g. in the vertical direction are required, the interaction volume is not the ultimate limit for patterning applications. It can be overcome by milling (comp. section 6.2.1, with limitations for nano patterning (comp. section 7.2)). A further alternative are pattern transferring techniques like in EBL e.g. resist exposures (comp. section 6.2.4), sacrificial layers as masks for the following processes steps or combinations can be used.

6.4 Instrumental set-ups for exploiting ion surface interactions

Three quite different instrumental set-ups for ion generation are briefly introduced: one for processing complete surfaces and two with µ/nm lateral resolution capabilities.

The first one generates a plasma (usually noble gas) around the sample. As a result ions hit the sample at all areas which are exposed to the plasma. It can be used to e.g. alter surface properties of polymers e.g. [197] or to clean surfaces [186]. A further wide spread application of a plasma around a target is sputter coating e.g.: non conducting electron microscope samples receive a thin conducting layer of the target atoms. Another potentially interesting result from this ion source type is a kind of self assembly: "periodic grove formation" [180].

The second instrument set-up possesses a volume ion source which is scanned over a semiconductor surface. Areas partially covered e.g. with resist will be protected from the ion bombardment (applications are implantation/doping comp. section 6.2.2) for e.g. computer memory and processor fabrication within the semiconductor industry.

The third instrument set-up uses a point ion source (e.g. from LMIS comp. chapter 4) and focuses the beam to a few nm spot onto the sample surface applying charged particle optics (comp. chapter 5) for direct write [198]. This is the instrument set-up we have chosen for our point source ion beam nano patterning instrument (comp. chapter 8).

All three cause ion-matter interactions, however results differ. A bright beam generated by a point LMIS (comp. chapter 4) focused into a sub 10 nm diameter spot of a few pico Ampere (comp. chapter 5) scanned over the sample surface at variable speeds has a different impact than a constant ion flux over large surface areas of usually less ions per time unit.

Usually one of the set-ups dominates a specific application in industry or research. E.g. volume beam implanters are optimised for the speed/throughput requirements of the semiconductor industry or point ion source instruments (employing e.g. Ga LMIS) are used for the creation of specimens for transmission electron microscopes ("TEM lamellas", comp. section 7.3.1) because of its versatility. Nevertheless, inspirations for application could come from neighbouring technologies, employing the other instrument set-ups. However, different ion doses per time unit on surface areas can lead to different results (comp. section 6.1.9). Especially as they possess the complementary capability to carry out ion-matter interactions locally and with arbitrary shapes.

6.5 Vice versa approach

Taking the involved mechanisms into account a "vice versa approach" is possible, in which one could search for mechanisms / effects in the chosen material system that are sensitive to ions in a certain way within the desired target feature dimension range (effective interaction volume, comp. section 6.3.4), then explore the potential application field. This patterning process alternative could assist in solving some of current nano patterning challenges.

For example highly oriented pyrolyitc graphite (HOPG) is a promising material system, even "a few ion events" cause monolayer atomic modifications with lateral extensions of a few nm after a controlled oxidation process [199] (comp. section 9.1).

6.6 Summary

Ion beam matter interactions and some ways to model them have been introduced.

The number of potentially exploitable or already exploited ion beam matter interactions in the linear cascade regime is huge, compared to the choice of electrons. Although the ultimate instrument resolution of point source electron beam instruments is usually higher than for e.g. focused point Ga LMIS instruments (comp. section 5.1, 5.1.11 compared to 2.1.2), Ga^+ ions result in a significantly smaller voxel (effective interaction volume). This opens fascinating direct nano patterning opportunities in all 3 dimensions with extremely high selectivity and high resolution. This has already been predicted/suggested at the end of the 1950s / beginning of the 1960s by e.g. R. Feynman [8] and S.P. Newberry [9] (comp. chapter 1 and section 2.2.5).

So far ion-matter interactions have been mainly studied, understood and optimised for e.g. semiconductor doping due to implantation of the incident ions, milling (comp. section 6.2.1) by sputtering away surface atoms, surface analysis (all three [119]) and deposition or increase the sputter yield due to gas assisted processing employing Ga LMIS [156] and [11] (comp. section 7.3).

Additional application inspirations could come from neighbouring technologies employing a different instrument set up, as the phenomena of focused point ion source beams and broad beams are quite similar. This opens new opportunities in nano fabrication research, e.g. by transferring classical ion beam processes to nano scale or developing new ones, especially as some results cannot be reached by conventional thermodynamic processes (comp. introduction to chapter 6) [1]. Further details about interaction mechanisms can be found in: [183] [152] [134] [11] [180] [150].

7 FIB instruments and standard applications

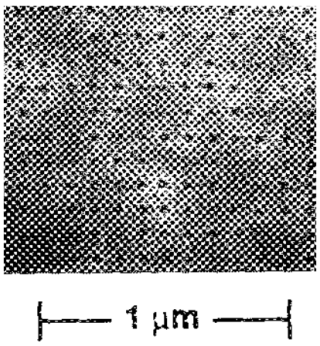

Since the end of the 1970s liquid metal ion source (LMIS) instruments carry out patterning (comp. Figure 24) as well as analysis applications, both rely on and influence each other.

There exist on one hand dedicated ion beam instruments for semiconductor industry needs, which have reached a high degree of automation. On the other hand there are versatile R&D platforms.

In this chapter a short overview will be given about existing instrumentation and exemplary applications. Afterwards in chapter 8, 9, 10 the necessary modifications for an ion beam nano patterning instrument and its application will be shown.

7.1 Overview over some analysis applications

In scanning ion microscopy (SIM) secondary electrons or ions can be detected. This is similar to scanning electron microscopy (SEM, comp. section 2.1.2) and one of the most commonly used applications of ion beam instruments [119]. However, different contrast creating effects offer complementary analysis opportunities [200]. Three examples are:

First it is possible to collect secondary ions in addition to secondary electrons [11]. Second the crystal orientation of the surface grains can be analysed using channeling (comp. section 6.1.7) [11] [200]. Third the much smaller interaction volume for heavy ions like Ga^+ (comp. section 6.3.3) results in more surface sensitive information at the same acceleration voltage (SIM/SEM).

A further analysis application exploits secondary ions (comp. section 6.1.8), which are not only collected, but also mass separated. This technique is called secondary ion mass spectroscopy (SIMS). It is a sensitive, flexible, powerful and commonly used surface composition analysis technique see e.g. [183].

In addition to the secondary electrons and ions -similar to SEMs- additional excitation products can be exploited like: Auger electrons [200] and x-rays (comp. section 6.1.8 and 6.2.4).

The ion microscopy capabilities are required to prepare and set-up the instrument for patterning applications e.g. to optimise the beam profile on the sample surface or for mark recognition in multi level structuring. However, ion beam analysis is destructive to the sample surface especially if heavy ions like Ga^+ are employed (sputtering comp. section 6.2.1), so the analysis results are influenced significantly. Finally, analysis techniques can be combined with the milling capabilities e.g. by first removing surface layers and then analyse regions below (e.g. metrology from cross sections, comp. section 7.3.1).

7.2 Ion beam patterning advantages and disadvantages

Kanaya's [85], Seliger's [86] [87] and Orloff's and Swanson's [89] pioneering work and especially the invention of the LMIS (comp. chapter 4) inspired more and more R&D labs all around the world to study the large amount of interaction mechanisms for their analysis and patterning applications. Especially the fact that the EBL resist PMMA (comp. section 6.2.4) has revealed an about two orders of magnitude higher resist sensitivity (IBL versus EBL,

comp. section 2.2.5) [86] [87], this encouraged further groups at the end of the 1970s to study patterning capabilities. Examples are: the already mentioned resists analysis [190] [201] or direct selective ion implantation [202].

Potential advantages like the large ion-matter interaction variety (6.1.8), the unique capability to create materials "...not obtainable by normal thermodynamic processes..." [1] (comp. introduction of chapter 6, 6.2.2), the possibly to reduce backscattering and hence the proximity effect have been reported. The latter one is possible due to the much lower penetration depth and less backscattering effects of heavy ions like Ga^+, see [136] [203]. In addition Komuro et al. [190] have discovered that the resist contrast is higher (steeper contrast curve) if exposed by ions, compared to electrons. Last but not least Kubena has achieved remarkable 7 nm dot sizes by ion beam resist exposure applying Ga^+ ions at 50 kV in 60 nm thick PMMA (comb. Figure 24) [115], which has been comparable to EBL results by that time, comp. e.g. [204].

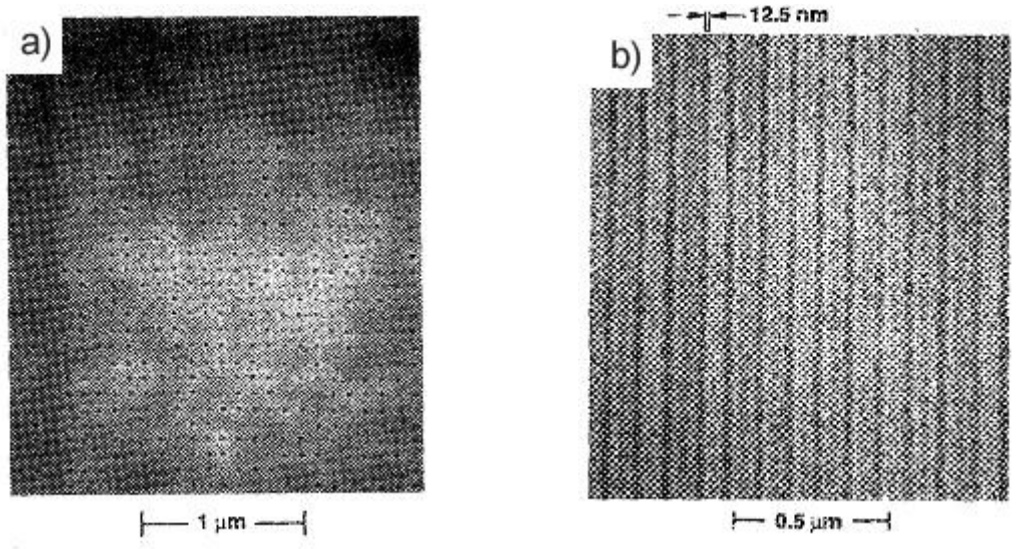

Figure 24: a) down to 7 nm dots and b) 12.5 nm lines in PMMA patterned by IBL (Fig. 6b and Fig. 4c in [115]

These promising results, the huge potential range of exploitable interactions (comp. section 6.1.8) in combination with the small interaction volume (comp. section 6.3.3) have caused enthusiasm in finding complementary patterning processes within the research community. In addition the commercially available instruments for industrial applications can reach a high level of automation (comp. 7.3.1). However, challenges have occurred, the list of reported nano patterning drawbacks appears long: discontinued lines; incident ion residuals;

impossible thick resist exposure; impossible mark detection below thick resists; unintended damage and the lack of accurate dose control. This resulted in a decline in ion beam nano patterning research activities at the mid of the 1990s, only a few groups kept carrying out research in this field e.g. [205] [206] [207]. The latter group works on a broad ion source projection instrument as potential next generation lithography candidate for the semiconductor industry.

The different challenges mentioned above will be described in more detail.

I. discontinued lines

A challenge is that narrow lines exposed at low doses (e.g. in poly(methyl-methacrylate), PMMA) are not continuous [201] [136] [208] [115].

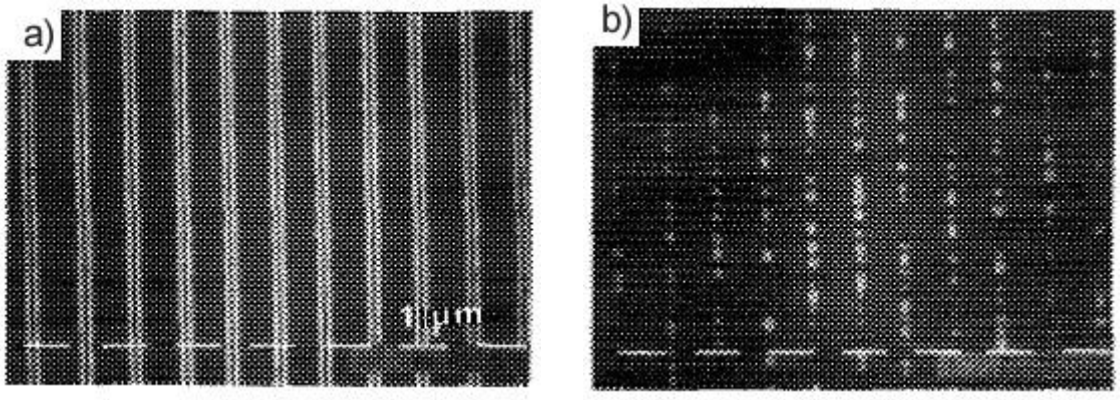

Figure 25: SEM micrographs of a) continued ($1.5e^{-7}$ As/cm^2) and
b) discontinued ($0.7e^{-7}$ As/cm^2) thin lines in PMMA resist Fig. 7 in [136]

Matsui has compared a resist named P($SiSt_{90}$-CMS_{10}) with PMMA. They have found out, that the more sensitive P($SiSt_{90}$-CMS_{10}) one starts to show the discontinued lines phenomenon at a lower dose ($1.2 \cdot 10^{-8}$ As/cm^2) compared to PMMA ($7 \cdot 10^{-8}$ As/cm^2). As a result electronic noise is unlikely, but the behaviour can be explained by the fact that shot noise is caused in the resist by low dose effects in combination with threshold like behaviour of the resist contrast curve or that this can be caused by oscillations at the end of the Taylor cone [136]. These oscillations are a fundamental LMIS characteristic which is also present in other FIB processes than organic resist IBL (comp. section 4.4). Later on Kubena has managed to decrease the minimum linewidth down to <10 nm and increase the necessary dose to about $1 \cdot 10^{-6}$ As/cm^2 until he observed this effect again [115].

II. incident ion residuals

A further disadvantage is the fact, that the incident ions remain partially in the sample surface (most commonly Ga) which is often not wanted [189] [69] [209].

III. impossible thick resist exposure

The smaller interaction volume (comp. section 6.3.3) of e.g. Ga^+ ions has not only advantages (comp. above), because in Ga ion beam resist exposure, it limits the usable resists thickness [69].

IV. impossible marks detection below thick resists

In addition marks cannot be seen by scanning ion microscopy (SIM, comp. section 7.1) below resists layer thicker than interaction volume [203].

V. damage

Further on unintended surface damage caused by milling (comp. section 6.2.1) is always present [189], so surface areas of interest might be partially destroyed. At the µm scale initial damage during e.g. the FIB instrument set-up (focussing comp. section 7.1, imaging to find the exact position) can be ignored. However, for nano patterning this is usually not the case anymore, therefore perfect alignment of an additional optical or electron imaging capability with the ion beam is required. Alternatively a high precision stage could be used [178], like those employed in EBL writers.

VI. accurate dose control

In FIB instruments a precise dose control is difficult as "... computer controlled (ion beam) micromachining presupposes that the tool operates at a constant etch rate ..." [178].

VII. "... the single most reason..." [69].

However, another argument could be the decisive one following Marrian et al.: "... But, and perhaps most telling, the available tooling for electron beam lithography (EBL) is much more sophisticated, which is perhaps the single-most reason it is much more widely used..." [69]. This may be due to the fact that EBL development has started earlier [203]. However, there have been efforts realising ion beam instruments which are similar to electron beam writer at the end of the 1980s [10], but the technology has not been accepted by the research community.

On one hand at least these 7 disadvantages exist. On the other hand there has been a significant commercial interest in FIB milling / deposition (comp. section 6.2.1 and 6.2.3) and increased need for complementary nano analysis. These two circumstances in combination with growing funding for nanotechnology research over the last 10 years has led to a wide spread and increasing usage of ion beam technology in nano research laboratories. As a result some researchers start off exploring nano patterning applications again and explore ion beam processes [210] [198] [211]. Maybe because they are limited by the current processes, fascinated by the advantages (comp. above) or potential future opportunities like e.g. single ion events even of multi species ion sources [212].

7.3 General instrument differences

Although the fundamental set-up of ion and electron beam instruments (comp. chapter 3) is similar, dedicated optimisations of the following parts allow a specialisation for certain applications:

- charged particle optics (CPO, comp. section 5.1) column (including e.g. ion beam generation, deflection)
- detectors
- driving electronics / software
- sample manipulation stage including reproducibility and position sensing

The major application fields in the semiconductor industry exploit only two of the possible ion beam interaction mechanisms (comp. section 6.1.8 and 6.6): sputtering (comp. section 6.2.1) and Gas assisted processing (comp. section 6.2.3) [11]. The latter one possesses a potential large variety of incident ion and gases combinations, but only a few gases are

routinely employed. In addition both are carried out using only one incident ion species (Ga), although there exists a possible large variety (comp. section 6.1.8). The application fields are called: **circuit edit (device / mask repair)** and **failure analysis**, here dedicated instrument set-ups exist. Further on, nowadays many nanotechnology research labs utilise a versatile ion beam instrument for various analysis and patterning applications. All these machines are commonly referred to as FIB (focused ion beam) instruments, the general architecture will be explained in more detail, followed by the one of an electron beam writer.

7.3.1 Industrial applications and instrument set-ups

The tasks of FIB instruments in "circuit edit" are:

On one hand surface material is milled (comp. section 6.2.1) away e.g. to remove short circuits in multi layer semiconductor devices [213]. However, care has to be taken, because residual Ga traces on the surface can be conducting.

On the other hand gas assisted processing (comp. section 6.2.3) is employed to add or deposit missing interconnections [213]. For photo masks the equivalents are: removing unintended features by rendering the processed areas almost transparent again. In the additive case opaque features are grown on the surface. The latter one is called additive mask repair [150]. Further details about mask repair can be found in e.g. [208] [213].

Instrument tasks in failure analysis are mainly the preparation of samples for further analysis e.g. in the same or other instruments. These tasks employ milling with and without gas assistance (comp. section 6.2.1 and 6.2.3). Milling a thin foil out of a solid substrate for high resolution analysis in a transmission electron microscope (TEM, comp. section 2.1.2) is called "TEM lamella preparation" [214]. Creating "viewing trenches" into the sample surface, so objects below the surface can be observed. This technique is called cross sectioning [215]. In addition SIM / SEM imaging or further analytical methods can be employed.

The requirements for these Instruments are quite similar: high process speeds, short cycling times, high level of automation, capability to handle samples of various sizes and additional less destructive imaging capabilities to the inherent ion microscopy ones (comp. section 7.1).

As a result the general tool set-up is similar for both groups of tasks: The instruments use a Ga liquid metal ion source (comp. chapter 4). They are equipped with charged particle optics (CPO, comp. section 5.1) columns optimised for high ion beam probe currents (comp. chapter 3) above 1nA. This enables high process speeds. In addition the stage driving time between

tasks is kept small by positioning stages with high travel speeds (>>10mm/s). Fast automated load lock systems ensure short cycle times. The software in FIB instruments (comp. section 7.3.2) has four major tasks: first interface the instrument hardware (adjust lenses, stigmator, vacuum control...), second carry out imaging of the sample surface, third design basic features and fourth pattern them with constant etch/deposition rates [178]. In addition instruments for industrial applications have reached a high level of automation for some tasks, by dedicated software routines. They render processes more reproducible and minimise operator interaction, however operator intervention is still required from time to time: "... automated job, sequencing to ensure maximum tool use with minimal operator intervention" [216]. In addition tasks requiring a reproducible process stop apply an automated "end point detection" function.

As many semiconductor companies have 200 and 300 mm processes lines, the FIB instruments require optional front-end modules designed to simultaneously handle 200mm and 300 mm wafers.

The scanning ion microscopy capabilities are required for the instrument set-up, but alter the scanned surface areas (comp. section 7.1), therefore these instruments have a need for a less destructive navigation, process control and visualisation capability. This can be either realised by an accurate position sensing, high reproducibility of the stage position (comp. section 7.2) in combination with light optical imaging (OptiFIB-IV [217]) or more commonly by an additional integrated high resolution scanning electron microscope. The software is used to focus the beams, take images, design features on the image and pattern them with constant etch/deposition rates.

Differences in the tool set-ups arise for gas processing (comp. section 6.2.3) e.g. in circuit edit a gas injection system is required. In failure analysis further detectors can be added e.g.: in-situ scanning transmission electron microscopy (STEM) or Auger analysis. Finally, applications like in-situ 3 dimensional imaging have a need for 5 axis tilt eucentric positioning stages, they keep the feature of interest in the centre of the image when the positioning stage is tilted or rotated.

Commercially available circuit edit instruments are: the already mentioned OptiFIB-IV [217] and V600CE [218] or failure analysis ones: Expida Family (FEI), Certus 3D Wafer DualBeam (FEI), CLM 3D (FEI), Defect Analyzer 3000 HP (FEI), JFS-9855s (Jeol), XVision 300 (Seiko, Zeiss) [219].

7.3.2 Further applications and a versatile instrument class

Various analysis, material removal, deposition, injection of surface modifications and pattering applications are carried out also in many nanotechnology R&D labs using a versatile FIB instrument. Further details about mainstream applications can be found in e.g. [44] [152] [134] [11] [156] [194]. An exemplary wide spread application of this instrument class is also TEM lamella preparation (comp. section 7.3.1).

They can be equipped with two charged particle columns (FIB and SEM), for similar reasons as described above (comp. 7.3.1). The SEM one is usually assembled on the top and the FIB one at an angle to the vacuum chamber ceiling. The positioning stage can be tilted to have e.g. 90° incident of the electrons or the ions. These instruments offer a high versatility for all kinds of different patterning and analysis applications. The Ga LMIS beam columns can be the same as in some of the instruments for industrial applications (comp. section 7.3.1) or especially optimised ones for a high instrument resolution (comp. section 5.1). In many R&D applications the latter one is of higher importance than process speed. In addition they are equipped with a raster scan electronic for analysis and patterning purposes. Imaging employs a SE detector. For further analysis applications the appropriate detectors can be attached. The software in versatile FIB instruments carry out the same four major tasks as described above (comp. section 7.3.1). Some patterning tasks can be automated. Further on the instruments can be complemented by “lithography attachments” (dedicated pattern generator plus software) for more demanding and unattended batch nano patterning tasks. These systems can be equipped with sample manipulation stages of various sizes depending on the applications.

Commercially available instruments are e.g.: FEI Helios Family (5 nm, FIB instrument resolution, comp. section 5.1) [174], Seiko Zeiss (4 nm) [173], Zeiss Auriga (<2.5 nm) [220] and the Tescan Lyra (<5 nm) [221].

Usually the only -ion beam relevant- acceptance test is to proof the instrument analysis resolution (comp. section 5.1), shown by imaging on “ideal samples” in the SIM mode (comp,. section 7.1).

These systems enable the users to explore a large variety of analysis and patterning application fields and develop processes. In addition all of the industrial applications above can be carried out, but the versatility can sacrifice the automation level, however none of the currently commercially available FIB instruments is comparable to an electron beam writer (comp. drawback VII in section 7.2).

7.3.3 Patterning applications of gas field ion sources (GFIS)

As described in section 4.2.1 a new source technology has been developed. So far this technology has been mainly employed for analysis purposes [107].

Winston et al. [109] and Sidorkin et al. [110] have connected a pattern generator to this He ion microscope and have carried out patterning experiments. The first one has reached down to about 6 nm dot diameter and the second one to below 20 nm pitch in hydrogen silsesquioxane (HSQ) resist (comp. section 8.4 I). In addition Winston has published promising results employing Ne ions in the same instrument [222]. All three prove the promising capabilities of this technology enlarging the variety of employable ions (comp. section 6.1.8 for standard LMIS) for high resolution applications. However, the technology "is still in its infancy" and will need some time to be able to fulfil demanding unattended batch nano patterning applications.

7.3.4 Electron beam lithography (EBL) writers

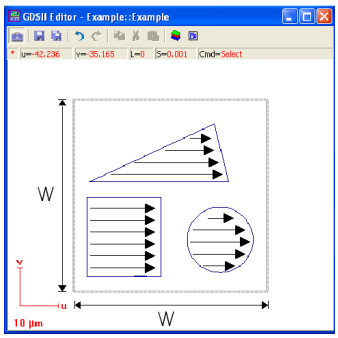

Marrian (comp. drawback VII in section 7.2) has meant ultra high resolution Gaußian beam vector scan electron beam lithography (EBL) instruments e.g. [56], when he has written: "... the available tooling is much more sophisticated..." [69] (comp. section 7.2).

Figure 26: Sketch of the vector scanning process and a write-field of edge length (w)

The history of the EBL instruments is summarised in section 2.2.2. Their general set-up is similar to the ion beam instruments above (comp. chapter 3 and section 7.3), but they are equipped with only one high end charged particle optics (CPO, comp. section 5.1) column. During the patterning process there is no need for live visual process control. This column is assembled at the top of the chamber with 90 degree incident electrons onto the sample surface. These columns are optimised for maximum instrument resolution (comp. section 5.1) at reasonable probe currents (e.g. < 2 nm at about 170 pA for 20 kV [223]), linear and calibrated write fields (field of view, ≥50 µm, comp. Figure 26) with little beam shape as well as size deterioration away from the optical axis.

The electron source is optimised for long term beam current stability and the instruments offer a selection of possible probe currents matching the application, e.g. optimised for a high application resolution (comp. section 5.2), a low one for sensitive processes, ... This is usually done with the assistance of an automated beam defining aperture (comp. section 5.1.2) exchanger. If the suitable one has been selected, it will be employed for a certain patterning period.

The software in versatile FIB instruments (comp. section 7.3.2) has four major tasks (comp. section 7.3.1), with some process automation capabilities. However, EBL writers offer an additional fifth one: program and execute complex unattended computer aided design (CAD) based patterning sequences, including the necessary machine parameter control loops (e.g.: probe current, focus, dose,... comp. above), sometimes with the capability to design and store CAD patterns.

If a pattern design (CAD structure) exceeds one write-field, the instruments stitch. Stitching requires a laser interferometer position sensing. During this procedure the design is automatically cut into sub structures of one write-field. Then the content of the first one will be patterned at the desired position, followed by a stage movement to the next position, here a second write-field will be patterned and so on. Finally, complex and unattended batch nano structuring sequences can be programmed. E.g. patterning sequences “over night” or “over the week end” can be set up, these can cover large areas well above one write-field. During the patterning sequence different tool settings (e.g. probe current and size) can be employed suiting different patterning requirements.

EBL writer stages possess a high positioning reproducibility, allowing multi level patterning on top of existing patterns, generated by this or by other instruments: EBL, imprint or optical lithography (comp. section 2.2). The stage is driven with the accuracy of the laser interferometer position sensing to the desired sample position and an automatic mark recognition sequence including write-field recalibration is carried out.

Since future device characteristic research is carried out in semiconductor R&D sites, the stage travel range can be up to 300 mm (12” wafer capability), so semiconductor production lines R&D wafers can be partially patterned with the R&D instrument and otherwise be processed in the normal production line [224]. In addition the instrument design has to take care for the beam position stability.

Long term unattended operation requires control and feedback mechanisms:
The area dose is an important EBL process (control) parameter. It is proportional to the probe current (I_p), point dwell time (T_d) and inverse proportional to the square of the "step size" (comp. section 6.1.9). Therefore the beam current is measured accurately before (and optionally also during) the patterning process with the implemented pico-amperemeter. Taking the preselected patterning grid step size, the control computer calculates from this information the appropriate parameter for the 16 or more bit digital pattern generator (PG). These ensure the desired feature doses by adjusting the point dwell time (comp. section 6.1.9). In addition the interferometer position signal fed into the computer is employed for write-field alignment (calibration) and absolute stage position information. The computer and PG take also care for patterning (vector scanning, comp. Figure 26), as well as position, focus and stigmator corrections employing the corresponding sensor information. The instruments can be equipped with a height sensing system keeping the sample surface in focus over the sample area of interest.
These measures ensure the selected feature doses on the sample surface, an equidistant exposure grid, pattern placement accuracy, constant electron probe size and shape within the patterning field (write-field) over long periods (hours).
Due to the higher accuracy and long term stability demands of EBL writers compared to versatile FIB nano analytics and pattering workstations (comp. section 7.3.2), the acceptance test relevant specification list (which has to be proven at the customer site) includes more than just the instrument analysis resolution (comp. section 7.3.2 and 5.1): instrument patterning resolution, beam current stability, position stability, stitching accuracy and multi level pattern placement accuracy (for details comp. section 8.2).
Exemplary manufacturer are: [225] [226] [227] [228] [229].

7.4 Summary

Although the large variety of ion-matter interactions (comp. section 6.1.8) open fascinating patterning opportunities and Seliger has proven the practical feasibility of resist exposure already in 1973 [86] [87], still only a very few interactions are routinely employed: Ga^+ ions carry out milling (comp. section 6.2.1) and gas assisted processing (comp. section 6.2.3). The interest for patterning besides these two interactions has even declined since about the middle

of the 1990s until about the year 2004. It appears that the expectations in lateral nano patterning technologies have not been satisfactorily met so far. Reasons for this are: the encountered drawbacks, the little number of R&D instruments, the large commercial interest in only a few of the interactions and that EBL development started at least a decade before [203]. There have been attempts at the end of the 1980s e.g. [10], to create ion beam instruments similar to EBL writers, but for the described reasons, the nano research community hasn't accepted it as a routine tool and technique.

Commercially available ion beam tool concepts are either optimised for certain applications or versatile and multi purpose FIB instruments. The first category can reach a high degree of automation for these applications and the second ones offer many options for studying all different kinds of analysis or patterning applications. However, they have the need for operator attendance during the patterning sequence [216] and are limited in functionality as well as automated control and feedback mechanisms for long term unattended batch patterning.

However, since about 2004 the commercial interest, increased need for nano analysis and growing funding for nanotechnology research has led to a wide spread of these instruments within the nano research community. As a result some groups try again to use the technology for nano patterning e.g. [210] [198] [211]. In addition promising results from gas field ion source instruments prove the feasibility of ion nano patterning.

8 An ion beam complement to EBL writers

In 1988 Ochiai has published development results employing a similar instrument architecture [10], however it has not been accepted by the research community for various reasons (comp. section 7.2). Here a new ion beam nano patterning instrument (comp. Figure 28) is introduced, resembling more an electron beam writer with an ion beam than the focused ion beam (FIB) tools described in section 7.3.1 and 7.3.2.

The instrument is meant to facilitate systematic studies of ion-matter interactions for nano patterning applications. The development roots of this instrument are summarised in section 12.3.

8.1 System architecture (set-up)

Electron beam (EBL) writers (comp. section 7.3.2) possess a different tool architecture than e.g. versatile FIB instruments (comp. section 7.3.4), although the fundamental set-up is similar (comp. section 7.3).

During the "NanoFIB" project the team (comp. section 12.3) has exploited its complementary know-how (comp. section 12.3) to create a proof of concept tool of an ion beam complement to EBL writers and to explore patterning applications (comp. chapter 9, 10 and section 12.4,8.4) [13]. It has been partially funded under the fifth framework EC growth program (Contract G5RD-CT2000-0034, 2001-2004).

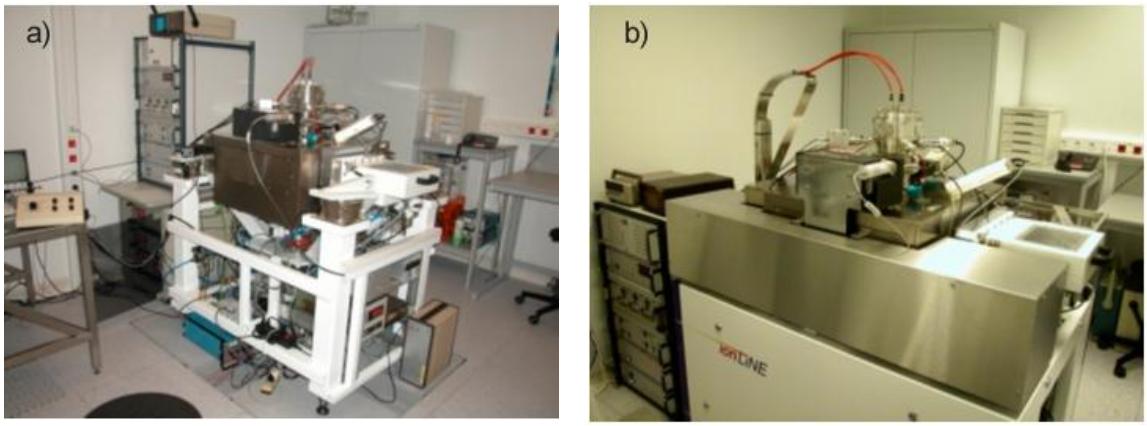

Figure 27: „NanoFIB" proof of concept tool a) 2003 and b) 2010 (LPN CNRS Marcoussis, France)

After the EC funding period the Raith GmbH with the assistance of the LPN CNRS has converted it into a product called ionLiNE [230].

This instrument shares the general system architecture, software and many elements with EBL writers and nano engineering workstations manufactured by the Raith GmbH. The tool is equipped with a single high end LMIS column (<10 nm @ 5 pA, comp. section 7.3.4). The 90° angle of incidence allows to operate at small working distances (WD), so a high demagnification, lower spherical and chromatic aberrations for the same charged particle optical set-up (column) are possible (comp. section 5.1.2 and 5.1.6, respectively). It is optimised for calibrated write fields ≥50 µm (field of view, comp. section 7.3.4).

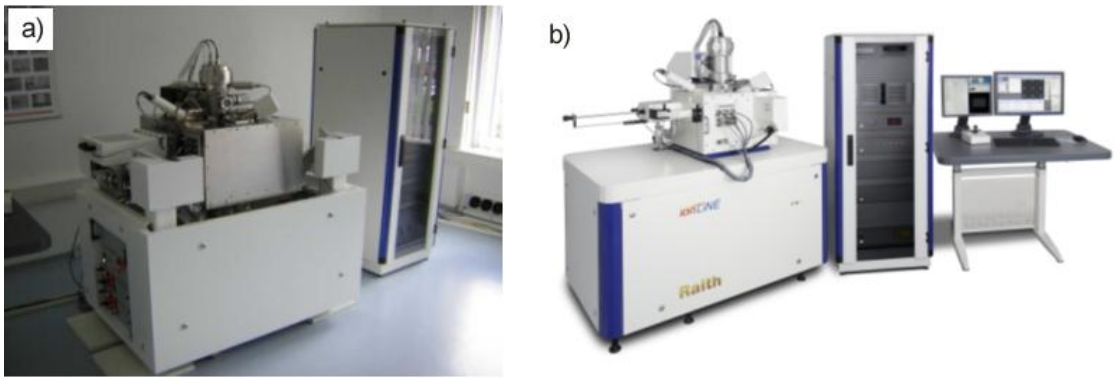

Figure 28: a) ionLiNE beta tool 2005 and b) final product 2009 (both Raith GmbH)

The successor at LPN CNRS inside the "Orsay group" (comp. section 4.3) J. Gierak has participated in the development of this instrument, they patented the refined NanoFIB technology [231]. It enables high beam currents in small patterning probe sizes and a long term beam current stability by employing a dedicated Ga LMIS [117], compared to the conventional technology (comp. chapter 4).

The software has the same five major functions as the one employed for EBL writers (comp. section 7.3.4 and 7.3.1). If structures are larger than one write-field, our instrument allows two different modes depending on the application. One of them is called stitching (comp. section 7.3.4) and the second one is called fixed beam moving stage (FBMS). Both require moving the sample stage with a high resolution and reproducible position sensing e.g. realised by a laser interferometer feedback. The second mode does not cut the CAD structure into individual write-fields. Here CAD elements extending write-field borders are continuously structured, whereas stage driving inaccuracies are constantly corrected by the beam. In addition multi days complex unattended batch nano structuring sequences can be programmed within a task list (comp. Figure 29 and section 7.3.4).

The beam generation allows together with the software a programmed, automatic selection of the desired beam current by changing the beam defining aperture (comp. section 5.1.2 and 7.3.4), in addition the instrument is equipped with an accurate beam current measurement system (comp. section 7.3.4). This enables an employable dose range from about 10^{12} to 10^{18} ions/cm^2 (comp. Figure 20) for nano patterning applications.

All control and feedback mechanisms available in Raith GmbH's EBL writers have been implemented into this instrument (comp. section 7.3.4).

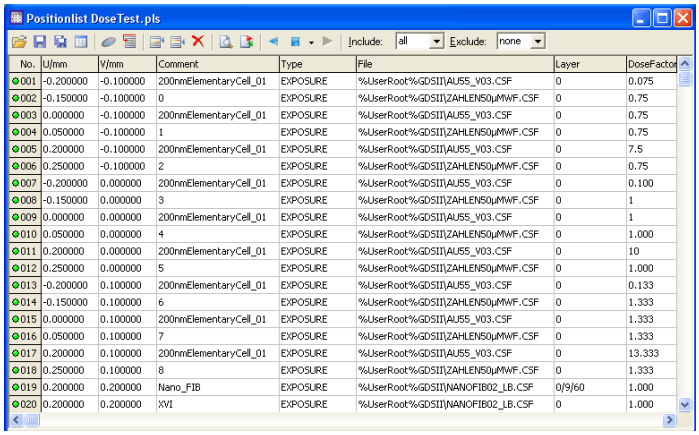

No.	U/mm	V/mm	Comment	Type	File	Layer	DoseFactor
001	-0.200000	-0.100000	200nmElementaryCell_01	EXPOSURE	%UserRoot%GDSII\AU55_V03.CSF	0	0.075
002	-0.150000	-0.100000	0	EXPOSURE	%UserRoot%GDSII\ZAHLEN50µMWF.CSF	0	0.75
003	0.000000	-0.100000	200nmElementaryCell_01	EXPOSURE	%UserRoot%GDSII\AU55_V03.CSF	0	0.75
004	0.050000	-0.100000	1	EXPOSURE	%UserRoot%GDSII\ZAHLEN50µMWF.CSF	0	0.75
005	0.200000	-0.100000	200nmElementaryCell_01	EXPOSURE	%UserRoot%GDSII\AU55_V03.CSF	0	7.5
006	0.250000	-0.100000	2	EXPOSURE	%UserRoot%GDSII\ZAHLEN50µMWF.CSF	0	0.75
007	-0.200000	0.000000	200nmElementaryCell_01	EXPOSURE	%UserRoot%GDSII\AU55_V03.CSF	0	0.100
008	-0.150000	0.000000	3	EXPOSURE	%UserRoot%GDSII\ZAHLEN50µMWF.CSF	0	1
009	0.000000	0.000000	200nmElementaryCell_01	EXPOSURE	%UserRoot%GDSII\AU55_V03.CSF	0	1
010	0.050000	0.000000	4	EXPOSURE	%UserRoot%GDSII\ZAHLEN50µMWF.CSF	0	1.000
011	0.200000	0.000000	200nmElementaryCell_01	EXPOSURE	%UserRoot%GDSII\AU55_V03.CSF	0	10
012	0.250000	0.000000	5	EXPOSURE	%UserRoot%GDSII\ZAHLEN50µMWF.CSF	0	1.000
013	-0.200000	0.100000	200nmElementaryCell_01	EXPOSURE	%UserRoot%GDSII\AU55_V03.CSF	0	0.133
014	-0.150000	0.100000	6	EXPOSURE	%UserRoot%GDSII\ZAHLEN50µMWF.CSF	0	1.333
015	0.000000	0.100000	200nmElementaryCell_01	EXPOSURE	%UserRoot%GDSII\AU55_V03.CSF	0	1.333
016	0.050000	0.100000	7	EXPOSURE	%UserRoot%GDSII\ZAHLEN50µMWF.CSF	0	1.333
017	0.200000	0.100000	200nmElementaryCell_01	EXPOSURE	%UserRoot%GDSII\AU55_V03.CSF	0	13.333
018	0.250000	0.100000	8	EXPOSURE	%UserRoot%GDSII\ZAHLEN50µMWF.CSF	0	1.333
019	0.200000	0.200000	Nano_FIB	EXPOSURE	%UserRoot%GDSII\NANOFIB02_LB.CSF	0/9/60	1.000
020	0.200000	0.200000	XYI	EXPOSURE	%UserRoot%GDSII\NANOFIB02_LB.CSF	0	1.000

Figure 29: Exemplary dose test task list

As a result it can carry out similar tasks like EBL writers, e.g. the stage's positioning reproducibility allows multi layer processing on pre patterned samples (comp. section 7.3.4). In addition the high resolution position sensing (comp. above), optical imaging capability and sample ("wafer") navigation, enables easy "blind" sample movements without unintendedly destroying surface areas by ion microscopy (comp. section 6.2.1, 7.1 and Figure 30).

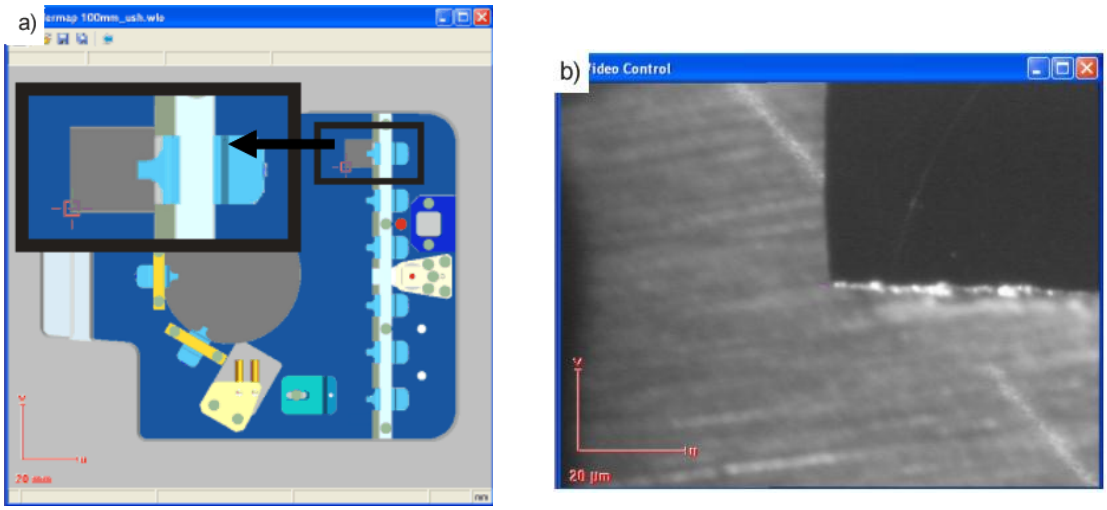

Figure 30: Exemplary: a) sample holder map, b) optical image allowing navigation and accurate pattern placement (the cross indicates in both pictures the centre point of the ion microscope (SIM) image's field of view, magnified area has been pasted into the image a)

Finally, our instrument has to pass specific stability and accuracy specifications similar to those for EBL writers (comp. section 7.3.4).

8.2 Instrument specifications and exemplary results

For our tool more specification relevant tests -similar to EBL writers (comp. section 7.3.4)- than for FIB systems (comp. section 7.3.1 and 7.3.2) or scanning electron microscopes (comp. section 2.1.2) are carried out: analysis resolution, patterning resolution, FBMS continuity and evenness, beam current stability, position stability, stitching accuracy and overlay accuracy. They are used to proof multi hour unattended batch nano fabrication capabilities and exemplary patterning resolution. It is common to optimise the beam profile for the desired target application and judge it by the final result. This is because the exact beam profile of high resolution charged particle optic (comp. section 5.1) instruments is difficult to determine, it relies on set-up parameters (e.g. focus) and the optimum can vary depending on the application (both comp. section 5.1.8 and 5.2). As a result in an acceptance test exemplary material systems and processes are selected to demonstrate the imaging and patterning resolution (comp. chapter 5) capabilities.

The first one is the instrument analysis resolution (comp. section 5.1) proven in the scanning ion microscope mode (comp. section 7.1). It is similar to those carried out on FIB systems (comp. section 7.3.2) or scanning electron microscopes (comp. section 2.1.2).

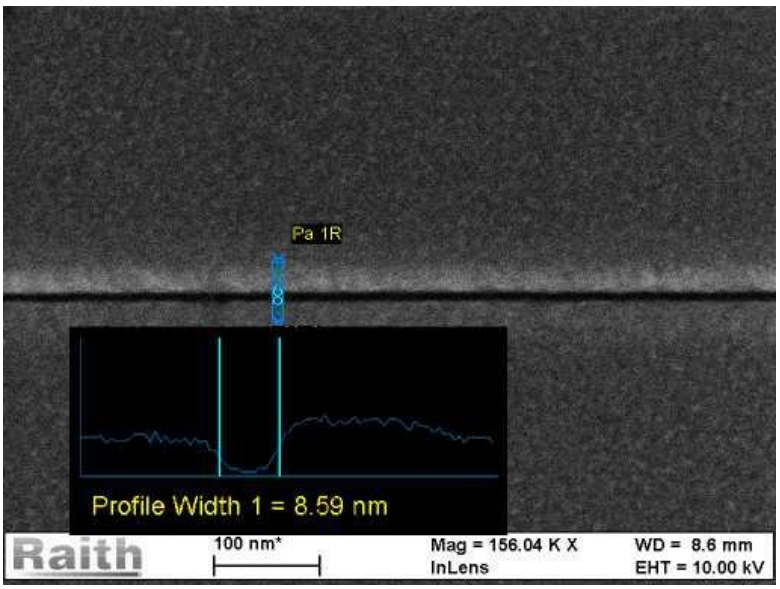

Figure 31 Exemplary etched line Cr (10 nm) on Si substrate (profile width measurement enlarged)

The instrument patterning resolution (comp. section 5.1) is a further one. Here a narrow line is milled (comp. section 6.2.1) into a thin Cr layer on a Silicon substrate within one write-field. In addition to the instrument patterning resolution within one write field, the continuity and evenness is measured after a patterning sequence in FBMS mode (comp. section 8.1): e.g. a 1 mm line is milled into an approx. 10 nm thick Cr layer on a Si substrate. The width of the line is measured at various locations.

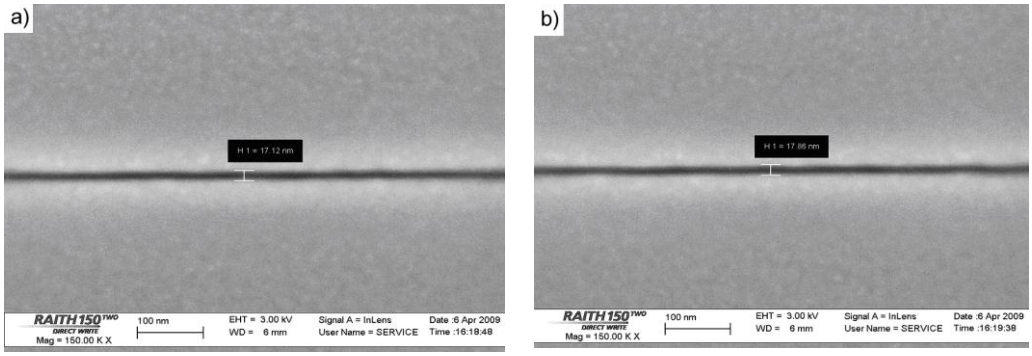

Figure 32: Exemplary SEM images of a 1mm FBMS line at a) 200 and b) 400 µm away from the start

The beam current stability is shown measured in the following way: The instrument operates more than 8 hours and the beam current is measured every 15 min with the aid of the implemented dedicated beam current measurement system.

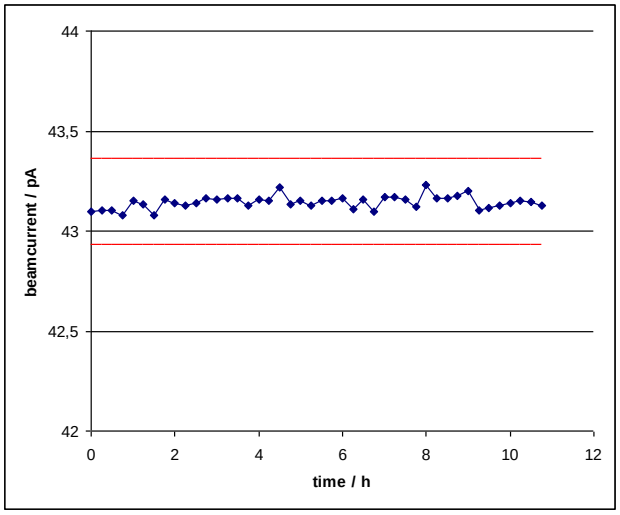

Figure 33: Exemplary beam current stability measurement result, (35 kV, every 15 minutes, red lines indicate ±0,5% around 43.15 pA)

The position stability is verified by checking how much the position of a feature of interest varies relative to the ion beam. The stage is driven to a mark position and the laser interferometer control keeps this position during the test. Every 15 min the mark position is registered by the automatic mark recognition capabilities for more than 8 hours.

In addition a stitching accuracy test (comp. section 7.3.4) is carried out: A multitude of write-fields are stitched together to create a pattern extending one field of view. Later on the pattern placement accuracies at stitch field borders are registered.

Finally, the multi level pattern placement (comp. section 7.3.4) accuracy is observed. The placement deviation of the second layer patterning process step with respect to the first one is detected.

8.3 Instrument architecture related application

We take a quick look at an exemplary application proofing the instrument stability over more than 15 hours during live patterning and that the instrument architecture is adequate. The milling ion-matter interaction (comp. section 6.2.1) is exploited to generate an x-ray zone lens on a silicon nitride membrane with a simple single step process [7]. The device has been milled over more than 15 h unattendedly incl. automated multiple position recalibration steps (comp. Figure 34b). The outer zone lens posses a patterned (milled) width of 100 nm.

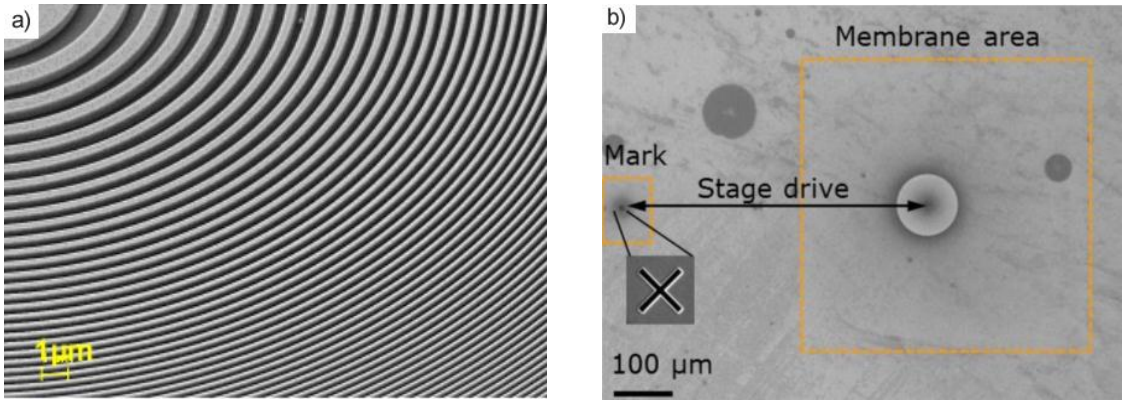

Figure 34: SEM micrographs a) showing a 45° tilted view of the zone plate: inner zones (Fig 3a in [7]), b) showing the silicon nitride membrane with active area including gold zone plate and position of reference mark for automatic positioning correction on bulk sample Fig. 1 in [7]

8.4 Overcoming the drawbacks

The development goal of our instrument has been to facilitate systematic explorations of ion-matter interactions (comp. section 6.1.8) for nano patterning applications.

On one hand there exists matured and established instrumentation with the related process know-how. Examples are: resist patterning by EBL writers (comp. section 7.3.4); gas assisted processing in circuit repair (comp. section 7.3.1) by electron beam [232] or FIB and further patterning technologies (comp. section 2.2). If these and similar ones will be studied with our instrument, some disadvantages (comp. section 7.2) remain. This is because our instrument is based on LMIS technology and they are inherent to carry out these applications especially employing Ga, in the linear cascade regime (comp. section 6.1.4).

However, on the other hand there are unsolved nano patterning challenges e.g. for 3D applications or complicated and unsatisfying results employing matured instrumentation and processes. In addition more than about 25 years have past since most of the drawbacks have been reported and the ion beam nano patterning enthusiasm has declined (comp section 7.2). During this time much complementary know-how has been accumulated in the research community, so there might now exist solutions for the 3 inherent drawbacks (discontinued lines, incident ion residuals, impossible thick resist exposure). For them we will present the current status and suggestions how to avoid these or mention the alternatives.

I. discontinued lines (comp. section 7.2 I)

If organic resists exposure will be studied with our instrument, the discontinued lines phenomenon is still present, depending on the selected resist and the applied dose. However, Matsui has already figured out in 1986 that the actual dose value at which the phenomenon occurs depends on the resist [136] (comp. section 7.2). After about 25 years of resist development, it makes sense to study a modern insensitive high resolution one like hydrogen silsesquioxane (HSQ). The experiments, results and their discussion are described in section 10.1.

Alternatively the etch resistance against reactive ion etching of an organic resist at the surface could be rendered by ion bombardment, “surface imaged resist” [203] [211].

Nevertheless, on one hand pure resist exposure by ion beam lithography (IBL) will always be faced with an about 40 years longer history and experience of EBL resist processing,

especially as the resists experiments above have not led to a technology breakthrough. On the other hand combining technologies to carry out fast final feature size enhancement or modification of resist patterns could be a useful complement [187] [233]. An example of a high resolution modification combined with an accurate feature overlay can be seen in Figure 35.

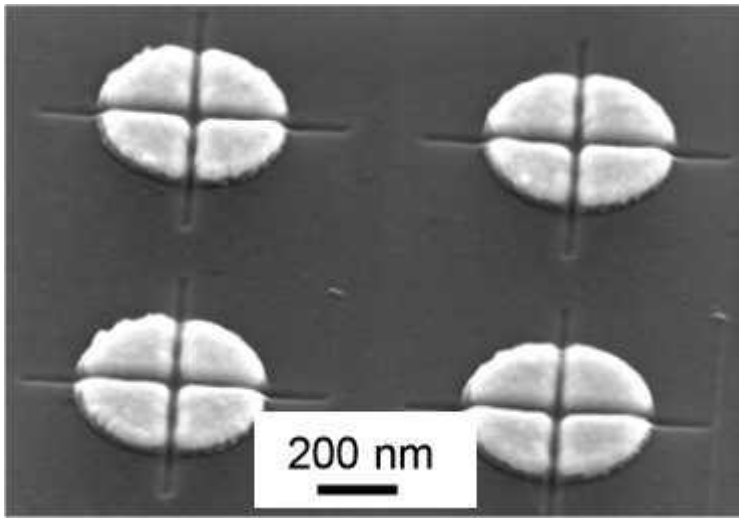

Figure 35: “SEM images of the through-cuts of Au-nano-particles by lines about 17 nm wide with IBL: “a slanted view” (Fig. 2a in [234])

II. incident ion residuals (comp. section 7.2 II)

The “drawback” that a part of the incident ion species (mostly Ga) is left behind, is still present with our instrument. It is again inherent to this ion beam technology. For some nano patterning applications it doesn’t matter, for others it is even wanted (e.g. local doping, [205], [235]), especially if different incident ion species could be employed [236] [237] (comp. section 6.1.8). Then the incident ion species could be tailored fitting to the material system and application of interest. Direct patterning with the desired ion species could significantly reduce process complexity compared to established techniques for some applications (comp. section 9.2 for the application and 6.2.2 for the ion-matter interaction). In addition for applications like atom intermixing (comp. section 6.2.2) or during resist exposure [203] the process can be set-up in a way that the incident ion species is mostly left behind inside the sacrificial layer. However, if it is really destroying the target application one of the established lateral nano structuring techniques (comp. above) might be the better choice.

III. impossible thick resist exposure (comp. section 7.2 III)

Shorter ranges and smaller interaction volumes (comp. section 6.3.3) of heavy ions require thin resists. This remains true also for our instrument as long as heavy ions like Ga^+ are employed (comp. section 6.3.1), but patterning transfer techniques are maybe an option (like lift-off, sacrificial layers,...). If nano structuring can only be done using thick resists, EBL (>1 kV) is usually more appropriate. However, the large variety of ion-matter interactions (comp. section 6.1.8) allow also patterning which can exploit this small interaction volume as an advantage (comp. 6.1.8 and 6.3) or -like suggested above- further incident ion species could be employed (comp. section 6.1.8), to tailor the interaction volume (comp. section 6.3.1, e.g. Figure 21).

Our new instrument allows different work flows compared to conventional FIB systems (comp section 7.3.2 and 8.1), which enables the users to overcome the following four reported disadvantages:

IV. impossible marks detection below thick resists (comp. section 7.2 IV)

Marks cannot be seen below a resist layer. This is a consequence of the short interaction volume (comp. section 6.3.3). On one hand another ion-matter interactions could be exploited (comp. section 6.1.8), instead of employing ion beam resist technology, to avoid this challenge. On the other hand the high precision sample manipulation of our instrument allows to drive “blindly” to a mark position (comp. section 7.2 and 8.1) without unintendedly destroying or modifying sample areas of interest. Then first the resist layer (automatic blind milling, comp. section 6.2.1) could be removed (by milling), followed by an automatic mark recognition procedure [187].

V. damage (comp. section 7.2 V)

In nano patterning applications the sample areas assigned for ion beam irradiation can usually not be imaged with the ion beam in advance.

A reason for this can be that the process is too sensitive to ions. Then even a single image scan would alter the complete surface properties of the image area (field of view) in an

unintended way. Another reason might be that the inherent sputtering interactions of e.g. Ga^+ ions (comp. section 6.2.1 and 7.1) could remove necessary surface layers.

Our instrument architecture overcomes this challenge by the system's high precision and reproducible sample manipulation (comp. section 7.2), in combination with a sample (wafer) navigation software and an optical imaging capability (comp. section 8.1 and Figure 30).

VI. accurate dose control (comp. section 7.2 VI)

Our tool shares the instrument architecture and software with our EBL writers, so the same precise beam current measurement and dose control mechanisms as well as control loops are available (comp. section 8.2).

VII. "... the single-most reason..." [69] (comp. section 7.2 VII)

As described above the instrument shares the architecture with Raith GmbH's EBL writers (comp. section 8.2), so it fulfils the requirements for nano pattering.

8.5 Summary

We have managed to create an ion beam complement to electron beam writers for nano patterning including a dedicated acceptance procedure dedicated to proof the patterning capabilities. In Figure 34a) patterning result has been presented which used the more than 15 hours instrument stability. Further successful application examples will be presented in chapter 9 and 10 as well as in section 12.4.

The status of the reported ion pattering drawbacks (comp. section 7.2 and 8.4) employing our instrument have been explained. It has revealed that some important ones can be overcome by the tool's concept, others maybe by the additionally gained know-how since the middle of the 1990s. An example is the technology improvement in resists (comp. section 10.1).

Nevertheless, some drawbacks are inherent especially to Ga ion-matter interactions, for these alternative routes have been proposed.

Finally, we can offer a new tool facilitating to study systematically the large variety of ion-matter interactions for nano patterning applications (comp. section 6.1.8).

The following two chapters describe application fields our project team and application partners have been exploring using this instrument technology.

9 Exemplary accessible applications

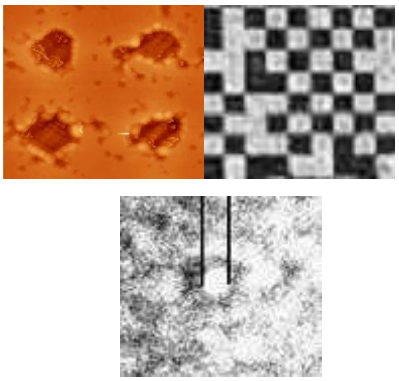

In addition to the creation of zone lenses and feature modification (comp. section 8.3 and 8.4, respectively) the team has studied many different applications (comp. section 12.4), employing our instrument technology. In our experiments we have exploited also additional ion-matter interactions to the two current main stream ones (sputtering and gas assisted processing, comp. section 7.3).

Three process examples will be described in more detail, visualising the nano patterning possibilities for ion beam technology. Examples one and two are the exploitation of two non main stream ion-matter interactions: atom intermixing (comp. Section 6.2.2) and intended local surface modifications (comp. section 6.2.1 and 6.2.2). The third example is a refinement of the classical ion-matter interaction called sputtering (comp. section 6.2.1). The desired results have been achieved by applying doses from all 3 regimes described in section 6.1.9.

9.1 A material for fast processing / surface modifications (low dose)

Volume production of nm minimum feature size electronic or optical devices require high resolution (currently <30 nm) in combination with fast and reproducible processing. Researchers look for nano fabrication techniques to complement existing ones or establish new ones. Today most volume electronic device fabrication in the semiconductor industry Is carried out by optical lithography as main lateral pattern definition technology (comp. section 2.2.1). Some advantages and disadvantages have been described in section 2.2.1. In R&D a large amount of lateral nano pattering is carried out by EBL (electron beam lithography 2.2.2 and 7.3.4), exemplary advantages and disadvantages have been described in section 7.3.4, 9.3 and 9.2.

HOPG (highly oriented pyrolyitc graphite) in combination with an oxidation process is extremely sensitive to ion bombardment. Already about ten Ar^+ ions at 1 kV can create a relevant modification of the surface atomic order [238]. This is similar for Ga^+ ions at 35 kV [199]. The exploited ion-matter interaction is surface modification (comp. section 6.2.2). Relevant HOPG surface modifications oxidise at lower temperature than surfaces without treatment [239]. Non patterened perfect HOPG is not oxidised, it will only oxidise at step edges and surface modifications, with for example broken sigma bonds [240]. The oxidation process which follows the ion interaction process step exploits this.

Ghaleh differentiates between two ion dose regimes: “nano pits” and “nano cavities” (> 3.4 nm but before material removal by milling (comp. section 6.2.1) [240]. The nano pit ones are only a single surface layer deep. Different depth steps occur, because a certain minimum ion dose (about 10^{15} ions/cm^2 [199]) exists which extends the oxidation below the surface layer. For lower ion doses only the surface modifications in the first monolayer react with the oxygen, though atomic disorder is also produced in layers below. In addition process control is rather difficult for the nano pits at very low doses, as the source current might is not be stable enough at this level (comp. section 4.4) further on not every ion induces a relevant surface modification at the first mono layer, so the oxidation result possesses a significant statistical contribution.

In these examples dots have been patterned applying different doses followed by an oxidation process [199] [240].

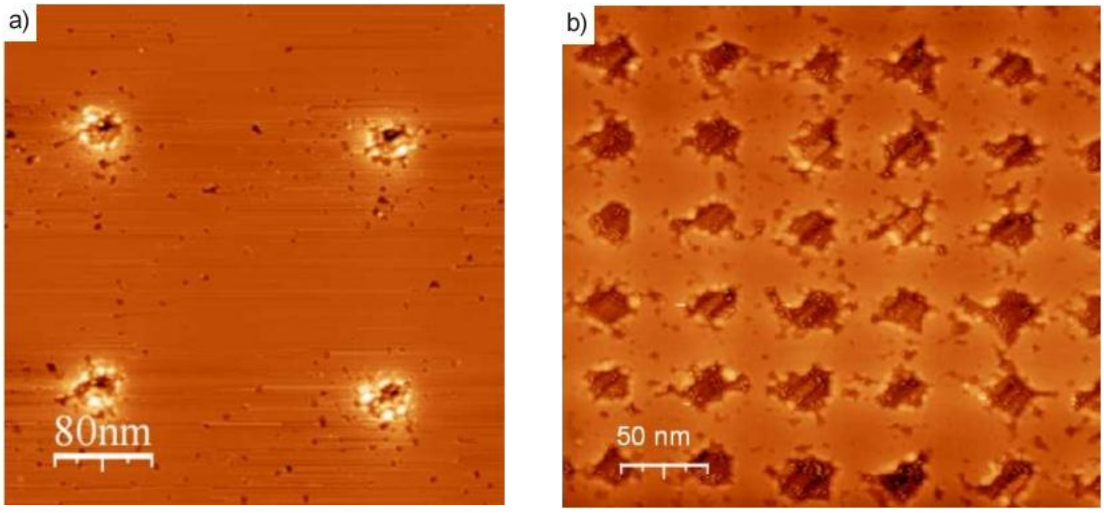

Figure 36: UHV STM micrographs of HOPG patterned by a Ga ion beam, after oxidation, resulting in:
a) sub 30 nm 2d resolution (ion dose 1870 ions/point) [240]
b) 50 nm period (ion dose $4 \cdot 10^{14}$ ions/cm^2 = 1963 ions/point assuming 25 nm diameter) Fig. 4 in [199] [240]

The results (comp. Figure 36) demonstrate the potential of this technique: nanometer size features (<30 nm) with down to 50 nm period. It is a direct lateral nano patterning technique without the need for intermediate media (resist, metallisation, RIE). Features like the ones displayed in Figure 36 could be filled with another material to create e.g. electronic devices [240].

These “nano cavities” belong to the low dose regime (comp. section 6.1.9) as only about 2000 ions ($4 \cdot 10^{14}$ ion/cm^2, assuming a 25 nm diameter) are required to form an about 25 nm diameter hole.

The results have encouraged the group to continue the collaboration and studies [241].

9.2 High density magnetic data storage / atom intermixing (medium dose)

Magnetic hard disks with larger data storage capabilities but same or smaller hardware dimension can be achieved by increasing the data density (bits/mm^2). As a result nano patterning processes are required to fabricate small single magnetic domain areas as 2D discrete media with perpendicular anisotropy [242].

This can be done by conventional lateral nano patterning techniques like EBL followed by a pattern transfer [243] or self assembling [244]. An advantage of the first one is the freedom in

feature shapes and position on the sample, whereas a disadvantage is the process complexity (pattern transfer). For the second process the advantages are the reported feature size down to 3 nm and the potential patterning speed for volume production purposes. However, self assembly conditions are sometimes difficult to create at sample positions of interest and it's difficult to tailor feature shapes.

Ion irradiation can locally alter magnetic properties of ultra thin magnetic films, down to the nm scale [245]. Depending on the ion dose the surface properties can be tailored from ferromagnetic with reduced coercitivity to paramagnetic [245] [242]. In the presented results, the ion beam has been employed to create domain walls (comp. Figure 37b).

The ion-matter interaction responsible for this is called atom intermixing (comp. section 6.2.2). During the ion irradiation atoms from the substrate and incident Ga^+ ions are mixed into the thin magnetic film. This alters locally its magnetic properties. The material composition has been: Pt(3.4 nm) / Co(1.4 nm) / Pt(4.5 nm) grown on transparent Al_2O_3(0001).

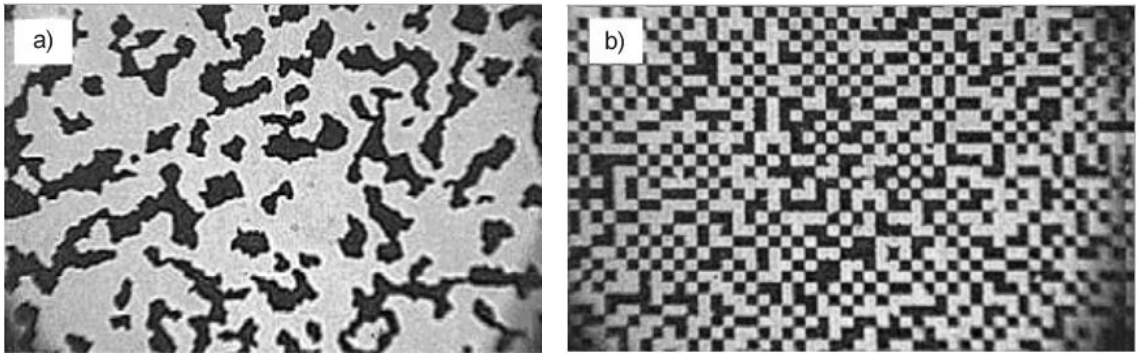

Figure 37: Magneto optical image of a thin line array patterned by Ga:
a) $2 \cdot 10^{13}$ ions/cm^2 and
b) with $2 \cdot 10^{16}$ ions/cm^2 Fig. 2 in [245]

Advantages of this technique are the process simplicity ("single step") and the freedom in feature shape and position. However, for volume production the over all process is usually slower than a self assembly processes.

The employed dose for this application ($6.3 \cdot 10^4$ ions/point, assuming 20 nm effective beam size or $2 \cdot 10^{16}$ ions/cm^2) is in the medium dose regime (comp. section 6.1.9).

As these remarkable direct patterning results open fascinating opportunities for magnetic hard disks or MRAM's (magnetic random access memory) fabrication, J. Ferré's and J. Gierak's teams will continue to explore the limits for this technology.

9.3 DNA encoding / sputtering (large dose)

A single molecule object detector can be created by electrically measuring the translocation of single molecules through a nano-pore (< 10 nm holes). This is done by applying a voltage between two electrodes in a conductive solution and measuring the resulting current. If molecules pass the nano-pore the current decreases shortly this effect is called "current blockade". Current changes indicate molecule compositions e.g. for in vivo virus analysis or DNA transcription [246] [247] [248].

The nano patterning challenge is to reproducibly create sub 10 nm holes, which are called nano-pores.

Such nano-pores can be fabricated by various techniques e.g. EBL (electron beam lithography, comp. section 2.2.2 and 7.3.4) followed dry a etch step (reactive ion etching, RIE) [249]. Another fabrication possibility is the sculpturing process [176] described in section 5.1.12. Advantages of EBL are: it is an established, wide spread and well understood process technology. However, a challenge exists for reproducible sub 5 nm holes creation: a resist resolution limit in combination with the required aspect ratio for the RIE process step [250]. The sculpturing technology can reproducibly create sub 5 nm holes, however it is a rather slow and manual process.

Simple direct milling (comp. section 6.2.1) of nano-pores is not possible, as ion solid interactions and lateral scattering of the primary beam limit the resolution [246] [250].

Therefore a refined process is required: Biance et al. [246] took a thin membrane instead of bulk material (thickness in the range of the projected range of the impinging ions, comp. section 6.1.6 and 6.3). As a result some of the displaced atoms are directly ejected at the rear side of the membrane. This reduces redeposition effects [177] (comp. section 6.2.1). In addition the membrane is patterned from one side and stopped as soon as a small diameter opening is created on the rear side [177] (comp. Figure 38a).

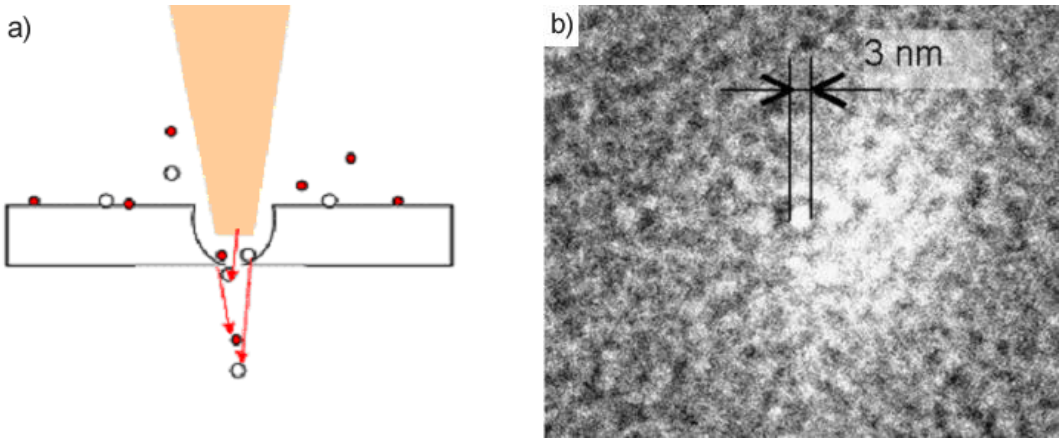

Figure 38: a) Patterning process Fig. 3c in [251]
b) TEM micrograph of a resulting nano-pore drilled by a Ga beam into a 20 nm thick SiC membrane Fig. 5 in [251] around $2.5 \cdot 10^7$ ions/point

The results achieved so far are competitive to those reached by other patterning techniques. The advantage is that it is a one process step technique, however for ultra small holes the dose process latitude is relatively small. As a result only 12 out of 20 holes have been opened in one experiment [177]. Although these tiny holes can be patterned relatively quickly, the employed dose has been $2.5 \cdot 10^6$ ions/point (equals $1 \cdot 10^{19}$ ions/cm^2 calculating with the 5 nm spot size as given in [177]), so the process belongs into the large dose regime (comp. section 6.1.9). Exemplary current blockades have been detected at different voltages 400 and 500 mV in Figure 34.

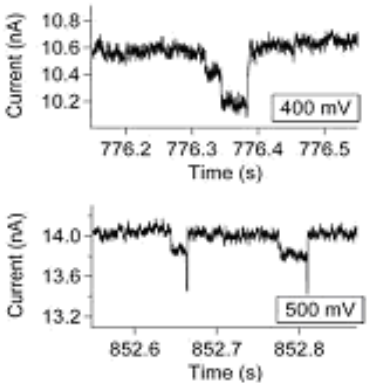

Figure 39: Current blockade measurements of λ DNA molecules through a Si_3N_4 nano-pore Fig. 3 in [247]

The team around Schiedt, Biance and Gierak will continue to improve this promising direct fabrication process.

9.4 Summary

These applications are examples of ion-matter interactions we have studied employing our instrument technology (comp. chapter 8): from intended surface modification, atom intermixing to refining classical sputtering. Even more processes and ion-matter actions have been studied over the recent years, a list of the corresponding publications is given in section 12.4.

The HOPG example (comp. section 8.4) is a low dose application with the potential for fast ion beam processing. Both need only a few thousand ions per point for pattern definition, but they require an additional oxidation or development process, respectively. Whereas nano-pores and magnetic domain wall creation have a need for medium and high doses, respectively. However, these two deliver the results immediately after the ion treatment, without the need for an additional process step.

In the following chapter we describe the application of this instrument technology to take a closer look at two “resist” processes.

10 Two applications in detail

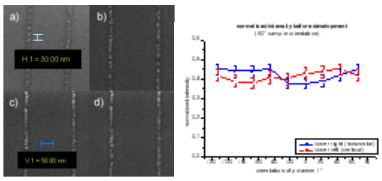

Since 2002 we employ this instrument technology (comp. 8) to study different application fields (comp. chapter 9, section 8.3, 12.1.2, 12.4).

We have employed the instrument to further analyse the following two examples:

a) potential causes for a long known effect in ion beam resist exposure (“discontinued lines phenomenon” (comp. section 7.2))
b) a metal organic resist to create conducting features as a potential material for process simplification opportunities in nano patterning

In addition we take a look at the corresponding application resolution for each process (comp. section 5.2).

10.1 EBL resist exposure

10.1.1 Introduction

For more than 25 years, a high edge roughness (compared to EBL) and a phenomenon called "discontinued lines" is present during the Ga LMIS exposure of organic resists [136]. The latter one limits the achievable minimum feature sizes: P(SiSt90-CMS10) resist starts to show the discontinued lines phenomenon at a dose of $1.2 \cdot 10^{-8}$ As/cm^2 and PMMA at $7 \cdot 10^{-8}$ As/cm^2 [136]. Nevertheless, in the early 1990s Kubena has demonstrated 85 nm period in 60 nm thick poly(methyl-methacrylate) (PMMA) resist [252] and sub-10 nm minimum feature sizes (isolated lines) in 30 nm PMMA ($2.4 \cdot 10^7$ ions/cm about 11 ions per dot or $1 \cdot 10^{-6}$ As/cm^2 (comp. section 6.1.9)) [115]. He has employed a Ga-LMIS instrument at an acceleration voltage of 50 kV and confirmed that an effect called "discontinued lines" limits the ultimate achievable feature size [115].

Potential causes have been described: shot noise, oscillations at the end of the Taylor cone of the Ga LMIS (both [136]), scattering/recoil effects [115] [253], or statistical dose fluctuations [115] [87].

Recently, promising results have been published for EBL [254] as well as for Helium ion beam lithography [110] [109] using the negative tone resist HSQ (lower sensitivity compared e.g. to PMMA). Both the minimum feature size of isolated lines and the achievable minimum period have been significantly improved by this process enabling down to 9 nm period in the EBL case.

We will present and detail our results obtained with a Ga-LMIS nano fabrication system aiming at the investigation of specific effects and the resolution limits related to LMIS-Ga-IBL. This work has been presented as a poster at MNE 2011 and has been accepted for paper publication in Microelectronic Engineering 2012 [255].

10.1.2 Experimental set-up

We have patterned designs at various conditions onto 6 and 20 nm thin HSQ (XR-1541.002 from Dow Corning, 2% in Methyl isobutyl ketone (MIBK)) on Si samples. In addition we have applied 3 different exposure strategies ("normal", "loops" and "shifted loops [187]") at similar doses. The resist development process we have utilised has been described in [254] and is called "salty development" (developer: 1% NaOH / 4% NaCl and stopper: ultra pure

water). All structures have been patterned at an acceleration voltage of 40 kV and a working distance (WD) of about 10 mm using the Ga-LMIS nano fabrication instrument described in chapter 8. Scanning electron microscope (SEM) micrographs have been taken at 3-5 kV and a WD of about 2.5 mm using an electron beam writer [256]. First we have studied minimum reachable feature sizes and then taken a closer look at the discontinued lines phenomenon (comp. section 7.2 and 8.4).

10.1.3 Results

I) Minimum feature size / period

A pattern for evaluating the minimum possible period (similar to the one described in [254]) has been exposed with an exposure step size of 1 nm, a beam current of 1.2 pA and different point dwell times for the evaluation of the optimum doses for minimum feature sizes and period.

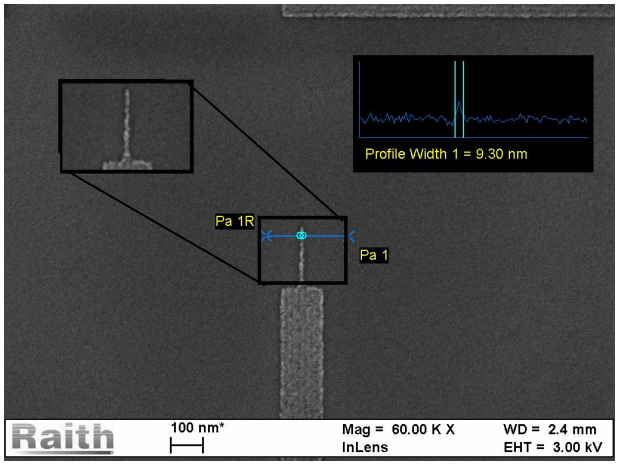

Figure 40: SEM micrograph, feature size <10 nm (6 nm HSQ on Si, exposed by 40 kV Ga, dose 19.4 pAs/cm equivalent to 20.9 µAs/cm^2, $1.2 \cdot 10^8$ ions/cm or 12 ions/point)

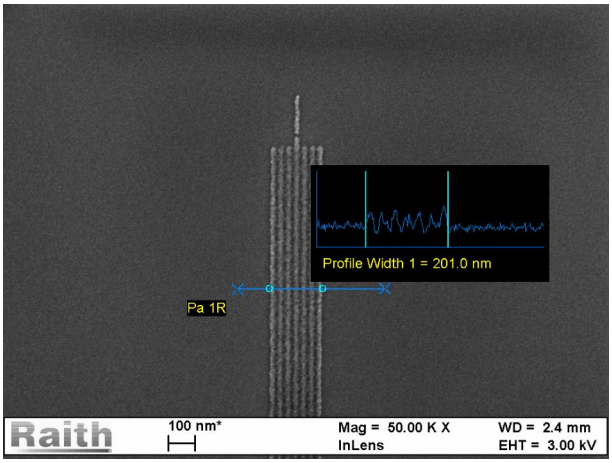

Figure 41: SEM micrograph of 30 nm period (6 nm HSQ on Si, exposed by 40 kV Ga, dose 23.6 pAs/cm equivalent to $1.5 \cdot 10^8$ ions/cm or 15 ions/point)

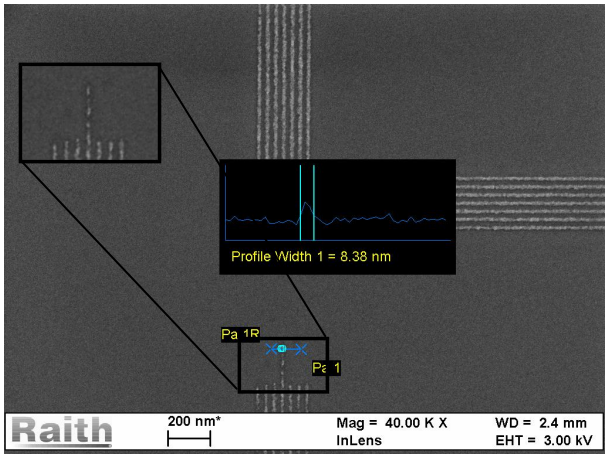

Figure 42: SEM micrograph showing line width limitation for lower dose, "discontinued lines" (6 nm HSQ on Si, exposed by 40 kV Ga, dose 18.4 pAs/cm, about 12 ions/nm, about $1 \cdot 10^{-5}$As/cm^2), inset discontinued line magnified without measurement

We have succeeded in reaching <10 nm minimum feature sizes (comp. Figure 40) and 30 nm minimum period (comp. Figure 41) by employing a line dose (comp. section 6.1.9) 19.4 pAs/cm and 23.6 pAs/cm, respectively.

In a 20 nm resist layer the minimum feature size reached has been around 15 nm.

If the doses are lowered below these values, the already mentioned "discontinued lines" phenomenon appears at an area dose of around $1 \cdot 10^{-5}$As/cm^2 (comp. Figure 42).

II) Analysing the impact of potential dose fluctuations

If emission process instabilities or other causes lead to dose fluctuations, varying the patterning (exposure) strategies could average these. We have selected 3 different ones: exposure step size (comp. section 6.1.9) variation, loops and shifted loops.

a) Variation of the exposure step size

GDSII patterns with lines separated by 200 nm have been exposed at varying dwell times, in addition the exposure step size has been varied from 1 to 30 nm (1,2,4,8,15,30 nm).

Up to 8 nm exposure step sizes no significant difference on the line edge roughness / discontinued lines phenomenon could be observed, although larger exposure step sizes mean more ions per point to reach the same exposure line dose.

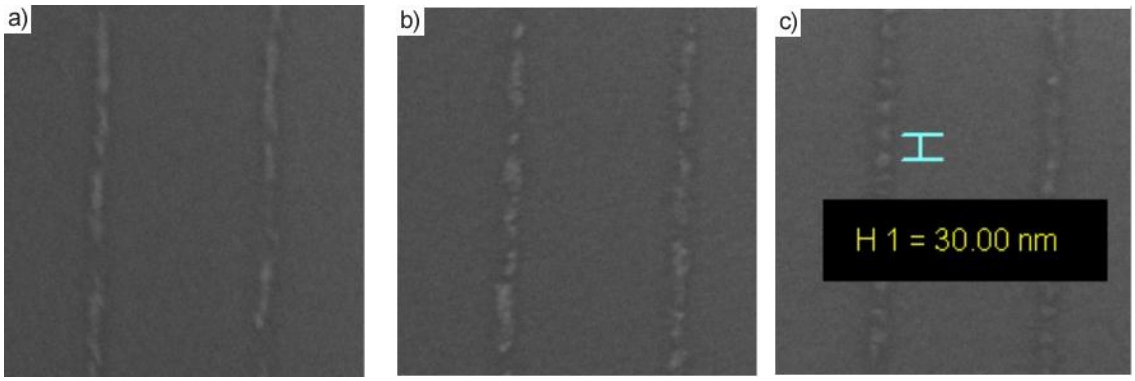

Figure 43 SEM micrographs of 200 nm separated lines, 6 nm HSQ on Si, exposed by 40 kV Ga, patterned with different exposure step sizes, SEM magnification 50,000 (c) valid for all three micrographs), line dose for all 3 about 11 ions/nm (area dose of about $1 \cdot 10^{-5}$As/cm^2)
a) exposure step size 1 nm about, dose 11 ions/point
b) exposure step size 8 nm about, dose 92 ions/point
c) exposure step size 30 nm, dose about 342 ions/ point scale bar in

For the 30 nm exposure step sizes individual points with this period become partially visible (comp. Figure 43c).

b) Loops

The same pattern as in IIa has been exposed applying different step sizes (1,2,4,8,15,30 nm) in addition each line has been "looped" (n = 1,9,16,25,36,81), meaning that the ion beam is not scanned only once over the line, but n times. Accordingly the dwell time employed in I/IIa have been divided by the number of loops (n) to reach the same effective total dose.
Between 1 and 81 loops per line no significant impact on the line edge roughness could be observed.

c) "shifted loops"

Again a similar pattern to IIa has been exposed, this time we have employed 32 and 16 nm exposure step size, with 8 slightly shifted lines on top of each other ("line package", comp. Figure 44), by 4 and 2 nm, respectively. In addition these line packages have been repeated n times (looped, comp. IIb).

However, even this shifted loop technique did not result in a significant line edge roughness difference between normal exposure und shifted loops (comp. Figure 45a)-c)).

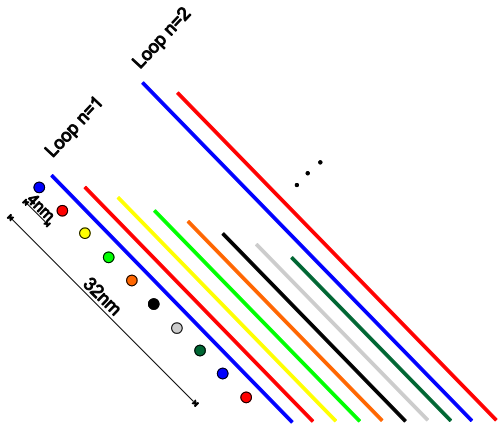

Shifted loops example: The instrument is set up to pattern with 32 nm exposure step size (e.g. blue dots Figure 44). In the design 8 lines have been created on top of each other ("pile of lines") whereas the start point of the following line has been each shifted by 4 nm: red, yellow, green, orange, black, grey, dark green, respectively. The selected doses have been adjusted to match this 4 nm effective exposure step. In addition these 8 shifted lines can be "looped" n times.

Figure 44: sketch of shifted loop exposure mode

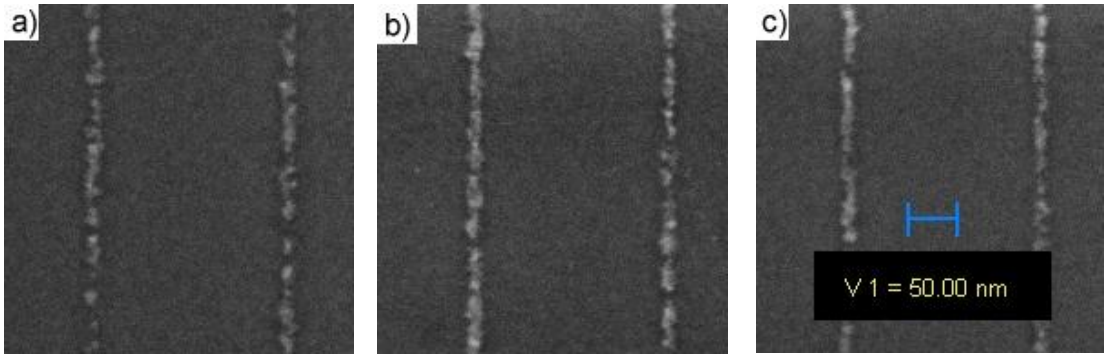

Figure 45: SEM micrographs of 200 nm separated lines, 6 nm HSQ on Si, exposed by 40 kV Ga, employing different "shifted loop" conditions, SEM magnification 60,000, total dose about 29 ions/dot (area dose of about $1 \cdot 10^{-5}$As/cm^2, scale bar in c) is valid for all three micrographs)
a) Reference w/o shifted loop, 4 nm exposure step size
b) Shifted loops 9 (32 nm exposure step size, 8 lines on top of each other, shifted by 4 nm each ("pile of lines") with 9 loops)
c) Shifted loops 36 (32 nm exposure step size, 8 lines on top of each other shifted by 4 nm each ("pile of lines") with 36 loops)

10.1.4 Summary and Discussion

Employing a very thin resist layer with low sensitivity ($1 \cdot 10^{-5}$ As/cm^2, like suggested in [115]) and evaluating 3 different exposure modes, we think we have managed to deconvolve effects due to potential dose fluctuations exceeding shot noise from other effects [115].

A variation of the exposure step size from 1 to 8 nm results in a factor of 8 increase for the total point dose. However, the threshold dose for the discontinued lines phenomenon remains the same. In addition we tried to average potential ion dose fluctuations by employing loops and shifted loops strategies, assuming that any ion dose variation is of a different period as the loops period or even the shifted loops period.

None of the tests have revealed a significant line width reduction below the discontinued lines barrier. As a result the resolution remains limited by the discontinued lines effect.

If the dose fluctuations exceed shot noise, we would have expected that one of the exposure methods would have been able to average the effect. There was no evidence of this, so we suppose either the physical limit of shot noise or the actual exposure process inside the resist as the dominating factor.

10.1.5 Conclusion and outlook

In our 40 kV Ga LMIS HSQ exposure experiments we have analysed a very thin resist layer (6 nm resist layer) and reached state of the art minimum feature sizes below 10 nm (continuous lines, Figure 40) and a minimum periodicity of 30 nm. Nevertheless, the discontinued lines phenomenon limits also the minimum reachable feature size in HSQ for Ga LMIS exposure. Our results indicate that the origin is more likely the exposure process inside the resist than probe current fluctuations above the shot noise level.

In spite of the discontinued lines effect, we believe that the reached high performance level opens promising perspectives for this IBL process employing hydrogen silsesquioxane resist.

10.2 Au_{55}

10.2.1 Introduction

Many nano fabrication processes have become quite complex involving many different process steps [6] [7] or are not possible by conventional methods [1]. An alternative to conventionally employed optical or electron beam lithography (EBL) is ion beam lithography (IBL). It is capable to deliver comparable lateral resolution to EBL [251]. It possesses a significantly smaller interaction volume and a larger number of ion-matter interactions exploitable for nano patterning applications, some of them even as direct nano fabrication [198]. Nevertheless, drawbacks of ion beam patterning exist [69] (comp section 7.2). However, we have already proven that these are not relevant for many applications (comp. chapter 9, section 8.3, 12.1.2, 12.4*)*. A simple process for patterning arbitrary conducting shapes has been suggested by Gierak and Hofman et al. [257] [258], respectively, employing a $Au_{55}(PPh_3)_{12}Cl_6$ "negative tone resist" (Au_{55}). The organometallic compound is locally fixed by the exposure process whereas the film composition is almost unchanged [258], the Au_{55} sticks to the surface at patterned areas and the non patterned areas are washed away during the development process. In addition small metal clusters exhibit exploitable quantum electrical behaviour [259].

We have adapted the technology to evaluate potential process complexity reduction opportunities for nano patterning applications. For this purpose we have analysed the dielectric film properties with a simple optical microscope set-up. For a conductor wire grid on an isolator incident light waves polarised in wire/grating lines direction ("parallel") could result in total reflexion if the vector of the electrical field is parallel to conducting lines of the grating [260]. However, if further effects dominate the results different optical anisotropic behaviour can be detected.

This work is in preparation for paper publication [261].

10.2.2 Experimental set-up

We have patterned various designs onto an about 50 nm $Au_{55}(PPh_3)_{12}Cl_6$ film on SiO_2 / Si samples (240 nm oxide thickness). Details about the resist process can be found in [257]. The structures have been patterned at different acceleration voltages and a working distance (WD) of about 10 mm using the Ga-LMIS nano fabrication instrument described in chapter 8.

Scanning electron microscope (SEM) micrographs have been taken at 10 kV and a WD of about 10 mm using an electron beam writer [256].

We have patterned gratings with different periodicity (comp. section 10.2.3a) and thin lines attached to large areas (comp. section 10.2.3a).

The optical microscope analysis set-up (comp. Figure 46) has been: an optical microscope with a camera attached, green filter (512-546 nm “green”), and polariser. The light is incident at about 15° with respect to the normal vector of the sample surface. At 0° orientation of the polarisator, the electric field vector is horizontally oriented in the taken optical microscope images and parallel to the plane of incidence (p-polarised).

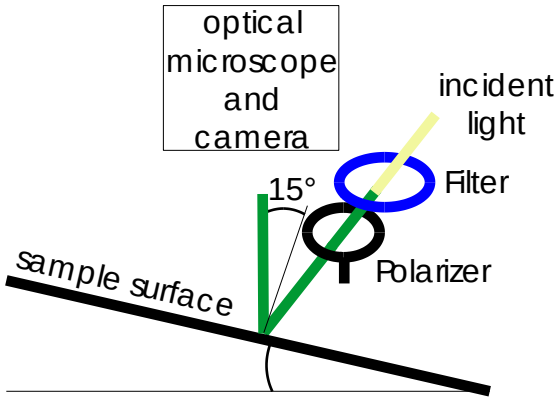

Figure 46: Set-up of the optical analysis

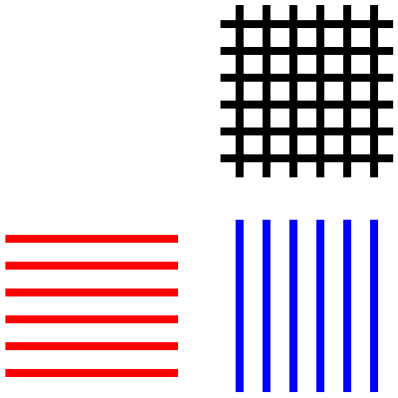

Figure 47: sketch of the patterned grating orientations at 0° sample orientation beneath the optical microscope

The images from the optical microscope at different polariser orientation angles have been stored. Afterwards the intensity of the unpatterned and patterned areas has been deduced by an imaging software [262].

The line orientations within the grating of our pattern is shown in Figure 47 .The atomic force microscope (AFM) image has been taken by an AFM [263] and the raw data have been processed employing a STM software [264].

The plots below display the results from the normalised intensity, which is defined in the following manner:

$$I_{norm} = \frac{I - I_{bc}}{I_{cross} - I_{bc}}$$

Equation 26: definition of normalised imaging intensity

I_{norm} = normalised intensity of the patterned area at a certain polarizer angle (displayed in the plots below)

I = average intensity measured inside for the "horizontal" or "vertical" gratings (two of the patterned areas)

I_{bc} = average intensity between the three patterns ("background")

I_{cross} = average intensity measured at the cross reference structure

10.2.3 Results

a) Gratings before and after development

The gratings have been patterned at a line dose (comp. section 6.1.9) of 1000 pAs/cm (equaling about 200 µAs/cm^2 or $1.3 \cdot 10^{15}$ ions/cm^2 (for a line width of about 50 nm).

Before development we have found the following optical anisotropy behaviour at about 0° sample orientation (comp. Figure 48a) and about 90° sample orientation (comp. Figure 48b), i.e. the structure in Figure 47 is rotated by 90°.

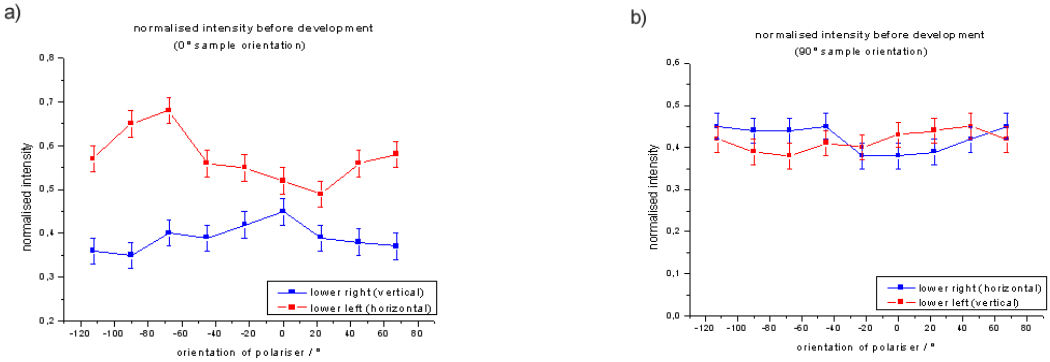

Figure 48: normalised intensity (applying Equation 26) plots for vertical and horizontal gratings before development, colours refer to the elements visible in Figure 47, a) at 0° sample orientation and b) at 90° sample orientation

The normalised intensity has been highly sensitive to the set-up, resulting in relative maxima and minima comp. Figure 48a) or absolute ones like in comp. Figure 48b) in the undeveloped condition. At horizontal polarisation (0° orientation of polariser) a relative maximum is

detected for the lower right structure (vertical lines comp. Figure 48a) at 0° sample orientation. Figure 48b) shows the results for 90° sample orientation, as a result the maxima and minima change from the lower left to the lower right grating in Figure 47 correspondingly.

In addition AFM images have been taken before development to study the topography. Figure 49 shows an example of the lower left structure (comp. Figure 47) scanned at 90° sample orientation.

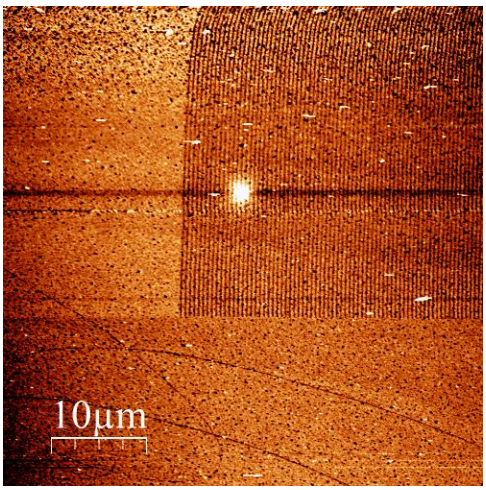

Figure 49: AFM image of the lower left pattern in Figure 47 before development at 90° sample orientation (filter flatten, z-control) in software [264]

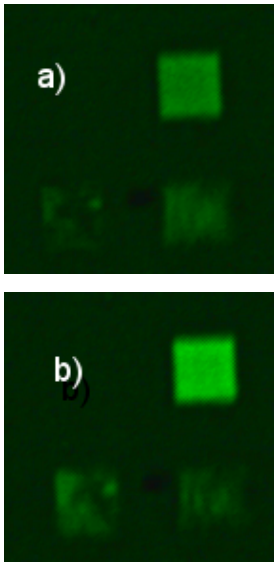

Figure 50: Optical microscope images after development of the lower right and left gratings cut from the images for 0° sample orientation (a) 0° and (b) -90° polariser orientation

After development of the samples, we have taken SEM micrographs (not shown) verifying the lines orientations with respect to the design (comp. Figure 47). The normalised intensity amplitude change due to polarisation orientation becomes more pronounced. As a result the intensity differences in the images are also more obvious (comp. Figure 50, Figure 51).

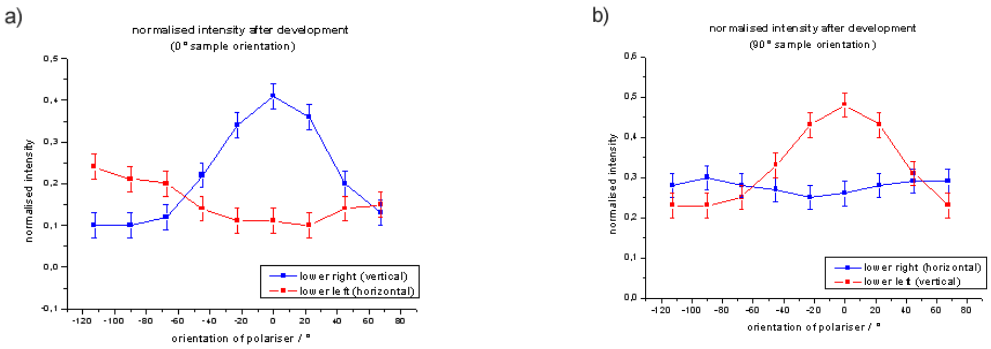

Figure 51: normalised intensity (applying Equation 26) plots for vertical and horizontal gratings after development, colours refer to the elements visible in Figure 47a) at 0° sample orientation and b) at 90° sample orientation

b) High resolution

We have patterned thin lines with varying doses at different contact pad distances to evaluate minimum feature sizes. The achieved high resolution results are displayed in Figure 52.

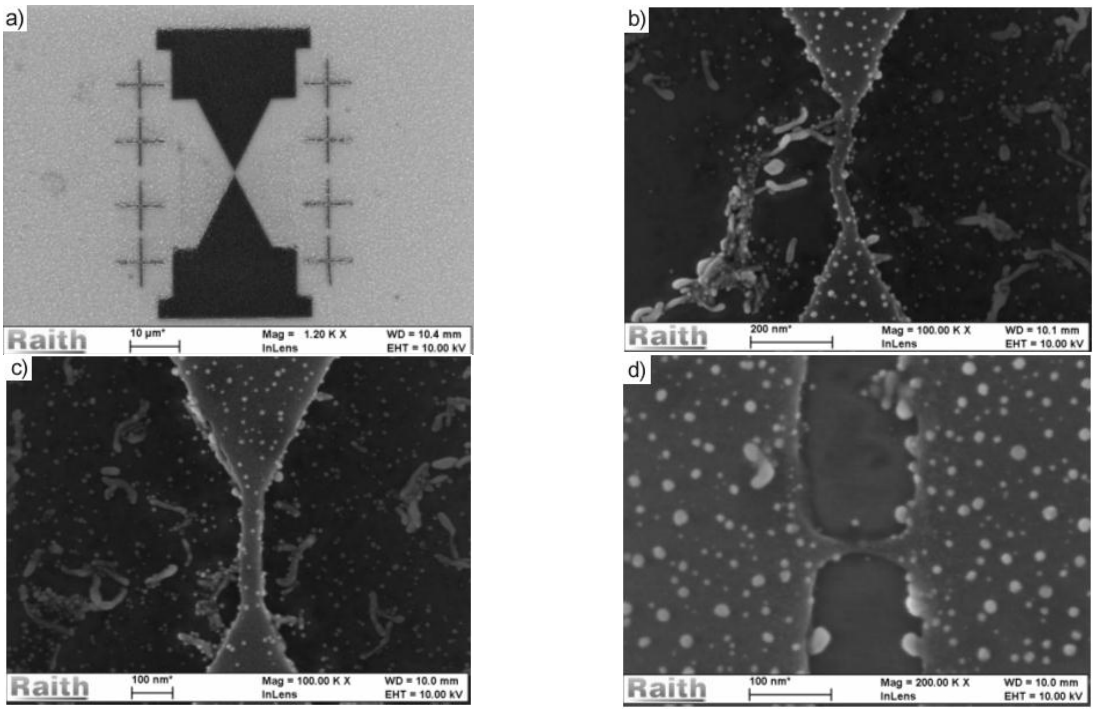

Figure 52: SEM micrographs of high resolution results after development
a) Au_{55} device with alignment marks, generated by Au_{55} cluster "exposure"
b) centre of a) 30 nm line, lost contact, 200 nm pad distance, dose 6pAs/cm
c) 50 nm wide well defined line at 200 nm pad distance, dose 12 pAs/cm
d) thin interconnection (<20 nm) with 100 nm contact pad distance < 6 pAs/cm

10.2.4 Summary and Discussion

a) Optical anisotropy for grating structures

Optical anisotropy to the orientation of polarisation is already detectable before development and gets more obvious after development. At the same orientation of polarisation the minima and maxima are swapped by rotating the sample by 90° underneath the optical analysis set-up (comp. Figure 46).

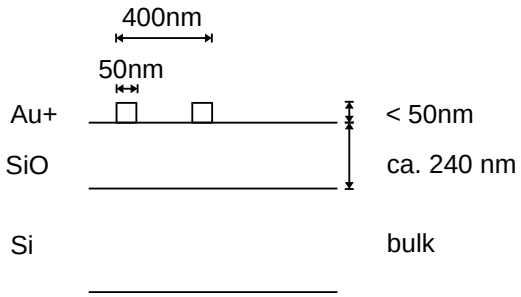

Figure 53: sample cross section of the $Au_{55}(PPh_3)_{12}Cl_6$ (Au+) grating on the sample surface

As described above an electrical field vector polarised parallel to the conducting lines of a grating on an isolator could result in an intensity maximum for reflection at 0° polarisator orientation [260], however this is not the case for our experiments. We have observed reflection maxima for light polarised perpendicular to the grating lines.

Theory as presented in [260] is applicable to large wavelength of the applied light with respect to the grating period and for small spacing (gaps between the thick metal lines). We have studied gratings with a period of 400 nm, which may not be small enough compared to the wavelength of the applied light (512-546 nm, mean 529 nm). In addition the created about 50 nm metal width and about 350 nm spacing, reduce the effect. Thus the approximation formulas given in [260] [265] cannot be applied.

Other effects must dominate our optical analysis. The material system cross section visualised in Figure 53 indicate the following effects being additionally involved: absorption at the metal lines [14]), diffraction at the grating [266], reflection and refraction at the air/SiO_2 interface, followed by an almost total reflection at the SiO_2/Si interface, then reflection and refraction again at the SiO_2/air interface and diffraction again at the grating.

We assume two of them could explain optical anisotropy to polarisation orientation and sample rotation by 90°:

- diffraction at the grating
- absorption at parallel grating lines and reflexion at the SiO_2 silicon interface beneath the actual grating

Taking a closer look at grating diffraction effects shows, that they are expected to be small: First the grating efficiency is expected to be small (almost zero) at low angles of incident (15°, comp. [267]). Second we observe the reflection under the same small angle (15°) as the incident light has normal to the sample surface, so we observe in specula reflection close to the 0^{th} order. Taking this into account we assume diffraction is not the main cause for our results.

Gierak shows in [257] that the irradiated areas indeed have a significant conductivity at a dose above $5 \cdot 10^{13}$ ions/cm^2. As the applied dose of $1.3 \cdot 10^{15}$ ions/cm^2 for the lines in the gratings lies above this value, we assume our optical analysis shows a significant electrical conductivity difference of the patterned and unpatterned areas, already in the non developed condition. Since development will not alter the electrical conductivity of the irradiated areas. Thus absorption in combination with reflection could be a reason for the results we see and explain them. A real metal possesses an Ohmic resistance > 0 (Joule loss), so we expect absorption to be present at the metal grating [14]. For electrical field parallel to the lines of the grating we expect in the transmitted light an intensity minimum (comp. e.g. for 0° sample orientation Figure 48a) and Figure 51b) the horizontal lines “red”). This gets reflected at the SiO_2/Si sample surface and is then partly absorbed in transmission. For the electrical field perpendicular to the lines we expect and see the opposite.

The larger amplitude after development could be explained by the more significant difference in dielectric properties of the exposed $Au_{55}(PPh_3)_{12}Cl_6$ lines with respect to the SiO_2 layer compared to the small difference between the $Au_{55}(PPh_3)_{12}Cl_6$ exposed areas compared to the $Au_{55}(PPh_3)_{12}Cl_6$ non exposed areas [258].

b) High resolution feature sizes

For separations between contact pads at and above 200 nm thin lines below 50 nm loose contact to the substrate during the development process. For 100 nm separation between supporting contact pads <20 nm line width have been reached. In addition to the electrical conductivity measurement results, the reached pattern fidelity and minimum feature sizes encourage us to carry out further experiments.

As seen in the experimental results the current process allows to fabricate thin gates if large supporting structures are in the vicinity (comp. Figure 52), but thin lines without supporting structures will not stick to the substrate posing a limit to the minimum grating periodicity in this process after development. Below about 50 nm line width the metal lines loose contact to the substrate (comp. Figure 52a) at distances of about 200 nm to the "large" supporting contact pads the 50 nm lines. This we think is due to the fact that the thin lines do not possess sufficient fixation to the sample surface comp. [258], so they partially loose contact to the sample surface. Thinner line width can be reached by decreasing the distance to the contact pads (comp. Figure 52c), so the thin line (gate) between the contact pads is not washed away during the development process. The reached minimum feature sizes are characteristically for our results on different samples and we have found them to be independent of the applied acceleration voltages (e.g. 30, 35, 40 kV).

10.2.5 Conclusion and outlook

We have used $Au_{55}(PPh_3)_{12}Cl_6$ as a negative tone resist for Ga LMIS nano patterning.

The achieved optical anisotropy behaviour employing a simple optical microscope set-up, could be explained by electrical conductivity differences of exposed and non-exposed areas already for non developed samples. As a result it might not even be necessary to develop the sample for some applications, which could result in a simple two step fabrication process to achieve conducting features: spin coating of the resist and irradiation by the ion beam.

Further on we have reduced the distances to supporting contact pads which results in smaller minimum feature sizes (e.g. < 20 nm Figure 51), however this is not fully reproducibly yet.

If the electrical conductivity is not yet sufficient after exposure, two additional simple steps can be added: a development and a temper step. This would still be a simple nano fabrication process with the potential to reach up to pure gold electrical conductivity [258].

We think the promising material/process we have further investigated opens process complexity reduction potential for different applications: for example: molecule encoding devices [268]. The results presented in this work could be combined with the ones from [251] which have utilised the same instrument technology, if we place the nano-pore displayed in Figure 54b) into the centre of Figure 54a). The complete device is shown in Figure 52a) at lower magnification.

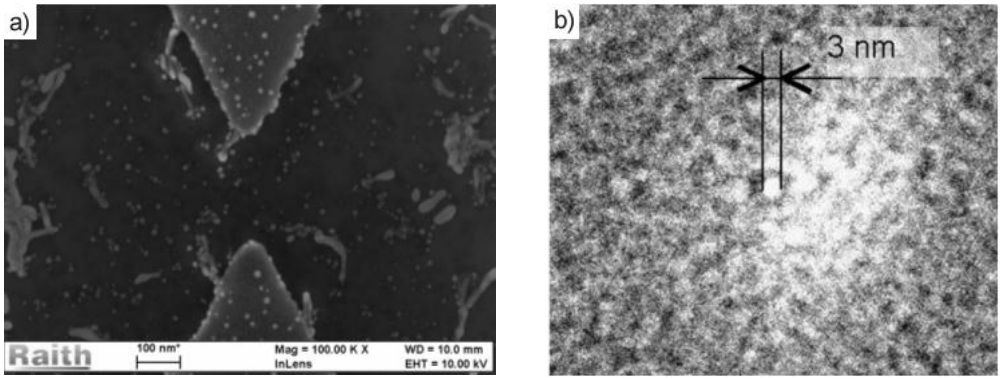

Figure 54
a) SEM micrograph of the inner part of a device (e.g. centre area of Figure 52a)
b) TEM micrograph of high resolution nano pore generated by FIB milling (comp. section 6.2.1), Fig. 5 in [251]

11 Summary and outlook

Although different kinds of established tools and processes exist for lateral nano patterning (comp. section 2.2 and 7.3.4), for some applications the process has become quite complex and others cannot be satisfactorily fulfilled at the moment (comp. chapter 1).

We think and have proven the feasibility and applicability of the LMIS FIB complement to an EBL writer presented in this work. We have employed a large variety of ion-matter interactions at competitive resolution levels even over many hours. Five examples are given in chapter 9 and 10 in combination with the zone lens fabrication process (comp. section 8.3). The instrument is a commensurate alternative nano patterning tool which has enabled us to explore a large amount of successful applications.

11.1 Summary

Already at the end of the 1950s beginninig 1960s, visionaries (e.g., Feynman [8] and Newberry [9]) have seen and predicted the potential of ion beam patterning (comp. chapter 1 and 6). Theory for resolution and exploitable ion-matter interactions (comp. chapter 5 and 6, respectively) predict a competitive three dimensional application resolution. For reasons, a similar instrument technology to ours did not reach the successful application level in nano research laboratories at the end of the 1980s (comp. section 7.2).

Since its invention at the end of the 1960s and early 70s [66] [67], electron beam lithography (EBL, comp. section 2.2.2 and 7.3.4) has become the most wide-spread lateral nano structuring technique. This was in large part due to its versatility and reached high level of sophistication of the instruments.

With the current technology, expertise from different fields (comp. section 12.3) and a different LMIS technology (comp. chapter 4) adequate for nano patterning requirements, we have managed to develop and commercialise a new LMIS FIB instrument dedicated to nano patterning (comp. chapter 8).

The system architecture's applicability has been proven by:

- the acceptance test (comp. section 8.2)
- high demanding applications which require stability over more than 15 hours (comp. section 8.3)
- sub 10 nm patterning capabilities compare [269] and section 10.1
- the large variety of leading edge results we have already reached in many different applications applying this instrument technology

The instrument's functionality facilitates process development (comp. chapter 8) and in-depth analysis of encountered challenges by enabling complementary nano patterning capabilities.

Nevertheless, drawbacks of gallium ion beam processing (comp. section 8.4) exist also with our instrument. However, comparing it with drawbacks of electron beam writers (comp. section 7.3.4), it has been shown by many successful applications (comp. chapter 9, 10 and section 8.3, 12.1.2, 12.4) that ion beam technology is a viable alternative, especially as there exist more ion-matter interactions exploitable for nano fabrication. Some of them are direct nano patterning, which allow simple processes, some even with only a single step. We have proven that the instrument capabilities (comp. chapter 8) are on the level of modern EBL

writers, so the “single most reason” for the non-acceptance of FIB nano structuring [69] (comp. section 7.2) has been overcome.

Focused ion beam nano structuring, being similar to EBL, is a serial and therefore relatively slow process. However, with complementary patterning capabilities to EBL, there is a chance that some of the current nano patterning challenges can be solved. For research or prototyping applications, it can be even faster than designing a photo mask, fabricating it, using the mask for optical lithography, creating the device, testing it, then possibly modifying the design in order to start over again. As a result focused ion beam technology can be a fruitful complement to currently established nano patterning techniques, especially in R&D / prototyping fields due to the beauty of “maskless” (“software masks”) patterning capabilities. However, the future of focused ion beam technology in nano patterning will depend on profound theory beyond conventional analysis and micro patterning applications. Both are closely linked to each other as dedicated tools facilitate systematically studying an application field and the creation of data as foundation for future theories and models.

11.2 Outlook

We think the fundamental instrument technology is mature and ready to start, enriching the researcher’s toolboxes.

We could continue studying current nano fabrication challenges to decide whether ion beam processing can be a viable solution. Here we have the selection between already exploited or further ion-matter interactions from the large variety described in section 6.1.8. It would make sense to enlarge the instrument capabilities and multiply the number of exploitable ion-matter interactions with Ga and additional liquid metal ion sources [270] [236] [271] [120] [121] [122].

In addition it is worthwhile further examining “conventional” nano patterning techniques at its limits to search for refining possibilities similar to the examples given in section 8.4 and 9.3.

Further on we look for instrument refinements to improve and accomplish the applications of nano researchers.

Potentially, the periodic grove formation [198] -so far observed in broad ion beam instruments- could be tested in a FIB instrument giving the opportunity to pattern the feature frame's at arbitrary shapes and at dedicated sample positions.

Finally, fascinating opportunities could arise by combining the instrument architecture with individual ion techniques [272].

12 Appendix

12.1 Personal contribution, publications and co-author

12.1.1 Personal contribution to the development process

I have been taking part at the NanoFIB growth research project since the beginning in 2001 as the main project partner inside the Raith GmbH.

During this time I have led, carried out parts of the engineering work and assembled parts of the proof of concept tool as well as the beta tool (comp. Figure 27a) and Figure 28a), excluding the column and filament work which has been carried out at LPN CNRS, during that time.

In addition to this my main role has been merging the Raith EBL writer architecture, know-how and software with the LPN CNRS ion beam technology.

Since the end of the EC project I have been responsible for parts of the product development project, for example the system architecture. In addition I use the instruments to explore the capabilities, applicability and ways to further improve it.

12.1.2 Publications as Author / Co-author

Author

L. Bruchhaus, H. Hövel, and J. Gierak,

Conductivity differences in Au_{55} nano clusters patterned by Ga FIB,

in preparation

L. Bruchhaus, S. Bauerdick, L. Peto, U. Barth, A. Rudzinski, J. Mussmann, J. Klingfus, J. Gierak, and H. Hövel,

High resolution and high density Ion Beam Lithography employing HSQ resist,

to be published in Microelec. Eng. 2012, http://dx.doi.org/10.1016/j.mee.2012.04.033

Co Author

A. Morin, G. Patriarche, E. Bourhis , A. Madouri, J. Pelta, L. Auvray , R. Jede, L. Bruchhaus, and J. Gierak,
FIB carving of nanopores into suspended monolayer graphene films
submitted to Microelectronics Engineering 2012

B. R. Appleton, S. Tongay, M. Lemaitre, B. Gila, J. Fridmann, P. Mazarov, J. E. Sanabia, S. Bauerdick, L. Bruchhaus, R. Mimura, and R. Jede,
Materials modifications using a multi-ion beam processing and lithography system,
Nucl. Instr. and Meth. B **272**, 153 (2012)

B. Gila, B. R. Appleton, J. Fridmann, P. Mazarov, J. E. Sanabia, S. Bauerdick, L. Bruchhaus, R. Mimura, and R. Jede,
First Results From A Multi-Ion Beam Lithography And Processing System At The University Of Florida
AIP Conf. Proc. **1336**, 243 (2011)

J. Gierak, B. Schiedt, D. Lucot, A. Madouri, E. Bourhis, g. Patriarche, C. Ulysse, X. Lafosse, L. Auvray, L. Bruchhaus, and R. Jede,
Challenges and opportunities for focused ion beam processing at the nano-scale,
Microscopy and Microanalysis **15** (Suppl. 2), 320 (2009)

J. Gierak, E. Bourhis, G. Faini, G. Patriarche, A. Madouri, R. Jede, L. Bruchhaus, S. Bauerdick, B. Schiedt, A.L. Biance, and L. Auvray
Exploration of the ultimate patterning potential achievable with focused ion beams,
Ultramicroscopy **109**, 457 (2009)

J. Gierak, E. Bourhis, D. Mailly, G. Patriarche, A. Madouri, R. Jede, S. Bauerdick, L. Bruchhaus, P. Hawkes, A.-L. Biance, B. Schiedt, L. Auvray, L. Bardotti, B. Prével, P. Mélionon, A. Perez, J. Ferré, J.P. Jamet. A. Mougin, C. Chappert, V. Mathet, L. Aigouy, I. Robert-Philip, I. Sagnes, R. Braive, A. Beveratos, and I. Abram,
Exploration of the ultimate patterning potential achievable with focused ion beams, Materials Research Society Symposium Proceedings **1089**, 7 (2008)

F. Ghaleh, R. Köster, H. Hövel, L. Bruchhaus, S. Bauerdick, J. Thiel, and R.. Jede,
Controlled fabrication of nanopits patterns on a graphite surface using focused ion beams and oxidation,
J. Appl. Phys. **101**, 044301-1 (2007)

J. Gierak, A. Madouri, A.L. Biance, E. Bourhis, G. Patriarche, C. Ulysse, D. Lucot, X. Lafosse, L. Auvray, L. Bruchhaus, and R. Jede,
Sub-5 nm FIB direct patterning of nanodevices,
Microelec. Eng. **84**, 779 (2007)

M. Villarroya, N. Barniol, c. Martin, F. Pérez-Murano, J. Esteve, L. Bruchhaus, R. Jede, E. Bourhis, and J. Gierak,
Fabrication of nanogaps for MEMS prototyping using focused ion beam as lithographic tool and reactive ion etching pattern transfer,
Microelec. Eng. **84**, 1215 (2007)

P. Kitslaar, M. Strassner, I. Sagnes, E. Bourhis, X. Lafosse, C. Ulysse, C. David, R. Jede, L. Bruchhaus, and J. Gierak,
Towards the creation of quantum dots using FIB technology,
Microelec. Eng. **83**, 811 (2006)

J. Gierak, E. Bourhis, M.N. Mérat Combes, Y. Chriqui, I. Sagnes, D. Mailly, P. Hawkes, R. Jede, L. Bruchhaus, L. Bardotti, B. Prével, A. Hannour, P. Mélinon, A. Perez, J. Ferré, J.-P. Jamet, A. Mougin, C. Chappert, and V. Mathet,
Exploration of the ultimate patterning potential achievable with focused ion beams,
Microelec. Eng. **78-79**, 266 (2005)

J. Gierak, D. Mailly, P. Hawkes, R. Jede, L. Bruchhaus, P. Mélinon, A. Perez, R. Hyndman, J.-P. Jamet, J. Ferre, A. Mougin, C. Chappert, V. Mathet, P. Warin, and J. Chapman,
Exploration of the ultimate patterning potential achievable with high resolution focused ion beams,
Appl. Phys. A **80**, 187 (2005)

J. Gierak, E. Bourhis, R. Jede, L. Bruchhaus, B. Beaumont, and P. Gibart,
FIB technology applied to the improvement of the crystal qualtiy of GaN and to the fabrication of organised arrays of quantum dots,
Microelec. Eng. **73-74**, 610 (2004)

H. Zhou, A. Midha, L. Bruchhaus, G. Mills, L. Donaldson, and J. M. R. Weaver,
Novel scanning near-field optical microscopy/atomic force microscope probes by combined micromachining and electron-beam nanolithography,
J. Vac. Sci. Technol. B **17**, 1954 (1999)

R.M. Cramer, L. Bruchhaus, and L.J. Balk,
Charcterisation of thermal device properties with nanometer resolution,
Microelectron. Reliab. **37**, 1583 (1997)

Given conference talks

L. Bruchhaus, S. Bauerdick, J. Thiel, R. Jede, F. Ghaleh, R. Köster, H. Hövel, J. Gierak, E. Bourhis, and the NanoFIB partners,
Surface functionalisation and other applications using newly developed FIB "nanowriter",
talk at the EFUG meeting during the ESREF conference 2006 in Wuppertal (Germany)

L. Bruchhaus, (invited)
...possible future trends and uses... "Different" application fields for ion beams,
talk at the NanoFIB conference 2005 London (Great Britian)

L.Bruchhaus, J. Gierak and the NanoFIB partners,
NanoFIB,
talk at the Phantoms Network Workshop 2001 in Würzburg (Germany)

Poster Author

L. Bruchhaus, T. Kliem, R. Jede, P. Hawkes, NanoFIB partners, Y. Lagadex, and J. Gierak,
Nano FIB: Instrument qualification tests,
poster at Phantoms Network Workshop 2002 in Catania (Spain)

Co-author Talks

J. Gierak , A. Madouri , E. Bourhis , J.-Y. Marzin , G. Oukhaled , L. Bacri , B. Cressiot , J. Pelta , R. Jede , and L. Bruchhaus,
FIB direct fabrication of sub-10 nm synthetic nanopores
APS March Meeting 2011, Volume 56, Number 2

Invited: J. E. Sanabia, S. Bauerdick, L. Bruchhaus, and R. Jede,
ionLiNE - a New Tool Concept for Nanofabrication,
20th International Conference on the Application of Accelerators in Research and Industry (www.caari.com), 2008

J. Gierak, A. Madouri, A.L. Biance, E. Bourhis, G. Patriarche, C. Ulysse, X. Lafosse, L. Auvray, L. Bruchhaus, S. Bauerdick, and R. Jede,
Nano-FIB from research to applications - a European scalpel for nanosciences,
XV MSM conference, 2007 Cambridge (Great Brittian)

F. Ghaleh, R. Köster, H. Hövel, L. Bruchhaus, J. Thiel, and R. Jede,
Production of ordered nanometer sized pits on HOPG,
DPG Frühjahrstagung 2006

J. Gierak, E. Bourhis, D. Mailly, R. Jede, L. Bruchhaus, T. Kliem, B. Lencova, P. Hawkes, and the NanoFIB partners,
Nano-fabrication with Focused Ion Beams: An enabling technique for nanoscience,
EuroNanoForum 2003, Trieste Italy

Co Author Posters:

F. Ghaleh, N. Grönhagen, H. Hövel, L. Bruchhaus, S. Bauerdick, J. Thiel, and R. Jede,
Production of metal cluster patterns using Focused Ion Beams (FIB),
DPG Tagung 2008

F. Ghaleh, N. Grönhagen, H. Hövel, L. Bruchhaus, S. Bauerdick, J. Thiel, and R. Jede,
Nanostrukturierung von Graphit mit fokussierten Ionenstrahlen und Oxidation,
NRW Nano Konferenz 2008 Dortmund

F. Ghaleh, H. Hövel, L. Bruchhaus, J. Thiel, and R. Jede,
Production of ordered nanometer sized pits with Focused Ion Beam (FIB),
Cluster Treffen 2005

M. Villaroya, C. Martin, F. Pérez-Murano, J. Esteve, N. Barniol, L. Bruchhaus, R. Jede, E. Bourhis, and J. Gierak,
Focused Ion Beam lithography on aluminium mask combined with Reactive Ion Etching,
MNE 2004, Rotterdam, NL

J. Gierak, E. Bourhis, R. Jede, L. Bruchhaus, B. Beaumont, and P. Gibart,
FIB technology applied to the improvement of the crystal quality of GaN and to the fabrication of organised arrays of Quantum dots,
MNE 2003, Cambridge, GB

J. Gierak, D. Mailly, Y. Lagadec, P. Hawkes, R. Jede, L. Bruchhaus, T. Kliem, and the NanoFIB partners,
Instrument specifications and highlighted applications
Phantoms Network Meeting 2003, Grenoble (Switzerland)

J. Gierak, D. Mailly, P. Hawkes, R. Jede, L. Bruchhaus, L. Bardotti, B. Prével, P. Mélion, A. Perez, R. Hyndman, J. Ferré, A. Mougin, J.P. Jamet, C. Chappert, V. Mathet, P. Warin, and J. Chapman,
Nano-fabrication with Focused Ion Beams
EIPBN 2002 Annaheim (USA)

12.2 References

[1] P.D. Townsend, J.C. Kelly, and N.E.W. Hartley, in *Ion Implantation, Sputtering and their applications*, (Academic press, London, GB, 1976), ISBN 0-12-696950-7

[2] Nanotechnology definition (NSET, February 2000)
http://www.nsf.gov/crssprgm/nano/reports/omb_nifty50.jsp (10.07.2008)

[3] Schlüsseltechnologien http://www.bmbf.de/de/6616.php (15.07.2011)

[4] K. Holmberg, in *Tribology of Mechanical Systems: A Guide to Present and Future Technologies*, edited by J. Vizintin, M. Kalin, K. Dohda, S. Jahanmir, (ASME Press NY, USA, 2004), ISBN 0791802094

[5] R. Bappert, S. Benner, B. Häcker, U. Klein, and G. Zweckbronner, in *Biologie Technik*, (SiemensForum Munich/Berlin Germany, 1999)

[6] S.R. Nassif, in International Conference on Simulation of Semiconductor Processes and Devices, SISPAD, 5 (2007)

[7] A. Nadzeyka, L. Peto, S. Bauerdick, M. Mayer, K. Keskinbora, C. Grévent, M. Weigand b, M. Hirscher and G. Schütz, MNE conference 2011

[8] R.P. Feynman, Engineering and Science **23**, 22 (1960)
the actual talk has been given at Caltech at 29.12.1959,
http://calteches.library.caltech.edu/47/02/1960Bottom.pdf or.
www.zyvex.com/nanotech/feynman.html 29.01.2008

[9] S.P. Newberry, in Proceedings of the Fourth SEBT , edited by R. A. Bakish, 81 (1962)

[10] Y. Ochiai, Y. Kojima, and S. Matsui, J. Vac. Sci. Technol. B **6**, 1055 (1988)

[11] L.A. Giannuzzi, B.I. Prenitzer, and B.W. Kempshall, in *Introduction to Focused Ion Beams*, edited by L.A. Giannuzzi and F.A. Stevie (Springer, NY, USA, 2005), ISBN 0-387-23116-1, Chap. 2, pp. 13-52

[12] EC growth project Contract No. G5RD-CT2000-0034, project team members
www.nanofib.com (25.01.2009)

[13] J. Gierak, D. Mailly, P. Hawkes, R. Jede, L. Bruchhaus, P. Mélinon, A. Perez, R. Hyndman, J.-P. Jamet, J. Ferre, A. Mougin, C. Chappert, V. Mathet, P. Warin, and J. Chapman, Appl. Phys. A **80**, 187 (2005)

[14] E. Hecht, *Optics*, 2nd ed. (Addison-Wesley Publishing Company, Reading, USA,1987), ISBN 0-201-11611-1

[15] E. Abbe, Beiträge zur Theorie des Mikroskops und der Mikroskopischen Wahrnehmung“, Archiv für mikroskopische Anatomie **9**, 456 (1873), article starts at p. 413

[16] Bergmann Schäfer, *Lehrbuch der Experimentalphysik*, Band 3 Optik, 7th ed. (Walter de Gruyter, Berlin, 1978), ISBN 3 11 0074575, p. 368

[17] Olympus 2008 - Olympus UIS2 Series: UPLSAPO 40X2: http://microscope.olympus.com/uis2/UPLSAPO/40X2/ (29.07.2008)

[18] Olympus II 2008 - e.g. UPLSAPO 100XO UIS2 Series from Olympus http://microscope.olympus.com/uis2/PLAPON/60XOTIRFM/ (1.8.2008)

[19] T. T. Tsong, Phys. Today **59**, 31 (2006)

[20] D. Semwogerere & E.R. Weeks, "Confocal Microscopy", published in the Encyclopedia of Biomat. Biomed. Eng., (2005), http://www.physics.emory.edu/~weeks/lab/papers/ebbe05.pdf (01.10.2008)

[21] http://www.dkfz.de/de/microscopy/index.html (03.09.2008)

[22] A. Lewis, M. Isaacson, A. Muray, and A. Harootunian, Biophys. J. **41**, 405a (1983)

[23] L. Bruchhaus, Diplomarbeit, Bergische Universität und Gesamthochschule Wuppertal, Germany, 1997

[24] E. Ruska, Rev. Mod. Phys. **59**, 627 (1987)

[25] L. de Broglie, PhD thesis, Universtié de Paris, 1924, published in Ann. Phys. Paris, **10**, 3, 22 (1925)

[26] B. Lencová, in *Handbook of Charged Particle Optics*, edited by. J. Orloff, 2nd edition (CRC Press, Boca Raton, USA, 2009), Chap. 5, pp. 161-208, ISBN 1-4200-4554-7

[27] M. Knoll and E. Ruska, Ann. Phys. **5**, 607 (1932)

[28] E. Ruska, Z. Phys. **87**, 580 (1933)

[29] W. Glaser, *Grundlagen der Elektronenoptik*, (Springer Verlag, Wien, Austria, 1952)

[30] P. W. Hawkes and E. Kasper, *Principles of electron optics: Volume 1*, (Academic press, London, GB, 1989), ISBN 0-12-333351-2

[31] P. Hawkes, Annales de la Fondation Louis de Broglie, **29**, 837 (2004)

[32] M. Knoll and E. Ruska, Z. Phys. **78**, 318 (1932)

[33] SESAM/UHRTEM Project http://www.smt.zeiss.com/c1256e4600305472/Contents-Frame/e6dc2de22b08ae2dc1256e5b00512342 (1.8.2008)

[34] M. Haider, S. Uhlemann, E. Schwan, H. Rose, B. Kabius, and K. Urban, Nature **392**, 768 (1998)

[35] H.H. Rose, Sci. Technol. Adv. Mat. **9**, 1 (2008)

[36] M. Schmallenberg, http://www.eipbn.org/history.pdf (07.08.2008), 2007, p.1-16

[37] Vistec 2008 - http://www.vistec-semi.com/ „E-Beam Lithography“ (07.08.2008)

[38] FU-Berlin 2007 - http://www.physik.fu-berlin.de/einrichtungen/sfb/sfb658/tutorials/doente/tutorial_pascual.pdf (28.02.2012)

[39] R. Young, J. Ward, and F. Scire, Rev. Sci. Instrum. 43, 999(1972), p. 999-1011

[40] G. Binnig, H. Rohrer, C. Gerber, and E. Weibel, Phys. Rev. Lett. **49**, 57 (1982)

[41] G. Binnig and C. F. Quate Phys. Rev. Lett. **56**, 930 (1986)

[42] F. J. Giessibl, Science **267**, 68 (1995)

[43] Müller E. W., Adv. Electron. Phys. **13**, 83 (1960)

[44] P.D. Prewett and G.L.R. Mair, *Focused ion beams from liquid metal ion sources*, No.1 Electronic & electrical engineering research studies, Microengeneering series, Series, edited by P.S. Walsh, Research studies press Ltd. Taunton, Somerset GB, 1991)

[45] W.H. Escovitz, T.R. Fox, and R. Levi-Setti, Proc. Nat. Acad. Sci. **72**, 1826 (1975)

[46] R.G. Wilson and G. R. Brewer, *ION BEAMS With applications to Ion Implantantion*, (Robert E. Krieger Publishing Compnay, Huntington, New York 1979)

[47] J. Andrus, Patent “Fabrication of Semiconductor Devices,” U.S. Patent No. 3,122,817, 1964 http://v3.espacenet.com/textdoc?DB=EPODOC&IDX=CA640560&F=0, (16.09.2008)

[48] Computer history 2008 - http://www.computerhistory.org/semiconductor/timeline/1955-Photolithography.html (16.09.2008)

[49] Nobelprize.org 2008 - http://nobelprize.org/nobel_prizes/physics/articles/lecuyer/planar.html (16.09.2008)

[50] J. A. Hoerni, Patent *Method of Manufacturing Semiconductor Devices*, US3025589, 1962 http://v3.espacenet.com/textdoc?DB=EPODOC&IDX=US3025589, (16.09.2008)

[51] J. A. Hoerni, Patent *Semiconductor device*, US3064167, 1962, http://v3.espacenet.com/textdoc?DB=EPODOC&IDX=US3064167, (16.09.2008)

[52] M.S. Hibbs, in *Microlithography*, edited by J. R. Sheats, and B.W. Smith (M. Dekker Inc., New York, USA, 1998), Chap. 1, pp. 1-108, ISBN 0-8247-9953-4

[53] R.F. Pease and S.Y. Chou, in *Proceedings of the IEEE* **96**, edited by R. J. Trew, 248 (2008)

[54] ASML 2008 - http://www.asml.com/asml/show.do?ctx=5869&rid=35905 and http://www.asml.com/asml/show.do?ctx=6720&rid=35774 (29.07.2008)

[55] P. H. Carr, Rev. Sci. Instrum. AIP, NY, **1**, 711 (1930)

[56] G. Owen, and J. R. Sheats, in *Microlithography*, edited by J. R. Sheats, and B.W. Smith, (M. Dekker Inc., New York, USA, 1998), Chap. 6, pp. 367-402, ISBN 0-8247-9953-4

[57] D.A. Buck and K. Shoulders, in *Proceedings Eastern Joint Computer Conference*, Am. Inst. Elec. Engineers, Special Publication **t-114**, (New York, ATEE, 1958), p.55-59

[58] W.E. Glen, in *Proceedings of the second SEPB*, edited by R. A. Bakish, 4 (1960)

[59] W. Opitz, in *Proceedings of the second SEPB*, edited by R. A. Bakish, 32 (1960)

[60] G.J. Selvin and W.J. MacDonald, in *Proceedings of the Second SEBP*, edited by R. A. Bakish, 86 (1960)

[61] G. Moellenstedt and R. Speidel, Physik. Blaetter **16**, 192 (1960)

[62] O. Wells, in *Proceedings of the 3rd symposium on electron beam proesses*, (Alloyd Electronics Corp., Cambridge Mass., USA, 1961) p.291-321

[63] R.M.F. Thornley, A.V. Brown, and A.J. Speth, IEEE Trans. Electron Components **EC-13**, 36 (1964)

[64] R.F.M. Thornley, and M. Hatzakis, in *Record of the IEEE 9th Annual Symposium on electron, ion and laser beam Techn.*, 64 (1967)

[65] I. Haller, M. Hatzakis, S. Srinivasan, IBM J. Res. Dev. **12**, 251 (1968), http://www.research.ibm.com/journal/ (28.02.2012)

[66] T.H.P. Chang and A.D.G. Steward, in *record of the IEEE Annual Symposium on Electron, Ion and Laser Beam Technology,* (Inst. of Elect. San Fransico, USA, 1969), p. 97-106

[67] T.H.P. Chang and B.A. Wallman, in *Record of the 11th Symposium on Electron, Ion and Laser Beam Technol.*, (San Francisco Press, USA, 1971), p. 471-482

[68] D. R. Herriott, R.J. Collier, D.S. Alles, and J.W. Stafford, IEEE Trans. Electron Devices, **ED-22**, 385-392 (1975)

[69] C. R. K. Marrian, D. M. Tennant, J. Vac. Sci. Technol. **A 21**, S207 (2003)

[70] Cornell 2008 - http://www.cnf.cornell.edu/cnf5_tool.taf?_function=detail&eq_id=33&gtitle=ELECTRON%2DBEAM%20LITHOGRAPHY&area=ELECTRON%2DBEAM%20LITHOGRAPHY&cacName=JEOL%209300&labUser=&_UserReference=858AD0E9BA5A58E948C3BAD8 (06.09.2008)

[71] SC Technol. 2008 - http://www.semiconductor-technology.com/features/feature226/ (10.10.2008)

[72] AMTC 2008 - http://www.amtc-dresden.com/homepage/content/index.php?xmlfile=../content/xml/overview.xml&PHPSESSID=6b50ae9ffe15ceeab07fd6afa0f7622a (6.9.2008)

[73] T. H. P. Chang, M. Mankos, K. Y. Lee and L. P. Muray, Microelec. Eng. **57-58**, 117 (2001)

[74] L.R. Harriott, J. Vac. Sci. Technol. B **15**, 2130 (1997)

[75] P. Petric, C. Bevis, A. Carroll, H. Percy, M.Zywno, K. Standiford, A. Brodie, N. Bareket, and L. Grella, J. Vac. Sci. Technol. B **27**, 161 (2009)

[76] J. Kretz, PhD thesis TU Dresden, 2001 (GCA Verlag, Herdecke, Germany 2001), ISBN 3-89863-038-2

[77] A.A. Tseng, S.D. Sartale, M.F. Luo, and C.C. Kuo, in *Nanofabrication*, edited by A. A. Tseng (World Scientific Publishing Co. Pte. Ltd., Singapore, 2008), Chapter 1, pp.1-32, ISBN 981-270-076-5

[78] N. Kawasegi, D.W. Lee, N. Morita, and J.W. Park, in *Nanofabrication*, edited by A. A. Tseng (World Scientific Publishing Co. Pte. Ltd., Singapore, 2008), Chapter 2, pp.33-64, ISBN 981-270-076-5

[79] C. Santschi, J. Polesel-Maris, J. Brugger, and H. Heinzelmann, in *Nanofabrication*, edited by A. A. Tseng (World Scientific Publishing Co. Pte. Ltd., Singapore, 2008), Chapter 3, pp.65-126, ISBN-10 981-270-076-5

[80] D.M. Eigler, IBM, 1989, http://www.almaden.ibm.com/vis/stm/atomo.html, http://domino.research.ibm.com/comm/research_people.nsf/pages/eigler.index.html (3.9.2008)

[81] D.M. Eigler and E.K. Schweizer, "Positioning single atoms with a scanning tunneling microscope", Nature **344**, 524 (1990)

[82] A.J. Heinrich, C.P. Lutz, J.A. Gupta, and D.M. Eigler, Science **298**, 1381 (2002)

[83] S. Y. Chou, P. R. Kraus, P. J. Renstrom, Science **272**, 85 (1996)

[84] ITRS 2007 - 2007 international technology roadmap for semiconductors, http://www.itrs.net/Links/2007ITRS/2007_Chapters/2007_Lithography.pdf (10.10.2008)

[85] K. Kanaya, H. Kawakatsu, S. Matsui, H,Yomazaki, I. Okazaki, and K. Tanaka, *in Proceedings of the ELBS*, edited by A.B. El-Kareh, 489 (1965)

[86] R.L. Seliger and W.P. Flemming, J. Vac. Sci. Technol. **10**, 1127 (1973)

[87] R.L. Seliger and W.P. Fleming, J. Appl. Phys. **45**, 1416 (1974)

[88] R.L. Seliger, R.L. Kubena, R.D. Olney, J.W. Ward, V. Wang, J. Vac. Sci. Technol. **16**, 1610 (1979)

[89] J.H. Orloff and L.W. Swanson, J. Vac. Sci. Technol. **12**, 1209 (1975)

[90] infineon 2008 - http://www.infineon.com/cms/at/corporate/press/news/releases/2002/128411.html (9.9.2008)

[91] J. R. Minkel, *A tabletop UV microscope* (2006) http://www.spectrum.ieee.org/sep06/4378 (03.09.2008)

[92] T. Ueno, and J. R. Sheats, in *Microlithography*, edited by J. R. Sheats, and B.W. Smith (M. Dekker Inc., New York, USA, 1998), Chap. 7, pp. 403-428, ISBN 0-8247-9953-4

[93] P. Steinmann and J. M. R. Weaver, J. Vac. Sci. Technol. B **22**, 3178 (2004)

[94] B. Cord, J. Yang, H. Duan, D. C. Joy, J. Klingfus, K.K. Berggren, J. Vac. Sci. Technol. B **27**, 2616 (2009)

[95] I. Utke, P. Hoffmann, and J. Melngailis, J. Vac. Sci. Technol. B, **26**, 1197 (2008)

[96] Gierak 2007 and 2012 - J. Gierak (private communication)

[97] R. Forbes, in *Handbook of Charged Particle Optics*, edited by. J. Orloff, 2nd edition (CRC Press, Boca Raton, USA, 2009), Chap. 2, pp. 29-86, ISBN 1-4200-4554-7

[98] FEI-Nova 2008 - FEI Product brochure FEI Nova 200 Nano Lab, http://www.fei.com/uploadedFiles/Documents/Content/2006_06_Nova200NanoLab_pb.pdf (15.07.2008)

[99] Orsay 2008 - Orsay Physics „Cobra column“ http://www.orsayphysics.com/cobra.htm (21.06.2008)

[100] Seiko 2008 - Seiko Instruments http://www.siint.com/en/products/SMI3050.html (21.06.2008)

[101] F.A. Stevie, in *Introduction to Focused Ion Beams*, edited by L.A. Giannuzzi and F.A. Stevie (Springer, NY, USA, 2005), ISBN 0-387-23116-1, Chap. 1, pp. 1-12

[102] N. S. Smith, W. P. Skoczylas, S. M. Kellogg, D. E. Kinion, P. P. Tesch, O. Sutherland, A. Aanesland, and R. W. Boswell, J. Vac. Sci. Technol. B **6**, 2902 (2006)

[103] B. W. Ward, J. A. Notte, and N. P. Economou, J. Vac. Sci. Technol. B **24**, 2871 (2006)

[104] Postek 1997 - M.T. Postek, in *Handbook of charged particle optics*, edited by J. Orloff (CRC Press, Boca Raton, USA, 2009), Chap. 9, pp. 363-402, ISBN 1-4200-4554-7

[105] Sato 2009 - M. Sato, in *Handbook of Charged Particle Optics*, edited by. J. Orloff, 2nd edition (CRC Press, Boca Raton, USA, 2009), Chap. 8, pp. 391-435, ISBN 1-4200-4554-7

[106] V.N. Tondare, J. Vac. Sci. Technol. A **23**, 1498 (2005)

[107] Zeiss 2008 - Zeiss Orion He Ion Microcope: http://www.smt.zeiss.com/c1256e4600305472/Contents-Frame/4e8922e90f2a5212c125732b002ebec2 (12.10.2008)

[108] Zeiss II 2008 - Specification Sheet of Zeiss Orion He Ion Microscope, http://www.smt.zeiss.com/C1256E4600307C70/EmbedTitelIntern/ORIONEssentialSpecificationPDF/$File/oriondata.pdf (12.10.2008)

[109] V. Sidorkin, E. Veldhoven, E. Drift, P. Alkemade, H. Salemink, and D. Maas, J. Vac. Sci. Technol. B 27, L18 (2009)

[110] D. Winston, B.M. Cord, B. Ming, D.C. Bell, W.F. DiNatale, L.A. Stern, A.E. Vladar, M.T. Postek, M.K. Mondol, J.K.W. Yang, and K.K. Breggren. J. Vac. Sci. Technol. B **27**, 2702 (2009)

[111] N.S. Smith, P.P. Tesch, N.P. Martin, and R.W. Boswell, Microscopy Today **15**, 18 (2009)

[112] FEI 2012 - http://www.fei.com/products/focused-ion-beams/vion.aspx (07.03.2012)

[113] P. Kruit and. G. H. Jansen, in *Handbook of Charged Particle Optics*, edited by. J. Orloff, 2nd edition (CRC Press, Boca Raton, USA, 2009), Chap. 7, pp. 341-389, ISBN 1-4200-4554-7

[114] G.L.R. Mair, D.C. Grindrod, M.S. Mousa, and R.V. Latham, J. Phys. D. Appl. Phys. **16**, L209 (1983)

[115] R.L. Kubena, J.W. Ward, F.P. Stratton, R.J. Joyce, G.M. Atkinson, J. Vac.Sci. Technol. B **9**, 3079 (1991)

[116] Sudraut 2009 - http://www.felmi-zfe.tugraz.at/FIB/WS3_Beitraege/01%20Sudraud.pdf (28.11.2011), p. 36

[117] J.J. Van Es, J. Gierak, R.G. Forbes, V.G. Suvorov, T. Van den Berghe, Ph. Dubuisson, I. Monnet, A. Septier, Elsevier, Microelectronic Engineering **73-74**, 132 (2004)

[118] R. Forbes, in *Handbook of Charged Particle Optics*, edited by. J. Orloff, 2nd edition (CRC Press, Boca Raton, USA, 2009), Chap. 3, pp. 87-128, ISBN 1-4200-4554-7

[119] A. V. Steele, B. Knuffmann, J.J. McClelland, and J. Orloff, J. Vac. Sci. Technol. B **29**, C6F1 (2010)

[120] C. Perez-Martinez, S. Guilet, N. Gogneau, and Pascale Jegou, J. Gierak and P. Lozano, J. Vac. Sci. Technol. B **28**, L25 (2010)

[121] C. Perez-Martinez, S. Guilet, J. Gierak, P. Lozano, Microelec. Eng. **88**, 2088 (2011)

[122] S. Guilet, C. Perez-Martinez, P. Jegou, P. Lozano, J.Gierak, Microelec. Eng. **88**, 1968 (2011)

[123] W. Gilbert, *De magnete*, (English translation of the original Latin document, Dover Publishing Inc., New York), ISBN 0-486-26761-x

[124] F.R.S. Rayleigh, in Proceedings of the Royal society of London 29, 71 (1879), http://rspl.royalsocietypublishing.org/content/29/196-199/71.full.pdf+html (28.02.2012)

[125] V.E. Krohn jr., in *Progress in astronautics and rockertry*, Vol. 5, edited by D. B. Langmuir, E. Stuhlinger, and J. M. Sellen, (Academ. Press., NY, USA 1961), p. 73

[126] J.F. Mahoney, A. Y. Yahiku, H. L. Daley, R. D. Moore, and J. Perel, J. Appl. Phys. **40**, 5101 (1969)

[127] V.E. Krohn, and G.R. Ringo, Appl. Phys. Lett. **27**, 479 (1975)

[128] R. Clampitt, and D.K. Jeffries, „Advanves in molten metal field ion sources“, Nucl. Instrum. Methods **149**, 739 (1978)

[129] R.L. Seliger, J.W. Ward, V. Wang, and R.L. Kubena, Appl. Phys. Lett. **34**, 310 (1979)

[130] G. I. Taylor, Proc. Roy. Soc. Lond. A **280**, 383 (1964)

[131] R. G. Forbes, Vacuum **48**, 85 (1996)

[132] G. Benassayag, P. Sudraut and B. Jouffrey, Ultramicroscopy **16**, 1 (1985)

[133] M. Komuro, H. Hiroshima, H. Tanoue, and T. Kanayama, J. Vac. Sci. Technol. B 1, 985 (1983)

[134] J. Orloff, M. Utlaut, and L. Swanson, in *High resolution focused ion beams*, (Kluwer Academic Plenum Publishers, New York, USA, 2003), ISBN 0-306-47350-X

[135] L. W. Swanson, G.A. Schwind, A.E. Bell, and J.E. Brady, J. Vac. Sci. Technol. B **16**, 1864 (1979)

[136] S. Matsui, K. Mori, K. Saigo, T. Shiokawa, K. Toyoda, and S. Namba, J. Vac. Sci. Technol. B, **4**, 845 (1986)

[137] J.W. Ward and R.L. Kubena, J. Vac. Sci. B **8**, 1923 (1990)

[138] R.L. Kubena, and J. W. Ward, Appl. Phys. Lett. **52**, 2089 (1988) 2089

[139] C. Vieu, G. Ben Assayag, and J. Gierak, Nucl. Instrum. Methods in Phys. Res. B **93**, 439 (1994)

[140] J. Orloff, J.-L. Li, M. Sato, J. Vac. Sci. Technol. B **9**, 2609 (1991)

[141] J.W. Ward, R.L. Kubena, and M.W. Utlaut, J. Vac. Sci. Technol. B **6**, 2090 (1988)

[142] L. W. Swanson, IEEE Trans. plasma science **19**, 746 (1991)

[143] Wieck 2008 - http://www.ruhr-uni-bochum.de/afp/downloads/ausstattung/ionen.pdf (15.09.2008)

[144] C.S. Galovich, J. Appl. Phys. **63**, 4811 (1988)

[145] G. Hakvoort and C.M. Hol, Journal of Thermal Analysis **52**, 195 (202)

[146] J.C. Beckman, T.H.P. Chang, A. Wagner, and R.F.W. Pease, J. Vac. Sci. Technol. B **15**, 2332 (1997)

[147] FEI 2008 - FEI, "Gallium Liquid Metal Ion Source Handling and Operating Instructions", http://www.feibeamtech.com/pdf/Gallium.pdf (27.10.2008)

[148] G.L.R. Mair, in *Handbook of charged particle optics*, edited by J. Orloff, (CRC Press Boca Raton, USA, 1997), Chap. 3, pp. 103-141, ISBN 0-8493-2513-7

[149] S.T. Purcell, Y.T. Binh, and P. Thevenard, Nanotechnology **12**, 168 (2001)

[150] M. Utlaut, in *Handbook of Charged Particle Optics*, edited by. J. Orloff, 2nd edition (CRC Press, Boca Raton, USA, 2009), Chap. 11, pp. 523-600, ISBN 1-4200-4554-7

[151] J.E. Barth, and P. Kruit, Optik **101**, 101 (1996)

[152] M. Nastasi, J.W. Mayer, and J.K. Hirvonen, *Ion-solid interactions: Fundamentals and applications*, (Cambridge University Press, GB, 1996), ISBN 0521 37376 X

[153] P. Grivet, P. W. Hawkes and A. Septier, *Electron Optics: Part 1 Optics*, 2nd ed. (English Edition, Pergamon Press, Oxford GB, 1972)

[154] Orloff 2008 - J. Orloff (private communication)

[155] J. Großer, *Einführung in die Teilchenoptik*, (Teubener Studienbücher, B.G. Steubener, Stuttgart, Germany, 1983), ISBN 3-519-03050-0

[156] N. Yao, in *Focused ion beam systems*, edited by N. Yao (Cambridge University Press, 2007), Chap. 1, pp. 1-30, ISBN 978-0521-83199-4

[157] O. Scherzer, Zeitschrift fuer Physik **101**, 593 (1936)

[158] L. Reimer and G. Pfefferkorn, Rasterelektronenmikroskopie, (Springer Verlag Berlin, Germany, 1973), ,ISBN 3-540-06100-9

[159] L. Reimer, *Scanning electron microscopy*, 2nd ed. (Springer Verlag Berlin, Germany, 1998), ISBN 3-540-63976-4

[160] X. Jiang, *Coulomb Interactions in Charged Particle Optical Columns*, (Delft University Press, Dleft, NL, 1996), ISBN 90-407-1369-3

[161] G.H. Jansen, J. Vac. Sci. Technol. B **6**, 1977 (1988)

[162] M. v. Ardenne, *Tabellen der Elektronenphysik, Ionenphysik und Übermikroskopie: Band 1*, (VEB Deutscher Verlag der Wissenschaften, Berlin, GDR, 1956)

[163] Hawkes 2010 - P. Hawkes (private communication)

[164] A.V. Crewe, Optik **88**, 118 (1991)

[165] P. W. Hawkes and E. Kasper, *Principles of electron optics: Volume 2*, (Academic press, London, GB, 1989), ISBN 0-12-333352-0

[166] S. Nomura, J. Vac. Sci. Technol. B **16**, 104 (1998)

[167] Sato 1991 - M.Sato, and J. Orloff, J. Vac. Sci. Technol. B **9**, 2602 (1991)

[168] T.H.P. Chang and R. Viswanathan, J. Vac. Sci. Technol. **15**, 878 (1978)

[169] G.A.C. Jones, and G. Owen, J. Vac. Sci. Technol. **15**, 896 (1978)

[170] SIMION 2009 - http://simion.com/ (11.02.2009)

[171] EOD 2012 - http://www.lencova.com/ (08.03.2012)

[172] OPTICS 2009 - http://www.mebs.co.uk/

[173] Seiko/Zeiss NVision 40 2009 -
http://www.siint.com/en/products/fib/ion_beam_microscope_list.html (02.03.2009)
http://www.smt.zeiss.com/C1256A770030BCE0/WebViewTopNewsAllE/279544520F27CCE3C12571B9002BA756?OpenDocument (02.03.2009)

[174] FEI-Helios 2009 - http://www.fei.com/uploadedFiles/Documents/Content/2006_12_HeliosFamily.PDF (02.03.2009) and http://www.fei.com/products/families/helios-nanolab-family.aspx (27.03.2009)

[175] J. Gierak, A. Septier, and C. Vieu, Nucl. Instum. Meth. Phys. Research A **427**, 91 (1999)

[176] J. Li, D.Stein, C. McMullan, D. Branton, M. Aziz, and J.A. Golovchenko, Nature **412**, 166 (2001)

[177] J. Gierak, A. Madouri, A.L. Biance, E. Bourhis, G. Patriarche, C. Ulysse, D. Lucot, X. Lafosse, L. Auvray, L. Bruchhaus, and R. Jede, Microelec. Eng. **84**, 779 (2007)

[178] W. J. MoberlyChan, D. P. Adams, M.J. Aziz, G. Hobler, and T. Schenkel, MRS bulletin **32**, 424 (2007)

[179] J.F.Ziegler, J.P. Biersack, and M.D. Ziegler, SRIM, (12/15/2008 / v05, www.LuLu.com (on demand internet publisher), 2008), ISBN 0-9654207-1X

[180] N. Imanishi, in *Focused ion beam systems*, edited by N. Yao (Cambridge University Press, 2007), Chap. 2, pp. 31-66, ISBN 978-0521-83199-4

[181] H. Kuchling, in *Taschenbuch der Physik*, (Harri Deutsch Verlag, Frankfurt a.M., Germany, 1986), ISBN 5 87144 097 3

[182] C.A. Volpert, and A.M. Minor, MRS Bulletin **32**, 389 (2007)

[183] A. Benninghoven, R.D. Rüdenauer, and H.W. Werner, in *Secondary ion mass spectroscopy*, (J. Wiley and Sons, New York, USA, 1987), ISBN 0-471-01056-1

[184] Tian 1996 - S. Tian, S.-H. Yang, S. Morrisa, K. Paraba, A.F. Tasch, D. Kamenitsa, R. Reece, B. Freer, R.B. Simonton, and C. Magee, Nucl. Instrum. and Methods in Physics Research B **112**, 144 (1996)

[185] B. Basnar, A. Lugstein, H. Wanzenboeck, H. Langfischer, E. Bertagnolli, and E. Gornik, J. Vac. Sci. Technol. B **21**, 927 (2003)

[186] M. Henzler and W. Göppel, *Oberflächenphysik des Festkörper*, (Teubner Studienbücher, Stuttgart, Germany, 1991), ISBN 3-519-03047-0

[187] Bauerdick 2009 - S. Bauerdick (private communication)

[188] F. Watt, A. A. Bettiol, J. A. van Kan, E.J. Teo, and M.B. Breese, Int. J. Nanoscience **4**, 269 (2005)

[189] S. Rejntjens, and R. Puers, Micromech. Microeng. **11**, 287 (2001)

[190] M. Komuro, N. Atoda, and H. Kawakatsu, J. Electrochem. Soc. **126**, 483 (1979)

[191] R.K. Watts, in *VLSI Technology*, edited by S.M. Sze, 2nd ed. (McGraw-Hill Book Company Singapore; 1988), ISBN 0-07-100347-9

[192] SRIM 2008 - SRIM software, "The stopping and range of ions in matter", J.F. Ziegler, M.D. Ziegler, J.P. Biersack, Chester, MD, USA, www.srim.org, comp. also [179]

[193] Casino 2001 - D. Drouin, A.R. Couture, R. Gauvin, P. Hovington, P. Horny, H. Demers, wincasino, *monte CArlo Simulation of electroN trajectory in sOlids*, Casino Version 2.42, Université de Sherbrooke, Sherbrooke, Quebec, Canada, http://www.gel.usherb.ca/casino/

[194] Ishianti, T. Ohnishi, and T. Yaguchi, in *Nanofabrication*, edited by A. A. Tseng (World Scientific Publishing Co. Pte. Ltd., Singapore, 2008), Chapter 13, pp.431-470, ISBN 981-270-076-5

[195] Wucher 2010 - A. Wucher http://www.ilp.physik.uni-essen.de/wucher/movies/movies.html (16.01.2010)

[196] Rudenauer 1981 - F.G. Rudenauer, and W. Steiger, Microchemika Akta **76**, 375 (1981) p. 375-389

[197] N. Sprang, D. Theirich, J. Engemann, Surf. Coat. Technol. **74-75**, 689 (1995)

[198] A.A. Tseng, in *Focused ion beam systems*, edited by N. Yao (Cambridge University Press, 2007), Chap. 7, pp. 187-214, ISBN 978-0521-83199-4

[199] F. Ghaleh, R. Köster, H. Hövel, L. Bruchhaus, S. Bauerdick, J. Thiel, and R.. Jede, J. Appl. Phys. **101**, 044301-1 (2007)

[200] K. Ohya and T. Ishianti, in *Focused ion beam systems*, edited by N. Yao (Cambridge University Press, 2007), Chap. 4, pp. 87-125, ISBN 978-0521-83199-4

[201] H. Ryssel, K. Haberger, and H. Kranz, J. Vac. Sci. Technol. **19**, 1358 (1981)

[202] J.R.A Cleaver, and H. Ahmed, J. Vac. Sci. Technol. **19**, 1145 (1981)

[203] J. Melngailis, Nucl. Instrum. and Methods in Phys. Research B **80/81**, 1271 (1993)

[204] V. Boegli, PhD thesis, RWTH Aachen, 1988

[205] J. Gierak, C. Vieu, M. Schneider, H. Launois, G. Ben Assayag, and A. Septier, J. Vac. Sci. Technol. B **15**, 2373 (1997)

[206] A. Stanishevsky, S. Aggarwal, A. S. Prakash, J. Melngailis, and R. Ramesh, J. Vac. Sci. Technol. B **16**, 3899 (1998)

[207] H. Loeschner, G. Stengel, R. Kaesmaier, and A. Wolter, J. Vac. Sci. Technol. B **19**, 2520 (2001)

[208] J. Melngailis, J. Vac. Sci. Technol. B **5**, 469 (1987)

[209] C. Lehrer, L. Frey, S. Petersen, H. Ryssel, M. Schäfer, and T. Sulzbach, J. Vac. Sci. Technol. B **22**, 1402 (2004)

[210] A. Imre, L. E. Ocola, L. Rich, and J. Klingfuss, J. Vac. Sci. Technol. B **28**, 304 (2010)

[211] K. Arshak, M. Mihov, S. Nakahara, A. Arshak, D. McDonagh, J. Vac. Sci. Technol. **22**, 3016 (2004)

[212] Appleton 2009 - B. Appleton private communication

[213] K. N. Hooghan, in *Introduction to Focused Ion Beams*, edited by L.A. Giannuzzi, and F.A. Stevie (Springer, NY, USA, 2005), ISBN 0-387-23116-1, Chap. 5, pp. 87-106

[214] J. Mayer, L.A. Giannuzzi, T. Kamino, and J. Michael, MRS bulletin **32**, 400 (2007)

[215] B. Holdford, in *Introduction to Focused Ion Beams*, edited by L.A. Giannuzzi, and F.A. Stevie (Springer, NY, USA, 2005), ISBN 0-387-23116-1, Chap. 6, pp. 107-132

[216] Defect Analyzer 2009 -
http://www.fei.com/uploadedFiles/Documents/Content/2006_06_DefectAnalyzer300Advanced_pb.pd
(31.03.2009)f

[217] dcg systems 2009 - http://www.dcgsystems.com/optifib.html (31.03.2009)

[218] FEI 2010 - http://www.fei.com/products/focused-ion-beams/v600.aspx 29.04.2010

[219] suppliers 2009 -
http://www.fei.com/products/families/product-families.aspx
http://www.fei.com/products/types/dualbeam-systems.aspx
http://www.jeol.com/Default.aspx?tabid=158
http://www.siint.com/en/products/fib/ion_beam_microscope_list.html
(31.03.2009)

[220] Zeiss Auriga 2010
http://www.smt.zeiss.com/C1256E4600305472/Contents-Frame/1A1FF14FB0CDA53FC125723D00566AFC 29.04.2010
and
http://www.smt.zeiss.com/C1256E4600305472/Contents-Frame/1A1FF14FB0CDA53FC125723D00566AFC 29.04.2010

[221] Tescan Lyra 2011
http://www.tescan.com/products.php?id_menu=26 (11.07.2011)

[222] D. Winston, V. R. Manfrinato, S.M. Nicaise, L.L. Cheong, H. Duan, D. Ferranti, J. Marshman, S. McVey, L. Stern, J. Notte, and K.K. Berggren, Nano Lett. **11**, 4343 (2011)

[223] *Technical description of Raith 150-TWO*. V TD_ RAITH150TWO _3.2, April 2010

[224] Kretz 1998 - J. Kretz (private communication)

[225] Jeol 2010 - http://www.jeol.com/PRODUCTS/SemiconductorEquipment/ElectronBeamLithography/tabid/99/Default.aspx, (28.06.2010)

[226] Ellionix 2010 - http://www.sts-elionix.com/content/category/4/18/26/, (28.06.2010)

[227] Vistec 2010 - http://www.vistec-semi.com/; (28.06.2010)

[228] Nanobeams 2010 - http://www.nanobeam.co.uk/, (28.06.2010)

[229] Raith 2010 - http://www.raith.de/?xml=solutions%7CLithography+%26+nanoengineering, (28.06.2010)

[230] Raith 2007 - *Raith Info* **27**, (2007)

[231] J. Gierak. Y. Lagadec, A. Septier, *DISPOSITIF DE GENERATION D'UN FAISCEAU D'IONS ET PROCEDE DE REGLAGE DE CE FAISCEAU*, Patent No. FR000002823005A1, 2001

[232] EB Mask Repair 2010 - e.g. MeRiT HR 32 Zeiss SMT GmbH, http://www.zeiss.de/c1256c1500431210/Contents-Frame/6531cac4d5c10402c1256df7003f3cbc, (25.06.2010)

[233] Peto 2008 - L. Peto (private communication)

[234] L. Rosa, K. Sun, V. Mizeikis, S. Bauerdick, L. Peto, and S. Juodkazis, J. Phys. Chem. C **115**, 5251 (2011)

[235] D. Recht and N. Yao, in *Focused ion beam systems*, edited by N. Yao (Cambridge University Press, 2007), Chap. 12, pp. 318-336, ISBN 978-0521-83199-4

[236] B. R. Appleton, S. Tongay, M. Lemaitre, B. Gila, J. Fridmann, P. Mazarov, J. E. Sanabia, S. Bauerdick, L. Bruchhaus, R. Mimura, R. Jede, Nucl. Instr. and Meth. B **272**, 153 (2012)

[237] Tongay 2011 - S. Tongay, M. Lemaitre, T. Schumann, K. Berke, B. R. Appleton, B. Gila, and A. F. Hebard, Appl. Phys. Lett. 99, 102102-1 (2011)

[238] H. Hövel, T. Becker, A. Bettac, B. Reihl, M. Tschudy, and E.J. Williams, J. Appl. Phys. **81**, 154 (1996)

[239] H. Chang, and A. J. Bard, J. Am. Chem. Soc. **113**, 5588 (1991)

[240] F. Ghaleh, PhD thesis, TU Dortmund 2008, https://eldorado.tu-dortmund.de/handle/2003/26000

[241] L. Patryarcha, PhD thesis, TU Dortmund 2011, https://eldorado.tu-dortmund.de/handle/2003/29118

[242] J-P. Adam, J-P. Jamet, J Ferré, A. Mougin, S. Rohart, R. Weil, E. Bourhis and J. Gierak, Nanotechnology **21**, 1 (2010)

[243] S. Y. Chou, M. S. Wei, P.R. Krauss, and P.B. Fischer, J. App. Phys. **76**, 6673 (1994)

[244] S. Sun, C.B. Murray, D. Weller, L. Folks, A. Moser, Science **287**, 1989 (2000)

[245] R. Hyndman, A. Mougin, L.C. Sampaio, J. Ferre, J.P.Jamet, P. Meyer, V. Mathet, C. Chappert, D. Mailly, J. Gierak, J. Magnetism Magnetic Materials **240**, 34 (2002)

[246] A.-L. Biance, J. Gierak, E. Bourhis, A. Madouri, X. Lafosse, G. Patriarche, G. Oukhaled, C. Ulysse, J.-C.Galas, Y.Chen, L. Auvray, Microelc. Eng. **83**, 1474 (2006)

[247] B. Schiedt, L. Auvray, L. Bacri, G. Oukhaled, A. Madouri, E. Bourhis, G. Patriarche, J. Pelta, R. Jede, and J. Gierak, Microelec. Eng. **87**, 1300 (2010)

[248] G. Oukhaled, L. Bacri, E. Bourhis, B. Schiedt, A. Madouri, G. Patriarche, R. Jede, JM. Betton, P. Guegan, L. Auvray, J. Pelta, and J. Gierak, Mater. Res. Soc. Symp. Proc. **1253**, 1253-K10-33 (2010=

[249] A.N. Boers, A.C.F. Hoole, and J.M. Ryan, Microelectron. Eng. 32 (3), 131 (1996)

[250] T. Schenkel, V. Radmilovic, E.A. Stach, S.-J. Park, and A. Persaud, J. Vac. Sci. Technol. B **21**, 2720 (2003)

[251] J. Gierak, E.Bourhis, G.Faini, G.Patriarche, A.Madouri, R.Jede, L.Bruchhaus, S.Bauerdick, B. Schiedt, A.L.Biance, and L.Auvray, Ultramicroscopy **109**, 457 (2009)

[252] R. L. Kubena, F.P. Stratton, J.W. Ward, G.M. Atkinson, and R.J. Joyce, J. Vac. Sci. Technol. B **7**, 1799 (1989)

[253] N. Rau, F. Stratton, C. Fields, T. Ogawa, A. Neureuther, R. Kubena, and G. Wilson, J. Vac. Sci. Technol. B **16**, 3784 (1998)

[254] J. K. W. Yang, B. Cord, H. Duan, and K.K. Berggren, J. Vac. Sci. Technol. B **27,** 2622 (2009)

[255] L. Bruchhaus et al. to be published in Microelec. Eng. 2012, http://dx.doi.org/10.1016/j.mee.2012.04.033

[256] Raith instrument - Raith150-TWO, Raith GmbH, www.raith.com

[257] J. Gierak, E. Cambril, M. Schneider, C. David, D. Mailly, J. Flicstein, G. Schmid, J. Vac. Sci. Technol. B **17**, 3132 (1999)

[258] P. Hoffmann, G. BenAssayag, J. Gierak, J. Flicstein, M. Maar-Stumm, H. van Bergh, J. Appl. Phys. **74** , 7588 (1993)

[259] V. Torma, G. Schmid, and U. Simon, ChemPhysChem **5**, 321 (2001)

[260] L. Zhang, C. Li, J. Li, F. Zhang, L. Shi, J. of Optolelectronics and Adv. Materials **8**, 847 (2006)

[261] Bruchhaus 2012 II - plan to apply for paper

[262] Gimp 2011 - imaging software - Gimp V GIMP 2.6.8, http://www.gimp.org

[263] Topometrix instrument - Topmetrix explorer 1996 (software SPM Lab V3.03.06)

[264] I. Horcas, R. Fernandez, J.M. Gomez-Rodriguez, J. Colchero, J. Gomez-Herrero and A. M. Baro, Rev. Sci. Instrum. **78**, 013705 (2007)

[265] Logufatu 2008 - P.C. Logofatu, D. Apostol; A. Dinescu; R. Muller; D. Cristea, in *Semiconductor Conference, CAS 2008*. **1**, 10.1109/SMICND.2008.4703345, pp. 121-124

[266] H.J. Eichler, in *Bergmann Schäfer Experimentalphyik III Optik*, (de Gruyter, Berlin, Germany, 1987), edited by H. gobrecht, 8th edition, Chap. 3 pp. 325-480, ISBN 3-11-010882-8

[267] Enger 1983 - R.C. Enger, and S.K. Case, J. Opt. Soc. Am. **73**, 1113 (1983)

[268] Economist 2011 - http://www.economist.com/node/18304268/print 10.03.2011

[269] J. Gierak, A. Madouri, A.L. Biance, E. Bourhis, G. Patriarche, C. Ulysse, D. Lucot, X. Lafosse, L. Auvray, L. Bruchhaus, and R. Jede, Microelectron. Eng. **78-79**, 266 (2005)

[270] Ullmann 2008 - F. Ullmann, M. Schmidt, F. Grossmann, V.P. Ovsyannikov, J. Gierak, E. Bourhis, and G. Zschornack, VDI Berichte **2027**, 241 (2008)

[271] Gierak 2010 - J. Gierak, A. Madouri, E. Bourhis, L. Travers, D. Lucot, and J.C. Harmand, Microelec. Eng. **87**, 1386 (2010)

[272] Shinada 1999 - T. Shinada, Y. Kumura, J. Okabe, T. Matsukawa, and I. Ohdoman, J. Vac. Sci. Technol. B 16, 2489 (1998)

[273] Raith 1980 - *Raith Info* **1**, (1980)

[274] Raith 1987 - *Raith Info* **11**, (1987)

[275] Raith 1997 - *Raith Info* **20**, (1997)

[276] P.A. Tipler, *Physik* (Spektrum akademischer Verlag, Heidelberg, 1998) 2. Nachdruck 1988, of the first edition 1994

[277] Nicol 2004 - „The word format/template of this document is based on *AWDiss4.dot* from N. Nicol, and R. Albrecht, *Wissenschaftliche Arbeiten schreiben mit Word* (Addison-Wesley Verlag, München, Germany, 2004) ISBN 3-8273-2159-X

12.3 Development project background

12.3.1 Historical background of the instrument development

The main roots of the product development are the L2M's (LPN) long term experience in ion beam technology, the Raith GmbH's EBL writer know-how (for both comp. section 12.3.1) and the complementary knowledge of the other EC growth project team members (comp. section 12.3.2). EC growth project team (comp. also www.nanofib.com):

L2M CNRS "the Orsay group" [44]	Raith GmbH	Further technology milestones
		Parts of the LMIS history are summarised in section 4.3
		Early ion beam instruments have been developed comp. section 2.1.4, 2.2.5
1974 P. Sudraut (Paris XI Orsay), later L2M CNRS, starts to work with LMIS [96]		
1979 P. Sudraud finishes his PhD about Au LMIS [132]		
Since the 1980`s the L2M research institute develops FIB instrumentation and LMIS	1980 Raith KG has been founded as a spin off of Cambridge Instruments [273]	

L2M CNRS “the Orsay group” [44]	Raith GmbH	Further technology milestones
1985 the L2M team carries out in situ imaging of operating LMIS in a MeV TEM [132]		
1985 Jacques Gierak joins L2M		
	1987 Raith KG sells the first EBL attachment “Elphy” [274]	
1989 P. Sudraut founds Orsay Physics	1989 Raith KG converts into Raith GmbH	
		1991 Kubena reaches 7nm minimum feature sizes by ion beam patterning [115]
		Mid 1990s the interest in ion nano pattering decreases.
1990`s the L2M team starts the evaluation of a new type of focused Ga nano structuring instrument [205]	1997 Raith GmbH sells the first EBL system [275]	

12.3.2 NanoFIB EC growth project:

At the end of the 1990s Jacques Gierak (L2M CNRS) has gathered a team of complementary European experts (2 companies and 10 research institutes / universities, www.nanofib.com). The complementary fields of expertise span from theoretical physicists, applied physicists to development engineers of commercial companies. Together we have managed to receive a fifth framework EC growth project grant (Contract G5RD-CT2000-0034, 2001-2004) for the development and application of the joinedly created instrument (comp. Figure 27, chapter 8):

LPN (formerly L2M) **CNRS** (F): optimisation of the column, filament, the application of the joinedly created instrument and project co-ordination.
FuG Elektronik GmbH (G): dedicated power supplies
Delft University's Charged Particle Optics Group (NL), the **Institute of Scientific Instruments** (Brno/CZ) and CNRS CEMES (F) have complemented the CPO development.
CEA Sacley have carried out the in-situ analysis of the LMIS emission using a MeV transmission electron microscope.
University of Surrey (GB) **LMIS theory group** research on the fundamental theory of LMIS
Laboratoire de Physique des Solides and Institut d'Electronique Fondamentale de Uni Paris Sud (F), **Universität Essen Institut für Chemie** (G) and the **LPN CNRS** (F) have been our internal application „customers" (for their results comp. section 12.4).
We (**Raith GmbH**) added our EBL writer technology (hardware/software), manufacturing and process know-how to the project and adjusted them to ion beam processes.
NFL University of Florida, B. Appleton has bought the first instrument.

L2M CNRS “the Orsay group” [44]	Raith KG / GmbH	Further technology milestones
2001 the NanoFIB EC growth project starts (Contract G5RD-CT2000-0034, 2001-2004)		
2002 the “L2M” research institute is renamed into “LPN” CNRS		
Joined results/publications from the proof of concept tool (comp. chapter 9 and section 12.4)		
2004 Jacques Gierak has finished his PhD about his work realising and utilising a proof of concept tool of an ion beam complement to EBL writer		
2004 the EC project ended		
	2005 the application co-operation between TU Dortmund and Raith GmbH has started	
some of the NanoFIB research project partners continue to co-operate		
	2006 the formal product launch of the ionLiNE [230]	
	2007 Raith GmbH sells the first ionLiNE system	

12.4 Publications utilising ionLiNE instrument technology

In addition to the ones listed under section 12.1.2:

S. Tongay, M. Lemaitre, J. Fridmann, A.F. Hebard, B.P Gila, B.R. Appleton,
Drawing graphene nanoribbons on SiC by ion implantation,
Appl. Phys. Lett. 100, 073501-1 (2012)

J. Jaworowicz, V. Zablotskii, J.-P. Jamet, J. Ferré, N. Vernier, J.-Y. Chauleau, M. Kisielewski, E. Bourhis,
Magnetic coercivity of focused ion beam irradiated lines in a Pt/Co(1.4 nm)/Pt film,
J. Appl. Phys. **109**, 093919 (2011)

L. Bacri, A.G. Oukhaled, B. Schiedt, G. Patriarche, E. Bourhis, J. Gierak, J. Pelta, and L. Auvray,
Dynamics of colloids in single solid-state nanopores,
J. Phys. Chem. B **115**, 2890 (2011)

L. Bacri, E. Bourhis, B. Schiedt, A. Madouri, G. Patriarche, R. Jede, G. Oukhaled, J. Gierak,
Tailoring nanopores for efficient sensing of different biomolecules,
Materials Research Society Symposium Proceedings **1253**, 91 (2010)

J. Gierak, D. Lucot, A. Ouerghi, G. Patriarche, E. Bourhis, G, Faini, D. Mailly,
Nano-patterning of graphene structures using highly focused beams of gallium ions,
Materials Research Society Symposium Proceedings **1259**, 47-58 (2010)

E. Palacios, L.E. Ocola, A. Joshi-Imre, S. Bauerdick, M. Berse and L. Peto,
Three-dimensional microfluidic mixers using ion beam lithography and micromachining,
J. Vac. Sci. Technol. B **28**, C611 (2010)

A. Ouerghi, A., Kahouli, D. Lucot, M. Portail, L. Travers, J. Gierak, J. Penuelas, P. Jegou, A. Shukla, T. Chassagne, and M. Zielinski,
Epitaxial graphene on cubic SiC(111)/Si(111) substrate,
Appl. Phys. Lett. **96**, 191910-1 (2010)

L. Lalouat, L. Billot, E. Saïdi, L. Aigouy, B. Wang, P. Lalanne, E. Bourhis, J. Gierak, and V. Mathet,
Near-field analysis of surface waves generated by nanostructures,
Proceedings of SPIE - The International Society for Optical Engineering, 7608, art. no. 76080V, (2010)

J. Gierak, A. Madouri, E. Bourhis, L. Travers, D. Lucot, J.C. Harmand,
Focused gold ions beam for localized epitaxy of semiconductor nanowires,
Microelec. Eng. **87**, 1386 (2010)

B. Schiedt, L. Auvray, L. Bacri, G. Oukhaled, A. Madouri, E. Bourhis, G. Patriarche, J. Pelta, R. Jede, and J. Gierak,
Direct FIB fabrication and integration of "single nanopore devices" for the manipulation of macromolecules,
Microelec. Eng. **87** , 1300 (2010)

C. Perez-Martinez, S. Guilet, N. Gogneau, P. Jegou, J. Gierak, and P. Lozano,
Development of ion sources from ionic liquids for microfabrication,
J. Vac. Sci. and Technol. B **28**, L25 (2010)

B. Schiedt, L. Auvray, L. Bacri, A.-L. Biance, A. Madouri, E. Bourhis, G. Patriarche, J. Pelta, R. Jede, and J. Gierak,
Direct FIB fabrication and integration of "single nanopore devices" for the manipulation of macromolecules,
Materials Research Society Symposium Proceedings **1191**, 93 (2009)

J. Penuelas, A. Ouerghi, C. Andreazza-Vignolle, J. Gierak, E. Bourhis, P. Andreazza, J. Kiermaier, T. Sauvage,
Local tuning of CoPt nanoparticle size and density with a focused ion beam nanowriter,
Nanotechnology **20**, 425304 (2009)

J. Gierak
Focused ion beam technology and ultimate applications,
Semiconductor Sci. Technol. **24**, 043001 (2009)

A. Ravasio, D. Gauthier, F.R.N.C. Maia, M. Billon, J.-P. Caumes, D. Garzella, M. Géléoc, O. Gobert, J.-F. Hergott, A.-M. Pena, H. Perez, B. Carré, E. Bourhis, J. Gierak, A. Madouri, D. Mailly, B. Schiedt, M. Fajardo, J. Gautier, P. Zeitoun, P.H. Bucksbaum, J. Hajdu, H. Merdji,
Single-shot diffractive imaging with a table-top femtosecond soft X-ray laser-harmonics source,
Phys. Rev. Lett. **103**, 028104 (2009)

D. Lucot, J. Gierak, A. Ouerghi, E. Bourhis, G. Faini, and D. Mailly,
Deposition and FIB direct patterning of nanowires and nanorings into suspended sheets of grapheme,
Microelec. Eng. **86**, 882 (2009)

B. Wang, L. Aigouy, E. Bourhis, J. Gierak, J.P. Hugonin, and P. Lalanne
Efficient generation of surface plasmon by single-nanoslit illumination under highly oblique incidence,
Appl. Phys. Lett. **94**, 011114 (2009)

J. Penuelas, A. Ouerghi, D. Lucot, C. David, J. Gierak, H. Estrade-Szwarckopf, and C. Andreazza-Vignolle,
Surface morphology and characterization of thin graphene films on SiC vicinal substrate,
Phys. Rev. B Condens. Matter Mat. Phys. **79**, 033408 (2009)

P. Mélinon, A. Hannour, L. Bardotti, B. Prével, J. Gierak, E. Bourhis, G. Faini, and B. Canut
Ion beam nanopatterning in graphite: Characterization of single extended defects,
Nanotechnology **19**, 235305 (2008)

D. Martrou and J. Gierak
Development of a STM compatible ion emitter capable of atomic imaging resolution
Microelec. Eng. **85**, 1403 (2008)

E.M. Huisman, A.-L. Biance, A. Madouri, G. Patriarche, E. Bourhis, G. Oukhaled, L. Auvray, and J. Gierak,
A new way to integrate solid state nanopores for translocation experiments,
Microelec. Eng. **85**, 1311 (2008)

F. Ullmann, M. Schmidt, F. Grossmann, V.P. Ovsyannikov, J. Gierak, E. Bourhis, and G. Zschornack
Extension of focused ion beam technology using highly charged ions from an electron beam ion trap,
VDI Berichte **2027**, 241 (2008)

D. Stanescu, D. Ravelosona, V. Mathet, C. Chappert, Y. Samson, C. Beign, N. Vernier, J. Ferré, J. Gierak, E. Bouhris, and E.E., Fullerton
Tailoring magnetism in CoNi films with perpendicular anisotropy by ion irradiation,
J. Appl. Phys. **103**, 07B529 (2008)

F. Ullmann, F. Grossmann, V.P. Ovsyannikov, J. Gierak, E. Bourhis, J. Ferré, J.P. Jamet, A. Mougin, and G. Zschornack,
Production of noble gas ion beams in a focused ion beam machine using an electron beam ion trap,
J. Vac. Sci. Technol. B **25**, 2162 (2007)

Zurschnak: Ullmann, F., Großmann, F., Ovsyannikov, V.P., Gierak, J., Zschornack, G., *Production of a helium beam in a focused ion beam machine using an electron beam ion trap*, Appl. Phys. Lett. **90**, 083112 (2007)

R.M. Langford, P.M. Nellen, J. Gierak, and Y. Fu,
Focused ion beam micro- and nanoengineering,
MRS Bulletin **32**, 417 (2007)

F. Ullmann, F. Großmann, V.P. Ovsyannikov, J. Gierak, and G. Zschornack
Production of a helium beam in a focused ion beam machine using an electron beam ion trap, Appl. Phys. Lett. **90**, 083112 (2007)

A. Ruotolo, S. Wiebel, J.P. Jamet, N. Vernier, D. Pullini, J. Gierak, and J., Ferré,
Magneto-optical microscopy as a favourite tool to probe focused ion beam patterning at low dose,
Nanotechnology **17**, 3308 (2006)

A.-L. Biance, J. Gierak, E. Bourhis, A. Madouri, X. Lafosse, G. Patriarche, G. Oukhaled, C. Ulysse, J.-C. Galas, Y. Chen, and L. Auvray,
Focused ion beam sculpted membranes for nanoscience tooling,
Microelec. Eng. **83**, 1474 (2006)

L. Aigouy, M. Mortier, J. Giérak, and E. Bourhis,
Rare-earth doped fluoride glass particles as three-dimensional near-field optical sensors,
Physics and Chemistry of Glasses: European Journal of Glass Science and Technology Part B **47**, 83 (2006)

J. Gierak, E. Bourhis, A. Madouri, M. Strassner, I. Sagnes, S. Bouchoule, M.N. Mérat Combes, D. Mailly, P. Hawkes, R. Jede, L. Bardotti, B. Prével, A. Hannour, P. Mélinon, , A. Perez, J. Ferré, J.-P. Jamet, A. Mougin, C. Chappert, and V. Mathet,
Exploration of the ultimate patterning potential of focused ion beams,
J. Microlithography, Microfabrication and Microsystems **5**, 011011 (2006)

Z.H. Wu, , J. Gierak, E. Bourhis, A.-L. Biance, and H.E. Ruda,
Highly oriented and ordered semiconductor nanowire arrays for photonic device applications,
Proceedings of SPIE - The International Society for Optical Engineering **5971**, 597117 (2005)

A. Hannour, L. Bardotti, B. Prével, E. Bernstein, P. Mélinon, A. Perez, J. Gierak, E. Bourhis, and D. Mailly,
2D arrays of CoPt nanocluster assemblies,
Surface Science **594**, 1 (2005)

P. Mélinon, A. Hannour, B. Prével, L. Bardotti, E. Bernstein, A. Perez, J. Gierak, E. Bourhis, and D. Mailly,
Functionalizing surfaces with arrays of clusters: Role of the defects
Journal of Crystal Growth **275**, 317 (2005)

Aigouy, L., Mortier, M., De Wilde, Y., Gierak, J., Bourhis, E.,
Near-field optical measurements using rare-earth-doped glass-ceramic particles,
Proceedings of SPIE - The International Society for Optical Engineering **5458**, 163 (2004)

L. Aigouy, Y. De Wilde, M. Mortier, J. Giérak, and E. Bourhis,
Fabrication and characterization of fluorescent rare-earth-doped glass-particle-based tips for near-field optical imaging applications,
Appl. Optics **43**, 3829 (2004)

J.J. van Es, J. Gierak, R.G. Forbes, V.G. Suvorov, T. van den Berghe, P. Dubuisson, I. Monnet, and A. Septier,
An improved gallium liquid metal ion source geometry for nanotechnology,
Microelec. Eng. **73-74**, 132-138 (2004)

J. Kapsa, Y. Robach, G. Hollinger, M. Gendry, J. Gierak, and D. Mailly,
STM and FIB nano-structuration of surfaces to localise InAs/InP(0 0 1) quantum dots,
Applied Surface Science **226**, 31-35 (2004)

B. Prével, L. Bardotti, S. Fanget, A. Hannour, P. Mélinon, A. Perez, J. Gierak, G. Faini, E. Bourhis, and D. Mailly,
Gold nanoparticle arrays on graphite surfaces,
Applied Surface Science **226**, 173 (2004)

V. Repain, J.-P. Jamet, N. Vernier, M. Bauer, J. Ferré, C. Chappert, J. Gierak, and D.Mailly,
Magnetic interactions in dot arrays with perpendicular anisotropy,
J. Appl. Phys., **95**, 2614 (2004)

A. Perez, L. Bardotti, B. Prevel, P. Jensen, M. Treilleux, P. Me´linon, J. Gierak, G. Faini, D. Mailly,
Quantum-dot systems prepared by 2D organization of nanoclusters preformed in the gas phase on functionalized substrates,
New Journal of Physics **4**, 76.1 (2002)

L. Bardotti, B. Prevel, P. Jensen, M. Treilleux, P. Melinon, A. Perez, J. Gierak, G. Faini, and D. Mailly,
Organizing nanoclusters on functionalized surfaces,
Applied Surface Science **191**, 205 (2002)

C. Vieu, J. Gierak, H. Launois, T. Aign, P. Meyer, J.P. Jamet, J. Ferré, C. Chappert, T. Devolder, V. Mathet, and H. Bernas,
Modifications of magnetic properties of Pt/Co/Pt thin layers by focused gallium ion beam irradiation,
J. Appl. Phys. **91**, 3103 (2002)

R. Hyndman, A. Mougin, L.C. Sampaio, J. Ferré, J.P. Jamet, P. Meyer, V. Mathet, C. Chappert, D. Mailly, and J. Gierak,
Magnetization reversal in weakly coupled magnetic patterns,
Journal of Magnetism and Magnetic Materials **240**, 34 (2002)

R. Hyndman, P. Warin, J. Gierak, J.N. Chapman, J. Ferré, J.P. Jamet, V. Mathet, and C. Chappert,
Structural and magnetic properties of FIB-irradiated microstructures on a Pt/Co multilayer,
Journal of Magnetism and Magnetic Materials **240**, 50 (2002)

L.C. Sampaio, R. Hyndman, F.S. De Menezes, J.P. Jamet, P. Meyer, J. Gierak, C. Chappert, V. Mathet, and J. Ferré,
Power-law relaxation decay in two-dimensional arrays of magnetic dots interacting by long-range dipole-dipole interactions,
Phys. Rev. B - Condensed Matter and Materials Physics **64**, 1844401 (2001)

R. Hyndman, P. Warin, J. Gierak, J. Ferré, J.N. Chapman, J.P. Jamet, V. Mathet, and C. Chappert,
Modification of Co/Pt multilayers by gallium irradiation - Part 1: The effect on structural and magnetic properties,
J. Appl. Phys. **90**, 3843 (2001)

J. Gierak, D. Mailly, G. Faini, J.L. Pelouard, P. Denk, F. Pardo, J.Y, Marzin, A. Septier, G. Schmid, J. Ferré, R. Hydman, C. Chappert, J. Flicstein, B. Gayral, and J.M. Gérard,
Nano-fabrication with focused ion beams,
Microelec. Eng. **57-58**, 865 (2001)

12.5 Calculations

12.5.1 Electron / ion mass / speeds / equivalent wavelength

Indices "$_{rel}$" indicate the relativistic formulas / values

Non relativistic (classical approximation) particle wavelength

$$\lambda = \frac{h}{p} = \frac{h}{m \cdot v} = \frac{h}{m \cdot \sqrt{\frac{2 \cdot q \cdot V}{m}}} = \frac{h}{\sqrt{2 \cdot q \cdot m \cdot V}}$$

non relativistic (classical) speed of a charged particle accelerated by a voltage (V)

$$v = \sqrt{\frac{2 \cdot q \cdot V}{m}}$$

relativistic speed of a charged particle accelerated by a voltage (V)

$$v_r = c \cdot \sqrt{1 - \frac{1}{1 + \frac{q \cdot V}{m_0 \cdot c^2}}} \quad \text{from} \quad E_{kin} = m_0 \cdot c^2 \cdot \left(\frac{1}{\sqrt{1 - \frac{v^2}{c^2}}} - 1 \right) \text{ and } E_{kin} = q \cdot V \text{ (e.g. [276])}$$

Relativistic Energy [276]

$$E^2 = (p_{rel} \cdot c)^2 \cdot (m_0 \cdot c^2)^2 \text{ can be written as } p_{rel} = \frac{1}{c} \cdot \sqrt{E^2 - (m_0 \cdot c^2)^2}$$

with $E = E_{kin} + m_o \cdot c^2$ and $E_{kin} = q \cdot V$ the relativistic momentum can be written as

$$p_{rel} = \sqrt{\left[(q \cdot V)^2 + m_0 \cdot c^2 \right]^2 - (m_0 \cdot c^2)^2} = \sqrt{\frac{q^2 \cdot V^2}{c^2} + 2 \cdot q \cdot V \cdot m_0}$$

factor out both $2 \cdot m_o \cdot q \cdot V$ results in

$$p_{rel} = \sqrt{2 \cdot m_0 \cdot q \cdot V} \cdot \sqrt{1 + \frac{q \cdot V}{2 \cdot m_0 \cdot c^2}} \text{ with } \lambda = \frac{h}{p}$$

$$\lambda_{rel.} = \frac{h}{\sqrt{2 \cdot m_0 \cdot q \cdot V}} \cdot \frac{1}{\sqrt{1 + \frac{q \cdot V}{2 \cdot m_0 \cdot c^2}}}$$

with q for electrons is: $1.6 \cdot 10^{-19}$ As

Rest masses ratio: six orders of magnitude between Ga^+ (69.72 u) = $1.16 \cdot 10^{-25}$ kg

versus the electron mass ($5.485 \cdot 10^{-4}$ u)) = $9.1 \cdot 10^{-31}$ kg

c = speed of light (299,792,458 m/s≈$3\cdot10^8$ m/s)

h = $6.626\cdot10^{-34}$ Js

5 kV Ga^+ 117 km/s

30 kV Ga^+ 288 km/s

50 kV Ga^+ 371 km/s

30 kV electrons: $v_{rel} = 9.8\cdot10^7$ m/s (non relativistic $1.027\cdot10^8$ m/s),

$m_{rel} = 9.63\cdot10^{-31}$ kg => λ_{rel} = 7.0 pm (non relativistic 7.1 pm)

50 kV electrons: $v_{rel} = 1.24\cdot10^8$ m/s (non relativistic $1.32\cdot10^8$ m/s), $m_{rel} = 9.99\cdot10^{-31}$ kg

=> λ_{rel} = 5.4 pm (non relativistic 5.5 pm)

$\lambda_{30keV\ Ga+} \approx$ 0.02 pm (non relativistic / classical)

Necessary acceleration voltage for 371 km/s electrons (<< c therefore non relativistic):

$V = \frac{v^2 \cdot m_{elec}}{2 \cdot q}$, with 371 km/s => V = 0,392 V

12.5.2 Aberrations away from the optical axis formulas

Deflection distortion

$$d_y = -\frac{1}{2}\cdot\left(L+\frac{l}{4}\right)\cdot\Theta^3 \quad [162]$$

L = distance between end of deflection field and patterning plane, l = length of the deflection field, Θ = deflection angle

Astigmatism of deflection

$$a \approx \left(L+\frac{l}{3}+\frac{2\cdot L^2}{l}\right)\cdot\alpha_L\cdot\Theta^2, \quad b \approx \frac{3}{2}\cdot\left(L+\frac{l}{3}\right)\cdot\alpha_L\cdot\Theta^2 \qquad [162]$$

L = distance between end of deflection field and patterning plane, l = length of the deflection field, Θ = deflection angle

Coma of deflection

$$a \approx \frac{3}{4}\cdot\left(L+\frac{l}{3}\right)\cdot\alpha_L^2\cdot\Theta, \quad b \approx \frac{3}{4}\cdot\left(\frac{3\cdot L}{2}+\frac{2\cdot l}{3}\right)\cdot\alpha_L^2\cdot\Theta \quad [162]$$

L = distance between end of deflection field and patterning plane, l = length of the deflection field, Θ = deflection angle

12.6 Casino simulation parameters [193]

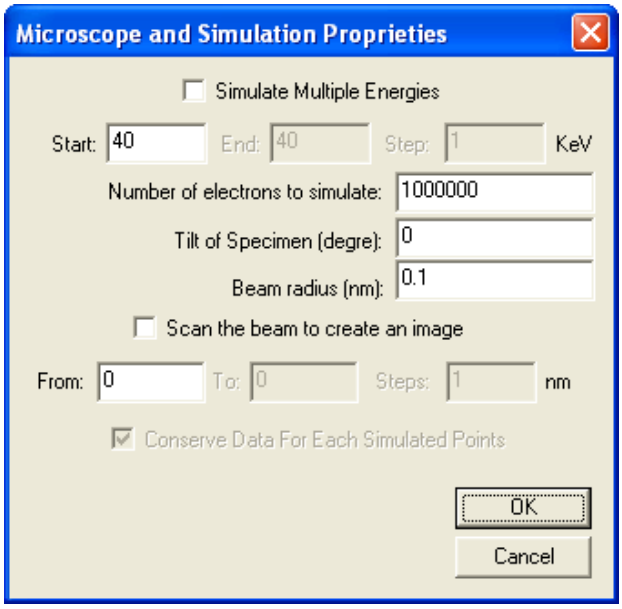

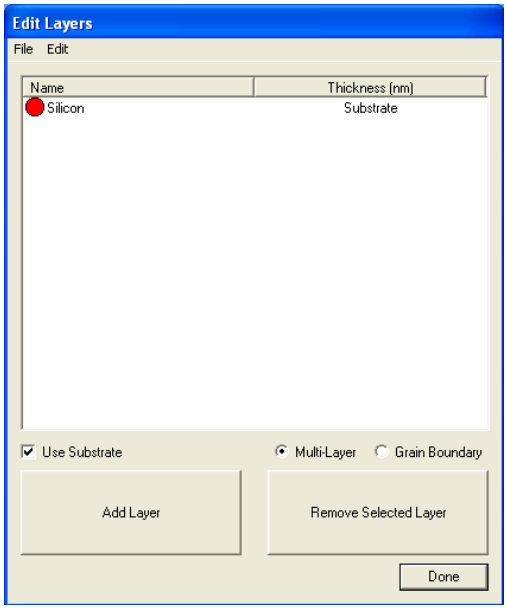

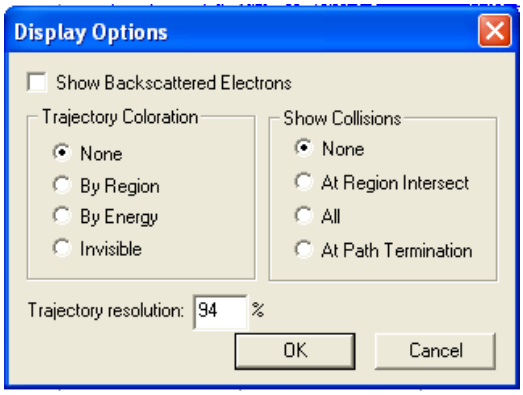

12.7 SRIM 2008 simulation parameters [192]

12.7.1 The interaction volume of Ga^+ ions hitting a Si sample surface

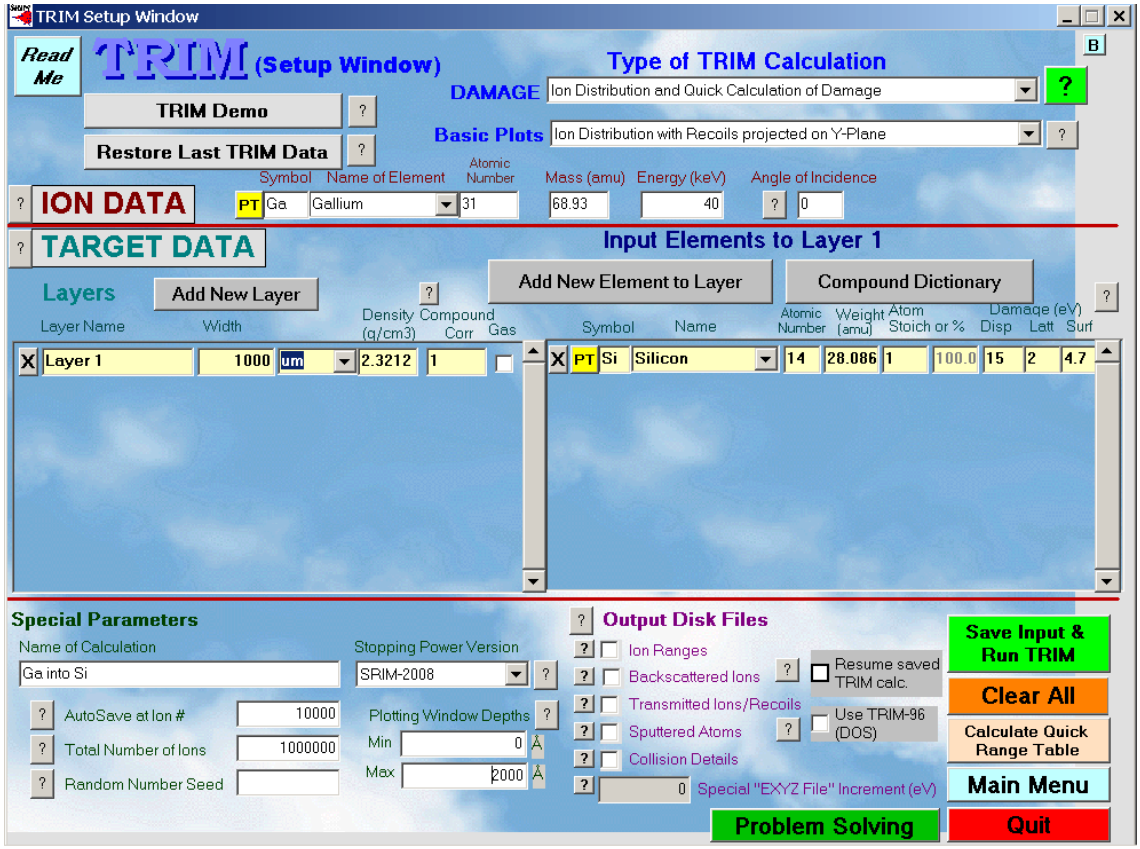

12.7.2 The interaction volume of Li ions hitting a Si sample surface

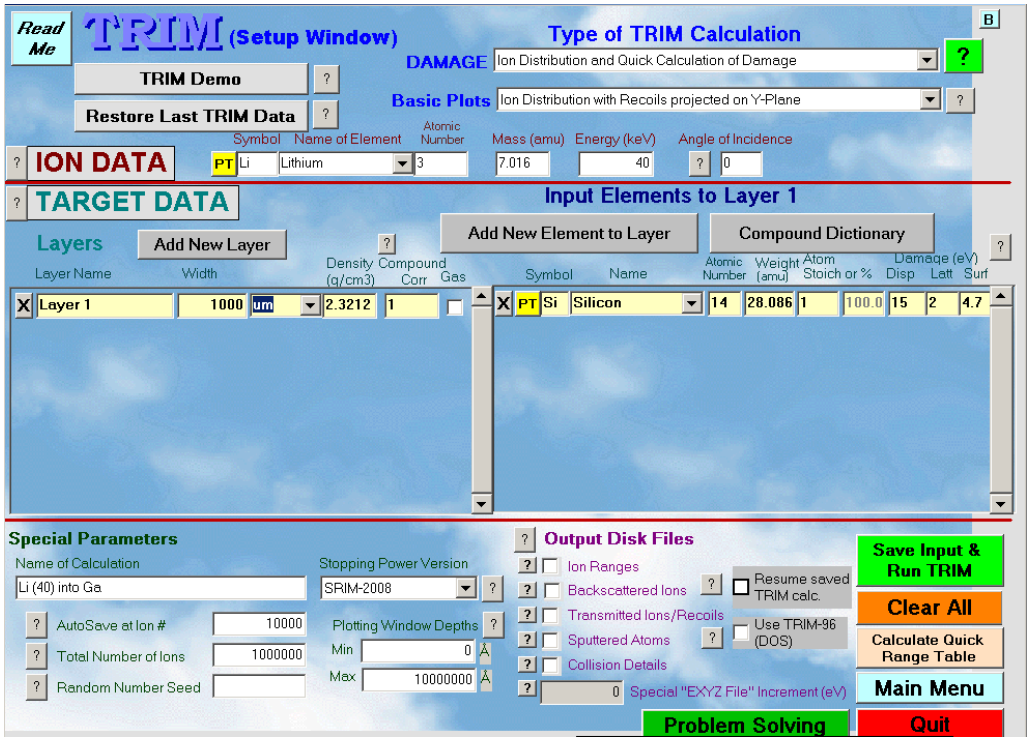

12.7.3 Ga^+ ions hitting a Si sample surface (nuclear and electronic interactions)

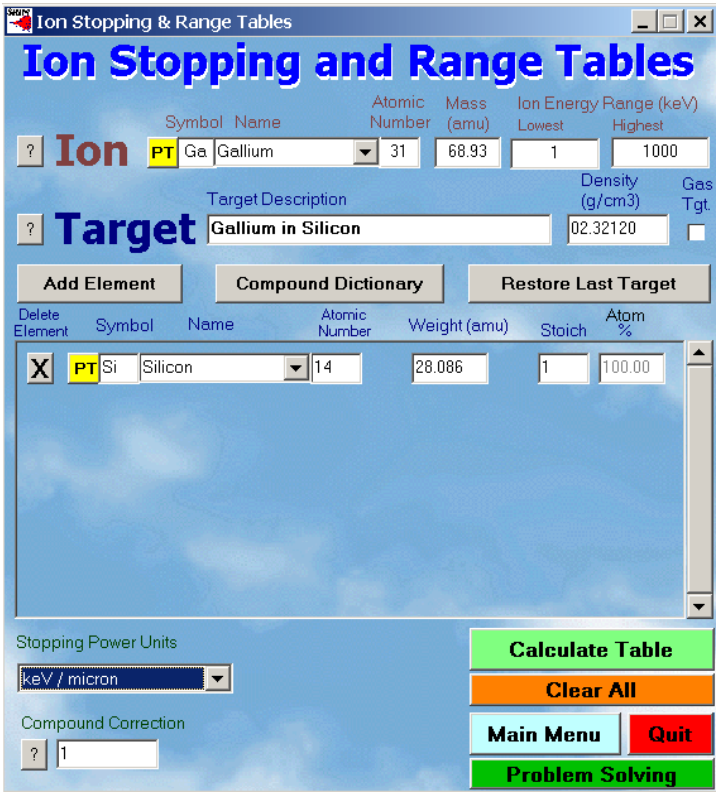

12.7.4 resulting values from 12.7.1

Ion Energy [keV]	dE/dx Elec. [keV/µm]	dE/dx Nucl. [keV/µm]	Projected range [nm]	Longitudinal Straggling [nm]	Lateral Straggling [nm]
1	21,38	407,9	3,4	1,6	1,2
1,1	22,43	425,1	3,6	1,7	1,2
1,2	23,42	441,2	3,7	1,7	1,2
1,3	24,38	456,3	3,9	1,8	1,3
1,4	25,3	470,6	4	1,8	1,3
1,5	26,19	484,1	4,2	1,9	1,4
1,6	27,05	497	4,3	2	1,4
1,7	27,88	509,2	4,5	2	1,5
1,8	28,69	520,8	4,6	2,1	1,5
2	30,24	542,6	4,8	2,2	1,6
2,25	32,08	567,5	5,2	2,3	1,7
2,5	33,81	590,2	5,5	2,4	1,8
2,75	35,46	611	5,8	2,5	1,8
3	37,04	630,1	6	2,6	1,9
3,25	38,55	648	6,3	2,7	2
3,5	40	664,6	6,6	2,8	2,1
3,75	41,41	680,1	6,9	2,9	2,1
4	42,77	694,7	7,1	3	2,2
4,5	45,36	721,5	7,6	3,2	2,4
5	47,81	745,5	8,1	3,3	2,5
5,5	50,15	767,2	8,6	3,5	2,6
6	52,38	787	9	3,7	2,7
6,5	54,52	805,1	9,5	3,8	2,9
7	56,58	821,9	9,9	4	3
8	60,48	851,7	10,8	4,3	3,2
9	64,15	877,6	11,6	4,5	3,4
10	67,62	900,3	12,5	4,8	3,6
11	70,92	920,4	13,3	5,1	3,9
12	74,07	938,4	14	5,3	4,1
13	77,1	954,6	14,8	5,6	4,3
14	80,01	969,2	15,6	5,8	4,4
15	82,82	982,5	16,3	6,1	4,6
16	85,53	994,5	17,1	6,3	4,8
17	88,17	1006	17,8	6,5	5
18	90,72	1016	18,5	6,8	5,2
20	95,63	1034	20	7,2	5,5
22,5	101,4	1052	21,7	7,7	5,9
25	106,9	1068	23,5	8,3	6,4
27,5	112,1	1080	25,2	8,8	6,8
30	117,1	1091	26,9	9,3	7,2
32,5	121,9	1100	28,5	9,8	7,5
35	126,5	1107	30,2	10,3	7,9

37,5	130,9	1113	31,9	10,8	8,3
40	135,2	1118	33,5	11,3	8,7
45	143,4	1126	36,8	12,2	9,4
50	151,2	1131	40	13,2	10,1
55	158,6	1133	43,3	14,1	10,8
60	165,6	1134	46,5	15	11,5
65	172,4	1134	49,7	15,9	12,2
70	178,9	1133	52,9	16,8	12,8
80	191,3	1127	59,3	18,5	14,2
90	202,9	1120	65,8	20,3	15,5
100	213,8	1110	72,2	22	16,8
110	224,3	1100	78,7	23,7	18
120	234,2	1089	85,1	25,4	19,3
130	243,8	1078	91,6	27	20,5
140	256,7	1066	98,2	28,7	21,8
150	280,1	1055	104,7	30,3	23
160	299,2	1043	111,2	31,9	24,3
170	315,2	1031	117,6	33,5	25,5
180	328,6	1020	124,1	35	26,7
200	350,3	997	137,1	38,1	29,1
225	371,6	969,6	153,4	41,8	32,1
250	390	943,5	169,9	45,5	35
275	407,6	918,7	186,5	49,2	37,9
300	425	895,2	203,3	52,8	40,8
325	442,4	873	220,3	56,3	43,7
350	459,9	851,9	237,3	59,8	46,6
375	477,4	831,9	254,4	63,2	49,5
400	494,7	813	271,6	66,6	52,3
450	528,7	778	306,1	73,2	58
500	561,7	746,2	340,7	79,6	63,7
550	593,6	717,4	375,5	85,8	69,2
600	624,4	691,1	410,2	91,8	74,8
650	654,1	666,9	444,9	97,5	80,2
700	683	644,7	479,6	103,1	85,6
800	738,6	605,1	548,6	113,8	96,1
900	791,8	570,8	617	123,7	106,3
1000	843,3	540,8	684,7	133	116,2

12.8 Index

12.9 Acknowledgements / Special thanks to

Hiermit bedanke ich mich recht herzlich bei allen, die zur Entstehung dieser Arbeit beigetragen haben.

Ein ganz besonderer Dank geht an Priv. Doz. Dr. Heinz Hövel für die exzellente Betreuung meiner Arbeit während der vielen Abendstunden, in denen er, mit viel Geduld, die Entstehung dieser Arbeit ermöglicht hat.

Merci beaucoup au Dr. Jacques Gierak pour sa vision de la technologie des faisceaux d'ions focalisés, la formidable coopération, boîte à idées, la correction des épreuves et le support expérimental.

Einen besonderen Dank geht an Herrn Dr. Ralf Jede, der mir die Chance gegeben hat der Koordinator des NanoFIB Projektes bei der Raith GmbH zu sein, seine CPO Bibliothek zur Verfügung gestellt und Teile der Arbeit Korrektur gelesen hat.

Special thanks to Prof. Dr. Peter Hawkes (CEMES/CNRS Toulouse) for his patient assistance, CPO literature tips and proof readings of the resolution chapter.

Dem Promotionsausschuss der Fakultät Physik an der TU Dortmund danke ich, dass ich die Promotion hier durchführen durfte.

Herrn Prof. Dr. Metin Tolan danke ich für die Möglichkeit meine Arbeit an seinem Lehrstuhl durch zu führen.

Frau Dr. B. Siegmann und Herrn Prof. Dr. Thomas Weis danke ich für das Interesse an meiner Arbeit, durch die Vertretung der wissenschaftlichen Mitarbeiter und die Übernahme des Korreferats.

Special thanks to Dr. Joseph Klingfus for proofreading.

Prof. Dr. Günter Schmid (Uni Duisburg-Essen) danke ich für die Entwicklung und die Erklärungen der Au_{55} Cluster.

Prof. Ulrich Simon (RWTH Aachen) danke ich für die Versorgung mit Au_{55} Clustern

Merci aussi à l'équipe du LPN-CNRS, en particulier à l'ingénieur Eric Bourhis, pour le support pendant mes visites, la formidable coopération, le support expérimental, les résultats scientifiques et le soutien pour ma thèse de doctorat.

Des weiteren danke ich meinen Raith Kollegen für die in den unterschiedlichsten Formen entgegengebrachte Unterstützung.

Thanks a lot for the great collaboration inside the NanoFIB project team and to the EC for partially funding this growth project (Contract G5RD-CT2000-0034).

Herrn Dipl. Ing. Hans-Georg Rademacher Lehrstuhl für Qualitätswesen TU Dortmund vielen Dank für die Bereitstellung des Rasterkraftmikroskops.

Der Arbeitsgruppe von Dr. Heinz Hövel danke ich für die Unterstützung bei der Fertigstellung der Arbeit und des Vortrages. Insbesondere danke ich Dr. Farhad Ghaleh und Dr. Lukas Patryarcha, die die mitentwickelte Anlage für Ihre Forschungen verwendet und uns wertvolle Beiträge zur Verbesserung gegeben haben.

Eidesstattliche Erklärung

Ich versichere an Eides statt, dass ich die vorliegende Dissertation mit dem Titel „An Ion Beam Complement to Electron Beam Writers“ selbständig und ohne unzulässige fremde Hilfe erbracht habe. Ich habe keine anderen als die angegebenen Quellen und Hilfsmittel benutzt, sowie wörtliche und sinngemäße Zitate kenntlich gemacht. Die Arbeit hat in gleicher oder ähnlicher Form noch keiner Prüfungsbehörde vorgelegen.

Dortmund, den ----------

(Lars Bruchhaus)